

Laser Pulse Control of Dissipative Dynamics in Molecular Systems

D I S S E R T A T I O N

zur Erlangung des akademischen Grades
doctor rerum naturalium
(Dr. rer. nat.)
im Fach Physik

eingereicht an der
Mathematisch-Naturwissenschaftlichen Fakultät I
Humboldt-Universität zu Berlin

von
Herrn Dipl.-Phys. Tomáš Maňcal
geboren am 23.4.1974 in Vlašim, Tschechische Republik

Präsident der Humboldt-Universität zu Berlin:
Prof. Dr. Jürgen Mlynek

Dekan der Mathematisch-Naturwissenschaftlichen Fakultät I:
Prof. Dr. Michael Linscheid

Gutachter:

1. Prof. Dr. Nikolaus P. Ernsting
2. Prof. Dr. Wolfgang Domcke
3. Dr. habil. Volkhard May

eingereicht am:	11. September 2002
Tag der mündlichen Prüfung:	19. Dezember 2002

Abstract

This work is dedicated to a further development of the density matrix theory and its application to the study of ultrafast laser pulse induced dynamics in molecular systems interacting with a thermal environment. Two topics are considered, first the so-called memory effects are analyzed which result from a reduced description of the molecular system excluding the environmental degrees of freedom. And secondly, the laser pulse control of dissipative molecular dynamics is examined.

The theoretical description of open quantum systems results in a time non-local equation of motion so that the evolution of the molecular system depends on its past. In this work a numerical method to solve the time non-local equations of motion has been developed and tested for a minimal model of a polyatomic molecule subject to the dissipative influence of an environment. An analytical solution of the equation of motion for the special case of very long standing memory is also achieved. To identify signatures of such memory effects in general case we compare this analytical solution with numerical calculations involving memory and with approximative computations ignoring time non-locality. For the excitation by a laser pulse shorter than the duration of the memory the molecular systems exhibit noticeably different dynamics than for the absence of the memory. The effects become significantly more pronounced with decreasing laser pulse durations.

The second part of the work concentrates on the application of the optimal control theory to guide molecular dynamics. Optimal control theory provides laser pulses which are designed in such a manner to fulfill certain control tasks, e.g. the population of a desired vibrational level of the molecular system or the placement of a wavepacket on a prescribed position on the molecular potential energy surface. As a first example the control of the dissipative photo-induced electron transfer in a donor-bridge-acceptor systems has been particularly considered ignoring the memory. The controllability of the electron transfer has been discussed and the mechanism by which it becomes possible has been identified. We have found the control of electron transfer reactions feasible even under the influence of dissipation although the yield of the control decreases drastically with increasing dissipation. In the presence of dissipation mechanism of the control has been found to change. The feasibility of the reproduction of the control pulses resulting for the optimal control theory in the experiment has been discussed and methods have been presented

how to check the efficiency of the reproduction of optimal control pulses by liquid crystal pulse shapers, prevailingly used in modern control experiments. To distinguish different control tasks a quantitative measure has been introduced characterizing complexity of the control task. The optimal control theory has also been formulated for molecular systems showing static disorder and applied on an ensemble of molecules exhibiting random orientations. Finally, the importance of memory effects for the control of dissipative dynamics has been discussed and the optimal control theory has been formulated to account for a time non-locality in the equation of motion for molecular systems.

Keywords:

Density matrix theory, non-Markovian dynamics, ultra-fast molecular dynamics, optimal control of dissipative molecular dynamics, optical control of electron transfer reactions, complexity of the control task

Zusammenfassung

Diese Arbeit wird einer Weiterentwicklung der Dichtematrixtheorie und ihrer Anwendung zum Studium ultraschneller laserpulsinduzierter Dynamik in Molekularsystemen in Wechselwirkung mit einem thermischen Bad gewidmet. Zwei große Themenkomplexe werden behandelt. Zuerst werden die sogenannten Gedächtniseffekte diskutiert. Diese folgen aus einer reduzierten Beschreibung des Molekularsystems, in der die Umgebungsfreiheitsgrade eliminiert werden. Im zweiten Teil wird die Laserpulssteuerung der dissipativen Molekulardynamik untersucht.

Die theoretische Beschreibung von offenen Quantensystemen führt zu einer zeitlich nicht-lokalen Bewegungsgleichung: Die Zeitentwicklung des Molekularsystems hängt von seiner Vergangenheit ab. In dieser Arbeit wird eine numerische Methode zur Lösung der zeitlich nicht-lokalen Bewegungsgleichung entwickelt und mit einem minimalen Modell eines polyatomaren Moleküls unter dissipativem Einfluss der Umgebung getestet. Eine analytische Lösung der Bewegungsgleichung für den speziellen Fall einer sehr langen Gedächtniszeit wurde hergeleitet. Zur Identifizierung solcher Gedächtniseffekte vergleichen wir diese analytische Lösung mit numerischen Rechnungen inklusive Gedächtnis und mit approximativen Rechnungen, die die zeitliche Nicht-Lokalität vernachlässigen. Für eine Anregung mit einem Laserpuls, der kürzer als die Gedächtniszeit des Systems ist, zeigt das Molekularsystem eine erkennbar unterschiedliche Dynamik als ohne Gedächtnis. Die Gedächtniseffekte werden mit abfallender Laserpulslänge deutlich ausgeprägter.

Der zweite Teil der Arbeit konzentriert sich auf die Anwendung der Theorie der Optimalen Kontrolle, um die molekulare Dynamik zu steuern. Aus der Theorie der Optimalen Kontrolle erhält man Laserpulse, die bestimmte Aufgaben erfüllen, z.B. die Besetzung gewünschter vibronischer Niveaus des Molekularsystems oder die Platzierung eines Wellenpakets auf einer vorgegebenen Position auf der molekularen Potentialfläche. Als erstes Beispiel haben wir die Kontrolle des dissipativen fotoinduzierten Elektronentransfers in einem Donator-Brückenmolekül-Akzeptor System betrachtet, wobei wir das Gedächtnis vernachlässigt haben. Die Steuerbarkeit des Elektronentransfers wird diskutiert und der Mechanismus, mit dem sie möglich wird, wird identifiziert. Wir haben festgestellt, dass die Steuerung der Elektronentransferreaktionen selbst unter dem Einfluss von Dissipation möglich ist, obwohl die Kontrollausbeute mit steigender Dissipation drastisch abfällt. In Anwesenheit

von Dissipation verändert sich auch der Mechanismus der Steuerung. Die experimentelle Ausführbarkeit der Herstellung des aus der Theorie der Optimalen Kontrolle resultierenden Kontrollpulses wird diskutiert und Methoden werden präsentiert, die die Abschätzung der Effizienz ermöglichen, mit der ein Flüssigkristall-Laserpulsformer, wie er heute in Experimenten verwendet wird, den gewünschten Puls erzeugen kann. Um zwischen verschiedenen Kontrollaufgaben zu unterscheiden, wird ein quantitatives Maß eingeführt, das die Komplexität der Kontrollaufgabe charakterisiert. Die Theorie der Optimalen Kontrolle wird auch für Molekularsysteme formuliert, die statische Unordnung zeigen, und wird auf ein Ensemble von Molekülen mit zufälligen Orientierungen angewendet. Zum Schluss wird die Bedeutung der Gedächtniseffekte für die Steuerung der dissipativen Dynamik diskutiert und die Theorie der Optimalen Kontrolle neu formuliert um eine zeitliche Nicht-Lokalität in der Bewegungsgleichung des Molekularsystems zu berücksichtigen.

Schlagwörter:

Dichtematrixtheorie, nicht-Markovsche Dynamik, ultraschnelle Molekulardynamik, optimale Steuerung der dissipativen Molekulardynamik, optische Kontrolle des Elektronentransfers, Komplexität der Kontrollaufgabe

Dedication

To all those back home who have missed me during my stay in Berlin.

Tuto práci věnuji všem těm doma, kterým jsem po dobu svého pobytu v Berlíně chyběl.

Contents

I	Introduction	1
II	Dynamics of Open Quantum Systems and Memory Effects	7
1	Dynamics of Open Quantum Systems	9
1.1	Density Matrix Theory	13
1.2	Quantum Master Equation	15
1.3	Markovian versus Non-Markovian Quantum Master Equation . .	19
1.3.1	Markov Approximation	20
1.3.2	Multi-Level Redfield Equation	21
1.3.3	Critical View on the Quantum Master Equation	22
2	Memory Effects and Ultrafast Optical State Preparation	24
2.1	The Molecular System	26
2.2	Memory Effects in the Frequency Domain	28
2.3	Effects of Initial Correlations	30
2.4	An Analytical Solution for the Case of Long Correlation Times .	33
2.5	Interplay of Non-Markovian Relaxation and Ultrafast Optical State Preparation	37
2.5.1	Density Operator Equation	38
2.5.2	Energy Representation	39
2.5.3	Numerical Results	44
2.6	Non-Markovian Dissipation via Multi-Quantum Processes	49
2.6.1	Non-Linear Coupling	51
2.6.2	Numerical Results	54
2.7	Summary of Chapter 2	58

III	External Field Control of Open Quantum Systems	61
3	Laser Pulse Control of Molecular Dynamics	63
3.1	Optimal Control Scheme for Dissipative Molecular Dynamics . .	68
3.2	Restriction to Mixed and Pure-State Dynamics	72
3.3	Reappearance of the <i>Pump-Dump</i> Scheme in the Optimal Control Theory	74
4	Optimal Control of Electron Transfer	79
4.1	The Electron Transfer Model	80
4.2	Optimal Control of Dissipation-Less Electron Transfer	81
4.3	Electron Transfer and Vibrational Relaxation	87
4.4	Interplay of Vibrational Relaxation and Internal Conversion . .	97
4.5	Acceleration of the Control Algorithm Convergency	99
4.6	Summary of the Chapter 4	102
5	Adapting Optimal Control Theory to Experimental Conditions	103
5.1	A Standard Experimental Set-Up	104
5.2	Complexity of the Control Task	107
5.2.1	Control Tasks with Growing Complexity	109
5.2.2	Pulse-Shaper Analysis and Definition of the Complexity	110
5.2.3	Complexity and Dissipation	113
5.2.4	Experimental Relevance of the Optimal Control Theory .	114
5.3	Optimal Control with Static Disorder (Orientational Averaging)	116
5.4	Optimal Control with the Non-Markovian Dissipation	120
5.5	Summary of the Chapter 5	122
IV	Conclusions and Outlook	125
V	Appendices	131
A	Nakajima–Zwanzig Equation with External Fields	133
B	Quantum Master Equation and the Introduction of the Reservoir Correlation Function	136
C	Microscopic Model for the Correlation Function	139

D	The Dissipative Part of the Quantum Master Equation and the Reduction to the Excited-State Potential Energy Surface	142
E	Solution of Non-Markovian Equations: Factorization of the Correlation Function	146
F	Solution of Non-Markovian Equations: Laguerre Polynomial Expansion	150
G	Evaluation of the Correlation Function Expansion Coefficients	153
H	Derivation of the Control Kernel	156
I	The Reverse Time Evolution Superoperator	157
J	Further Generalizations of the Optimal Control Theory	160
	J.1 Spectral Limitation of the Laser Pulse	160
	J.2 Generalized Target States	162
	J.3 Probe-Pulse Absorption as the Target of the Optimal Control .	163

Part I

Introduction

The dream to actively guide chemical reactions on a microscopic level can be traced back to sixties. In the first attempts to actively control chemical reactions the cw-laser has been used to excite special vibrational modes of the molecular system to break corresponding chemical bonds. Unfortunately, such a so-called *mode selective chemistry* which used a well defined frequency of the laser and its relatively high intensity failed due to the presence of strong intramolecular vibrational redistribution which leads to the fast flow of energy out of the selectively excited mode to other ones. A renaissance of the efforts to control a dynamics of small molecular systems came with the prospect of ultra-short laser pulses. Such radiation sources enable a coherent excitation of the system leading to wavepackets on the respective potential energy surfaces of molecular systems. Thus, control scenarios have been derived such as the so-called *pump-dump* scheme of Tannor and Rice [TKR86] and the method called *stimulated Raman scattering involving adiabatic passage* (STIRAP) [GRSB90] which use simple sequences of short pulses to achieve the population of some prescribed target states. They profit from the detailed knowledge of the potential energy surfaces and the energy spectra of the molecular system and have also been experimentally verified [BTS98] (see also [RZ00] and references therein).

A rather universal method to design laser fields for the control has been proposed by Rabitz and coworkers [PDR88, SWR88]. This so-called optimal control theory enables to compute control fields automatically utilizing propagations of their wavefunction or density matrix. The laser field designed by optimal control theory is usually denoted as the optimal laser pulse.

While utilizing simple pulse sequences similar to the pump-dump or STIRAP at early stages of the experimental developments, it was a breakthrough in experimental control to follow the proposal of [JR92a] to use feedback from the experimental measurement as an input for so-called evolutionary algorithms [BS]. The evolutionary algorithm provides the search for the optimal laser pulse parameters in order to achieve high yield in a given control task. In this way an experimental scheme could be designed with a modern pulse shaping device creating laser pulses according to the decision of a computer which analyzes the results of previous measurement.

Unfortunately, the application of the evolutionary algorithms in numerical simulations of control experiments becomes not feasible due to an enormous computational effort which would be connected with the multitude of corresponding numerical propagations of the molecular system. Rather, optimal control theory should be used to determine the theoretical optimal control pulses. These can be used e.g. as initial guesses in an evolutionary algorithm. A prerequisite for such an usage of the optimal control theory would be the

ability to estimate the possibility to generate the theoretical control pulse in experiment. To this end methods also have to be provided which enable a quantitative characterization of the complexity of the control pulse and the complexity of the control task [BKG01].

During the last 10 years the controllability of many types of molecules has been proven, both theoretically and experimentally. At the experimental field the pioneering work of the Gerber group has to be mentioned, for example in controlling the yield of photodissociation reactions [ABB⁺98, BBK⁺99] pushing even forward to the control in condensed phase [BDNG00]. In recent experiments the controlled systems range from atoms [BTS98] over polyatomic molecules [DFG⁺01] even to biological systems [HWC⁺].

In experiments on complex molecules, or in a condensed phase situation effects of relaxation and dissipation become unavoidable. There are only a few examples on theoretical discussions of control including dissipation [YOR99, Gev02] or including non-Markovian dissipation [KP97]. But the studied systems are few level ones only or the dissipation takes some special form. Therefore it becomes necessary to provide a formulation of the optimal control theory valid for more general types of dissipative systems. This formulation can be provided in the density matrix representation using the so-called quantum master equation. The density matrix formulation enables to derive optimal control equations in full analogy with the wavefunction description and enables to utilize previous experience with control of isolated systems [YOR99].

The exact formulation of the density matrix equation of motion for a small quantum system embedded in a solvent or another environment with a macroscopic number of degrees of freedom suggests that at any time the evolution of the system depends not only on the state of the system at that particular time, but also on its history (see e.g. [MK99]). This memory is the result of the removing of the environmental degrees of freedom from an explicit description in the equation of motion. The approximation neglecting the memory is usually termed the Markov approximation. This approximation is very useful in cases where the memory of the systems is much shorter than any typical time scale of the motion of the system. Considering short pulses with a duration on the 10 fs region which induce ultra-fast dynamics in the molecular system detailed description of the molecular dynamics becomes necessary. Particularly, the control pulses obtained from optimal control theory represent the whole trains of very short and intense pulses suggesting the necessity of the corresponding optimal control formulation which includes memory.

The main aim of this thesis is to investigate the optimal control of dissipative molecular dynamics. In line with what has been mentioned so far we concentrate on the following topics: (i) the clarification of the role of mem-

ory effects in the molecular dynamics; (ii) the formulation of the optimal control theory with Markovian dissipation for molecular systems with complicated electron-vibrational spectra; (iii) the methods to check the feasibility of an efficient experimental reconstruction of the optimal pulses obtained by optimal control theory; (iv) the simulation of more complicated experimental situation e.g. the disorder in the controlled systems; (iv) the formulation of the optimal control with non-Markovian dissipation.

The thesis are formally divided into five parts with Part I comprising this introduction. The main topic of the Part II is the description of memory effects in open quantum systems. It starts with an introductory chapter (Chapter 1) dealing with the description of the dynamics of open quantum systems. The density matrix theory is reviewed and the standard equation of motion for the density matrix of the system subject to the influence of a thermal bath is derived. Several types of approximations are used in the equation of motion and the Markov approximation is especially discussed. In Chapter 2 the non-Markovian dynamics (i.e. allowing for the memory effects) is studied for a reference model of a molecular systems. The memory effects are identified and discussed. Part III deals with the optimal control of electron transfer reactions. In Chapter 3 the optimal control theory is given in its most general form valid for the density matrix formulation of system dynamics. Thus, a formulation comprising both open as well as closed quantum systems is achieved. The theory is applied in Chapter 4 to the electron transfer reactions with and without dissipation and the controllability of electron transfer reactions is demonstrated and discussed. The questions of an experimental relevance of the optimal control theory, the complexity of the control task and some generalizations of the optimal control theory to describe some more complicated experimental situations are studied in the Chapter 5. The final part of the Chapter 5 is devoted to the formulation of the optimal control theory for the non-Markovian quantum master equation, which would make it possible to study the influence of the memory on the controllability of molecular systems. The conclusions and outlook from this work can be found in Part IV, many details of the presented theory have been shifted into the Appendices, which form Part V of this work.

Part II

Dynamics of Open Quantum Systems and Memory Effects

Chapter 1

Dynamics of Open Quantum Systems

The properties of a small open system embedded in a large one has been studied since the full recognition of the molecular theory. Pioneering works on Brownian motion conducted by Einstein and Langevin [Ein56, Lan08] started the development of the corresponding description of classical open microsystems resulting in two equivalent descriptions: master equations describing the evolution of the probability density of the microscopic system variables, such as Focker-Planck Equation [Ris89]; and the stochastic differential equations of the Langevin-type ruling the time evolution of the individual random trajectories of the microscopic system [vK92]. With the appearance of the Quantum Theory and with the remarkable progress in experimental techniques the description of the quantum situation became necessary. The success of the phenomenological Bloch equations [Abr61] in the description of the quantum relaxation processes and usability of the Pauli Equation for the description of the quantum transport phenomena [Pau28] initiated a rapid development of several types of the *generalized master equations* as a quantum analog to the Fokker-Planck equations [Nak58, Zwa60, Lin74]. Rather recently, the stochastic schemes reminding that of the Langevin-type equations, has been developed for open quantum systems [vK92, DCM92, GP92, PK98].

In modern experiments using e.g. an optical, infrared or NMR spectroscopies the information extracted from the system involves only some selected *degrees of freedom* (DOF). The dynamics of the rest of the system appears only in indirect manner through the dynamics of the observed DOF. For the further discussion we first remind some standard terminology (see e.g [MK99]). We denote the observed DOF as the *relevant system* and the rest of DOF as its *environment*. Sometimes the relevant system is denoted as *active system* or

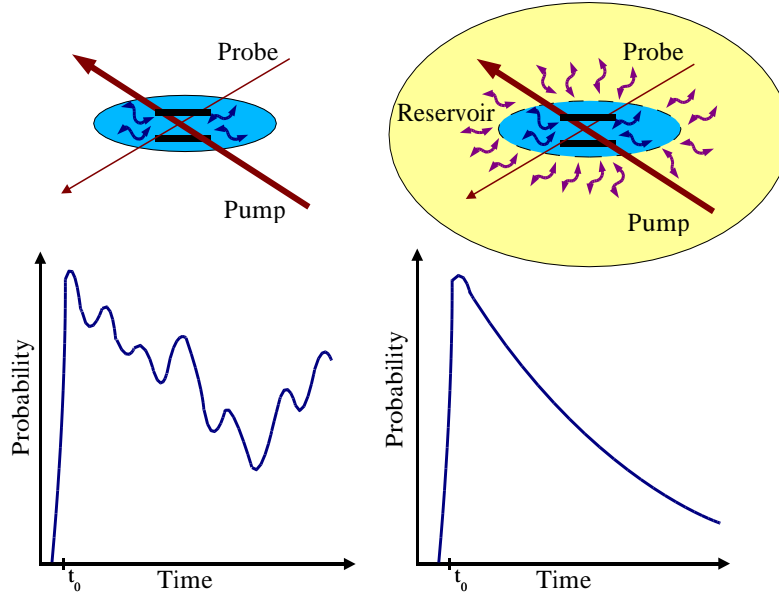


Figure 1.1: Pump-probe experiment and its results for a polyatomic molecule. The probabilities to find the system in its excited state are plotted as a function of time. The pump pulse is centered at time t_0 . Left, the molecule in gas phase where intra-molecular vibrations form an microscopic environment. Due to the finite dimension of the system it never reaches an equilibrium and the measurement shows some quasi periodic dynamics (recurrences) before optical recombination. Right, the same with the polyatomic molecule embedded in solution. The probe measurement shows just a relaxation due to the fast energy redistribution among an infinite number of reservoir DOF.

active set of DOF while we usually refer to the environment as to the *passive DOF*. Under this classification the environment can be both micro- and macroscopic depending on a given experimental situation. To name an example, for the electronic excitation dynamics of a polyatomic molecule in the gas-phase situation the intramolecular vibrational modes may act as a finite environment for the studied system of electronic levels which represents the relevant system. The characteristic feature of such a small microscopic environment is the presence of a coherence leading to the reversibility in its dynamics and appearance of the so-called recurrences. On the other hand, if the same molecule is situated on the surface of a solid body, it is embedded in a solid body or dissolved in a solution, the environment becomes macroscopic and the number of its DOF can be regarded as infinite. The interaction with such a macroscopic system

leads inevitably to the appearance of *irreversible dynamics*. The macroscopic environment is in such a case usually denoted as the *heat bath*, *thermodynamic bath* or *reservoir*. It is characterized by a small number of macroscopic variables or functions such as spectral density (see later detailed discussion). An example of the comparison between microscopic and macroscopic bath can be found e.g. in [MBS98]. On Fig. (1.1) a possible photo-induced dynamics of a system connected to such baths is depicted. Here we consider two electronic levels of a molecule. The system is excited from its ground-state by a strong pump pulse and then the population of the excited state is probed with certain delay with the second weak pulse. For an isolated molecule recurrences in the population of the excited state appear due to the system finite size, whereas the system connected to some macroscopic body shows just relaxation.

It may be advantageous to divide the system formally into the relevant part (denoted here with the letter S) and the reservoir (denoted as R) in such a way that the interaction between both parts can be regarded as weak. Approximative methods can then be recalled to treat the relevant system-reservoir interaction. To make our discussion more concrete we introduce the standard formal decomposition of the Hamiltonian of the compound system $S + R$. We denote the set of coordinates and their conjugated momenta corresponding to the system S as $s = \{s_j\}$ and similarly $Z = \{Z_j\}$ for the system R . The Hamiltonian of the system $S + R$ reads generally

$$H = H_S + H_R + H_{S-R}, \quad (1.1)$$

where H_S is the Hamiltonian of the relevant system, H_R the Hamiltonian of a reservoir and H_{S-R} represents the interaction between S and R . It is well-known, that due to the interaction term H_{S-R} , only the total wavefunction of the system exists and it is not possible to factorize it into the system part $\Phi_S(s)$ and a reservoir part $\chi_R(Z)$, so that $\Psi(s, Z) \neq \Phi_S(s)\chi_R(Z)$. To enable the quantum mechanical description of systems in interaction with the environment the concept of the *density operator* has been introduced by Landau and von Neumann shortly after the birth of the Quantum Theory. The density operator can describe not only the subsystems of a quantum system but also so-called *mixed state* which are represented by a set of its *pure states* weighted by their probabilities to be found in a given statistical mixture. The density matrix can be also assigned to the whole system $S + R$. It is the main task of the theory to find to correct time evolution of the density operator corresponding to the relevant system. The latter is obtained from the density operator of the whole system $S + R$ by means of the averaging over the DOF of the system R . Thus, the density operator of the relevant system S is usually called the *Reduced Density Operator* (RDO). In the state representation RDO is represented by

a matrix called *Reduced Density Matrix* (RDM). Sometimes the two terms are used as synonyms.

One of the most common approaches to the derivation of the equation of motion for RDO is to treat the interaction between systems S and R perturbatively and to derive the so-called Master equation. Depending on the problem one finds the second order approximations satisfactory [SM98] or may recall higher order [KP97], however the treatment of higher than 4th order becomes cumbersome. The Master equations provide the closed formulation of the equation of motion for the RDO and will be discussed in detail in section 1.1.

Trying to simulate larger relevant systems the scaling of the density matrix ($\sim N^2$, where N represents the number of involved quantum states) becomes a technical obstacle. As it was already mentioned a state of an open quantum system can be represented by a set of wavefunctions (in the similarity to the mixed state). The influence of the environment in this so-called Monte-Carlo Wavefunction Methods is described by stochastic action of certain dissipation operator. This operator provides e.g. for jumping between eigenstates which would not be possible in the isolated system. Between the jumps the wavefunction evolves freely according to some effective Schrödinger equation [DCM92, BKP99]. The corresponding density matrix can be obtained by averaging over the wavefunctions in the set. The important feature of the method is that in limit of the infinite number of wavefunctions in the set one reproduces the result obtained for the RDO within so-called Lindblad form of dissipation (explained shortly in section 1.3.3) so that the results are analog to those obtained from the master equation approach. Although we have to treat many wavefunctions instead of one density matrix the scaling of the wavefunction ($\sim N$) together with the suitability of such algorithm for parallel computers makes this approach an attractive alternative to QME. Recently, the method has been generalized also for other forms of dissipation than the Lindblad one [GN99a, BKP99].

Another approach enabling to find the time evolution of the reduced density matrix is based on the so-called *path integral* formulation of the quantum dynamics developed by R. P. Feynman [Fey48, FH65, Sch81, Mak98]. In the path-integral approach a transition amplitude or propagator is expressed as a sum of amplitudes along all paths that connect the initial and final points. Each of these amplitudes is a complex number with phase equal to the classical action along the path, measured in units of Planck's constant. This formulation goes in many aspects beyond the Master equation approach, since for a special case of the reservoir built up from the infinite number of harmonic oscillators it is possible to derive an exact, non-perturbative expression for the RDM. The

influence of the reservoir R on the relevant system S is incorporated via the so-called Feynman-Veron influence functional [FV63]. Despite this clear advantage over the Master equation approach in its non-perturbative incorporation of the environment, in the practical applications the path-integral approach is limited to the relevant systems with few levels only [Mak98].

Often, the reservoir DOF are of such a type, that they can be described in a classical manner. The dynamics of the relevant quantum system is computed with an additional potential resulting from presence of classical DOF. The DOF of the reservoir feel, on the other hand, the quantum mechanically averaged force of the relevant system [BHM97, Her94, SG96]. This approach is a mixed quantum-classical version of a more general approach also called *Time-Dependent Self-Consistent Field* (TDSCF) method [BJWM00]. Today, the TDSCF method enables to treat numerically systems consisting of about 10 atoms. Such calculations, if accurate enough, can play a role of the reference calculations for the approximative calculations which start with the system-”micro”-bath separation (e.g. electronic states versus vibrational modes). The most well-know system is here the *pyrazine* molecule (see [BJWM00, KWPD94]).

1.1 Density Matrix Theory

The density matrix theory provides a general formulation of the quantum dynamics of molecular system and enables a unified treatment of the quantum systems in interaction with a reservoir and isolated systems in mixed or pure state. Having once formulated the problem in the most general i.e. density matrix formulation, its subsequent reformulation for the special case of the isolated system is straightforward. The approach leading to the formulation of the concrete equation of motion for the RDO of a molecular system is explained in detail in the Appendices A, B and C. Here, we only review the important points of the derivation to present the logical construction of the theory we use throughout this work.

We regard the system $S + R$ as isolated, so that it can be described by a density operator

$$\hat{W}(t) = \sum_n w_n |\psi_n(t)\rangle \langle \psi_n(t)| \quad (1.2)$$

and its time evolution follows the so-called *Liouville-von Neumann equation*

$$\frac{\partial}{\partial t} \hat{W}(t) = -\frac{i}{\hbar} [H, \hat{W}(t)]_- . \quad (1.3)$$

Throughout this work we will often use the so-called *superoperator* notation, so that we define e.g. the *Liouvillian* acting on an operator as a commutator

with Hamiltonian, $\mathcal{L}\dots = 1/\hbar[H, \dots]_-$. With this definition one can write (1.3) as

$$\frac{\partial}{\partial t}\hat{W}(t) = -i\mathcal{L}\hat{W}(t). \quad (1.4)$$

As it is well-known the operator comprising the information about the state of the relevant system S only, regardless of the state of the system R can be obtained from \hat{W} by summing over some complete basis $\{|\alpha\rangle\}$ defined in the state space of R . This leads to the definition of the RDO

$$\hat{\rho}(t) = \sum_{\alpha} \langle \alpha | \hat{W}(t) | \alpha \rangle = tr_R \{ \hat{W}(t) \}. \quad (1.5)$$

The RDO is the central quantity of the following chapters. It involves the complete quantum mechanical information available about the relevant system S . To be able to apply the density matrix theory one needs to formulate the equation of motion for RDO.

A systematic derivation of the equation motion of the RDO is enabled by so-called *projection operator method*. We define an operator \mathcal{P} acting on the density operators (so-called projection *superoperator*), performing the summation over all reservoir (and/or other experimentally irrelevant) DOF

$$\mathcal{P}\hat{\rho}(t) = tr_R \{ \hat{\rho}(t) \} \hat{R}, \quad (1.6)$$

where \hat{R} is so-far arbitrary operator acting exclusively on the state space of the system R with the trace equal to 1. Using the projector operators it is possible to derive general expressions for the time evolution of the RDO without having to concentrate on any special form of the Hamiltonian (1.1). There are two formally equivalent ways how to achieve this goal resulting in so-called *Convolutionless Generalized Master Equation* (CL-GME) [CS79, ST77] taking a general form

$$\frac{\partial}{\partial t}\hat{\rho}(t) = \hat{\mathcal{I}}_{CL}(t, t_0; W(t_0)) + \hat{\mathcal{K}}_{CL}(t, t_0)\hat{\rho}(t) \quad (1.7)$$

and so-called *Nakajima-Zwanzig Equation* (NZE) [Nak58, Zwa60] with the general form

$$\begin{aligned} \frac{\partial}{\partial t}\hat{\rho}(t) &= \hat{\mathcal{I}}_{NZ}(t, t_0; \hat{W}(t_0)) - i\mathcal{L}_{NZ}\hat{\rho}(t) \\ &+ \int_{t_0}^t \mathcal{M}_{NZ}(t, t_0; \tau)\hat{\rho}(t - \tau). \end{aligned} \quad (1.8)$$

Here, in both Equations (1.7) and (1.8) the first terms on the right-hand side are called *initial correlation terms*. In the CL-GME the whole influence of the

reservoir DOF and the free dynamics is comprised to the operator $\hat{K}_{CL}(t, t_0)$ whereas for the NZE we can define an effective Liouvillian \mathcal{L}_{NZ} involving the free dynamics of the system and some meanfield term, and a dissipative term in form of a convolution of $\hat{\rho}(t)$ with the so-called memory kernel $\mathcal{M}_{NZ}(t, t_0; \tau)$. Despite their formal equivalence, there is one principal difference in both formulations. The convolutionless generalized Master equation is local in time i.e. the time evolution of the RDO in a given time t depends just on the state of the system in this given time t , while in the Nakajima-Zwanzig formulation, the time evolution of the RDO in a given time t is influenced by the contributions from the earlier times $t - \tau$ (with $\tau \geq 0$) of the system evolution.

The solutions of CL-GME and NZE represent still the same degree of difficulty as the solution of the original equation of motion for the density operator of the whole system $S + R$ since they still involve all DOF of $S + R$ explicitly. Thus, both CL-GME equation and NZE serve just as a starting point for the perturbation theory which enables the derivation of some treatable equations of motion for the RDO. To obtain them we can apply the perturbation theory with respect to the system-reservoir coupling represented by H_{S-R} . Provided H_{S-R} can be regarded as a small parameter, one neglects all contributions to the RDO time evolution of higher orders in H_{S-R} . It might be possible that the first non-trivial (second order) contribution is sufficient to account for the experimentally observed effects (see e.g. [SM98]). But in general it depends on the choice of the systems S and R and must always be thoroughly checked. Applying the second order perturbation theory, the approaches via CL-GME and NZE cease to be equivalent. The comparison of the expressions for both approaches in lower orders can be found e.g. in [BKP99]. Particularly the CL-GME in the second order approximation has the form of the second order NZE with additional Markov approximation applied.

In the rest of this chapter we will shortly review all the necessary steps leading to the so-called Quantum Master Equation (QME), which represents a particular second order perturbation theory version of the NZE. QME will be a starting point for our treatment of the effects of the relevant system interaction with a reservoir. Particularly we will be interested in memory effects.

1.2 Quantum Master Equation

In order to proceed from the exact NZE which solution is not feasible in any non-trivial case to an equation of motion for the RDO which enables such a solution we have to assume some special properties of the Hamiltonian (1.1). In most of the practical cases the assumption of H_{S-R} to be a small parameter

is justified. Thus, perturbation theory can be applied to obtain approximative equations of motion for RDO. Further we assume a special factorization *ansatz* on the form of the system-reservoir interaction Hamiltonian H_{S-R} . We will assume that it is of the form

$$H_{S-R} = \sum_n K_n(s) \Phi_n(Z), \quad (1.9)$$

where $K_n(s)$ and $\Phi_n(Z)$ are operators acting exclusively on the relevant system DOF and the reservoir DOF, respectively. Since no further assumptions about the functions $K_n(s)$ and $\Phi_n(Z)$ are made the Hamiltonian (1.9) can account for most cases of the practical importance [MK99].

Applying the second order approximation in the system-reservoir interaction H_{S-R} and the *ansatz* (1.9) we arrive at so-called *Quantum Master Equation* (QME) derived in detail in Appendix B

$$\begin{aligned} \frac{\partial}{\partial t} \hat{\rho}(t) = & -\frac{i}{\hbar} [H_S + \sum_m \langle \Phi_m \rangle K_m, \hat{\rho}]_- \\ & - \frac{1}{\hbar^2} \sum_{mn} \int_0^{t-t_0} d\tau \left(C_{mn}(\tau) [K_m, U_S(\tau) K_n \hat{\rho}(t-\tau) U_S^\dagger(\tau)]_- \right. \\ & \left. - C_{mn}^*(\tau) [K_m, U_S(\tau) \hat{\rho}(t-\tau) K_n U_S^\dagger(\tau)]_- \right). \end{aligned} \quad (1.10)$$

Here we transformed the expression (B.6) into the Schrödinger representation. The dissipative part of (1.10) will be denoted $\hat{\mathcal{D}}(t, t_0; \hat{\rho})$ so that we can write in similarity to Eq. (1.8)

$$\frac{\partial}{\partial t} \hat{\rho}(t) = -i\mathcal{L}_{eff} \hat{\rho}(t) + \hat{\mathcal{D}}(t, t_0; \hat{\rho}), \quad (1.11)$$

where the definitions of $\hat{\mathcal{D}}(t, t_0; \hat{\rho})$ and \mathcal{L}_{eff} are obvious from (1.10). To emphasize the integral structure of the dissipative term we define so-called *memory kernel* \mathcal{M} and write

$$\hat{\mathcal{D}}(t, t_0, \hat{\rho}) = \int_0^{t-t_0} d\tau \mathcal{M}(t, t_0; \tau) \hat{\rho}(t-\tau). \quad (1.12)$$

In Eq. (1.10) one immediately notices the presence of the operator H_S (in the first term on the right hand side and in the evolution operators $U_S(t)$) and of the operator K_n of the system part of (1.9). The reservoir operators H_R and Φ_n appear only in an averaged manner via the first contribution on the right

hand side and via so-called *correlation function* $C_{mn}(t)$ defined in Appendix B as

$$C_{mn}(t) = \langle \Phi_m(t) \Phi_n(0) \rangle_R - \langle \Phi_m \rangle_R \langle \Phi_n \rangle. \quad (1.13)$$

Here we used the abbreviation $\langle \dots \rangle = \text{tr}_R \{ \dots \}$. The correlation function comprises the whole information about the reservoir necessary to describe the time evolution of the RDO within our second order treatment of the system-reservoir interaction.

The RDO $\hat{\rho}$ appears with the retarded argument $t - \tau$ in the QME, so that the history of the system also determines its time development. Such a situation is commonly call the *non-Markovian*, in contrast to the *Markovian* situation when the future of the system depends on its current state only. The Eq. (1.10) is correspondingly called *non-Markovian* QME. The extension to which the history of the system plays a role in its time development is determined by the correlation function $C_{mn}(t)$, mainly by so-called *correlation time* t_c which characterizes the time scale on which the correlation function decays. We will often refer to the correlation time as to a *memory time* t_{mem} . The length of the correlation time also determines whether we can apply approximations to simplify the treatment of Eq. (1.10).

In order to be able to apply the QME on a particular molecular system we have to be yet more specific about the reservoir. In many cases it becomes possible to perform a normal mode analysis among the DOF of the reservoir. Assuming it was performed one can write H_R as a sum of independent harmonic oscillators. Concerning the system-reservoir interaction term we perform a formal Taylor expansion of H_{S-R} with respect to the reservoir coordinates $Z = \{Z_\xi\}$ and we take in account only the first order terms for the interaction Hamiltonian. It yields

$$H_{S-R} = K(s) \sum_{\xi} c_{\xi} Z_{\xi} \quad (1.14)$$

for the interaction Hamiltonian, where c_{ξ} is the system-reservoir coupling constant. Within this approximation and assuming the system is in thermal equilibrium we are able to write down a new expression for the Fourier transformed correlation function (see Appendix C)

$$C(\omega) = 2\pi\hbar^2\omega^2[1 + n(\omega)][J(\omega) - J(-\omega)]. \quad (1.15)$$

Here, $n(\omega)$ is Bose-Einstein distribution so that the temperature dependency of the system-reservoir interaction is now explicitly taken in account. The function $J(\omega)$ is the so-called *spectral density* which fully describes the reservoir for our purpose. It is defined as

$$J(\omega) = \sum_{\xi} g_{\xi}^2 \delta(\omega - \omega_{\xi}), \quad (1.16)$$

where g_ξ is the dimensionless coupling constant (C.13) of the reservoir mode with the frequency ω_ξ to the relevant system. The interpretation of this function is possible by comparing it to the well-know definition of the density of states of the reservoir

$$N(\omega) = \sum_{\xi} \delta(\omega - \omega_\xi). \quad (1.17)$$

Taking in account the definition of g_ξ according to (C.13) we see that $J(\omega)$ can be understood as the density of states weighted by the coupling of the particular states to the system S . The form of $J(\omega)$ decides which states of the system R couple to the system S and how. Usually, one prescribes some continuous function for $J(\omega)$. In this work we mainly use the form

$$\omega^2 J(\omega) = \Theta(\omega) j_0 \omega^p e^{-\omega/\omega_c}, \quad (1.18)$$

which is characterized by a cut-off frequency ω_c and an exponential decay into large frequencies. We use $p = 1$ in our latter applications.

In our equation of motion (1.10) the correlation function $C(\omega)$ appears in its time domain form $C(t)$. Using $J(\omega)$, Eq. (1.18) the cut-off frequency is one of the main factors determining the time dependence of $C(t)$. In our case with $p = 1$ the $C(t)$ decays with the time constant $t_c \approx 1/\omega_{cutt-off}$. The time t_c is the previously mentioned correlation time.

By prescribing the function $J(\omega)$ we completely described the reservoir interacting with our model system. But even if we define a convenient system Hamiltonian H_S and the system part of the interaction Hamiltonian $K(s)$, it would still be quite difficult to solve the equation (1.10) because of its integral nature. In the following section we will introduce some standard approximations which yield an ordinary differential equation for RDO.

To deal practically with QME it is convenient to convert it into the state representation. We consider the Hamiltonian H_S and the eigenvalue problem

$$H_S |\psi_\alpha\rangle = E_\alpha |\psi_\alpha\rangle, \quad (1.19)$$

we define the RDM as

$$\rho_{ab}(t) = \langle \phi_a | \hat{\rho}(t) | \phi_b \rangle \quad (1.20)$$

and similarly the matrix elements of all other necessary quantities. Introducing tetradic matrix

$$M_{ab,cd}(t) = \frac{1}{\hbar^2} \sum_{mn} C_{mn}(t) K_{ab}^{(m)} K_{cd}^{(n)}, \quad (1.21)$$

one may write the non-Markovian dissipative part of the QME as

$$\left(\frac{\partial}{\partial t} \rho_{ab} \right)_{diss} = - \sum_{cd} \int_0^{t-t_0} d\tau \left(M_{cd,db}(-\tau) e^{i\omega_{da}\tau} \rho_{ac}(t-\tau) \right)$$

$$\begin{aligned}
& -M_{ac,cd}(\tau)e^{i\omega_{bc}\tau}\rho_{db}(t-\tau) \\
& - [M_{db,ac}(-\tau)e^{i\omega_{bc}\tau} + M_{db,ac}(\tau)e^{i\omega_{da}\tau}]\rho_{cd}(t-\tau).
\end{aligned} \tag{1.22}$$

Besides the convenience of the numerical dealing with Eq. (1.22) one can also easily prove using this representation that the total probability is conserved here $\text{tr}_S\{\hat{\rho}\} = 1$ and the relation

$$\lim_{t \rightarrow \infty} \rho_{ab} = \delta_{ab} \frac{1}{\mathcal{Z}} e^{-E_a/k_B T}, \tag{1.23}$$

with $\mathcal{Z} = \sum_a e^{-E_a/k_B T}$ is fulfilled. This means that the asymptotic solution of the QME is the canonical thermal equilibrium with the reservoir.

1.3 Markovian versus Non-Markovian Quantum Master Equation

In the previous sections we have derived a closed equation of motion for the RDO correct in the second order perturbation approximation in system-bath interaction (1.10). We have seen in section 1.2 that the right hand side of the equation (1.10) depends on the RDO at earlier times of its propagation (non-Markovian case). The system inevitably *remembers* its previous evolution. To which extend these possible *memory effects* become noticeable the strength of the system-bath coupling and the concrete form of the correlation function decide. We refer to the memory effects often as to the *retardation effects* in the analogy with classical electrodynamics where the electromagnetic potentials exhibit retarded (delayed) dependency on the charge and current density due to the finite speed the electromagnetic signal travels between two points in space. So the charge- and current-densities act on itself in a retarded manner in an analogy to (1.10).

Whenever it is possible to neglect the retardation i.e. the memory time $t_{mem} \rightarrow 0$ (or in electromagnetism if one can regard $c \rightarrow \infty$) the treatment of the equation becomes much simpler. Usually one refers to the neglect of the memory as to the Markovian approximation. In the theory of open quantum systems such approximations found wide application. It is the main aim of the next chapter of this work to study retardation effects and to find differences between retarded and non-retarded dynamics. To this end we need to derive and solve also the Markovian form of QME.

1.3.1 Markov Approximation

If the coupling to the reservoir is not too strong, so that the change induced to the relevant system during the interval $\langle 0; t_{mem} \rangle$ by the reservoir is small one may invoke the approximation

$$\hat{\rho}(t - \tau) \approx \hat{\rho}(t). \quad (1.24)$$

Obviously this is too rough, since we also assume the change induced by the Hamiltonian H_S to be negligible. If it is not the case it is more appropriate to make the above approximation in the interaction picture as following

$$\begin{aligned} \hat{\rho}(t - \tau) &= U_S(t - \tau - t_0) \rho^{(I)}(t - \tau) U_S^\dagger(t - \tau - t_0) \\ &\approx U_S(-\tau) U_S(t - t_0) \hat{\rho}^{(I)}(t) U_S^\dagger(t - t_0) U_S^\dagger(-\tau) = U_S^\dagger(\tau) \hat{\rho}(t) U_S(\tau). \end{aligned} \quad (1.25)$$

Thus, the evolution of $\hat{\rho}(t)$ induced by the system Hamiltonian H_S is still exactly incorporated, while the influence of the reservoir and external fields during the interval $\langle 0; t_{mem} \rangle$ is neglected.

Utilizing this approximation the dissipative part of the QME becomes

$$\begin{aligned} \left(\frac{\partial}{\partial t} \hat{\rho} \right)_{diss} &= -\frac{1}{\hbar^2} \sum_{mn} \int_0^\infty d\tau \left\{ C_{mn}(\tau) \left[K_m, K_n^{(I)}(-\tau) \hat{\rho}(t) \right]_- \right. \\ &\quad \left. - C_{mn}^*(\tau) \left[K_m, \hat{\rho}(t) K_n^{(I)}(-\tau) \right]_- \right\}, \end{aligned} \quad (1.26)$$

where $K_n^{(I)}(-\tau) = U_S(\tau) K_n U_S^\dagger(\tau)$. Because the $C(t)$ dies out for $t > t_{mem}$ we could prolongate the upper interval of the integral to the infinity. Introducing the operator

$$\Lambda_m = \sum_n \int_0^\infty d\tau C_{mn}(\tau) K_n^{(I)}(-\tau) \quad (1.27)$$

and the non-Hermitian effective Hamiltonian

$$H_S^{eff} = H_S + \sum_m \langle \Phi_m \rangle K_m - \frac{i}{\hbar} \sum_m K_m \Lambda_m \quad (1.28)$$

we arrive at a very compact notation for the QME in Markov approximation

$$\begin{aligned} \frac{\partial}{\partial t} \hat{\rho}(t) &= -\frac{i}{\hbar} \left(H_S^{eff} \hat{\rho}(t) - \hat{\rho}(t) H_S^{eff\dagger} \right) \\ &\quad + \frac{1}{\hbar^2} \sum_m (K_m \hat{\rho}(t) \Lambda_m^\dagger + \Lambda_m \hat{\rho}(t) K_m). \end{aligned} \quad (1.29)$$

Throughout the next chapters two reference Markovian cases will be used. The Markov approximation of the dissipative part of (1.10) we get

$$\begin{aligned}\hat{D}(t, t_0; \hat{\rho}) &\approx \mathcal{R}(t, t_0; \mathbf{E})\hat{\rho}(t) \\ &\equiv \int_0^{t-t_0} d\tau \mathcal{M}(t, t-\tau; \mathbf{E}) \mathcal{U}_S^+(t, t-\tau) \hat{\rho}(t) .\end{aligned}\quad (1.30)$$

The definition of the dissipative superoperator \mathcal{R} is obvious. It realizes time-local but time-dependent dissipation which, additionally, is influenced by the presence of the external-field pulse. In the case where $t - t_0 \gg t_{\text{mem}}$ we can replace the upper limit of the τ -integral by ∞ . If the external field dependence is neglected the dissipative superoperator \mathcal{R}_0 (its matrix elements) becomes identical with the dissipative part of (1.29) which will be called the *standard Markovian QME* here

$$\frac{\partial}{\partial t} \hat{\rho}(t) = -i\mathcal{L}_{eff}(t)\hat{\rho}(t) - \mathcal{R}_0\hat{\rho}(t). \quad (1.31)$$

In the state representation one notices the relation between the Redfield tensor explained in the next section (1.35) and the superoperator R_0 being

$$R_{ab,cd} = Re\{(\mathcal{R}_0)_{ab,cd}\}, \quad (1.32)$$

where $(\mathcal{R}_0)_{ab,cd}$ is a the matrix representation of \mathcal{R}_0 .

We note that the dissipative superoperator \mathcal{R} remains time-dependent. It will be demonstrated below that the use of $\mathcal{R}(t, t_{\text{field}}; \mathbf{E} = 0)$ for times $t - t_{\text{field}}$ in the range of t_{mem} can give a reasonably good reproduction of the correct solution of the non-Markovian Eq. (2.16).

1.3.2 Multi-Level Redfield Equation

Working again in the state representation, we can proceed analogously to the section (1.2) and obtain the Markov version of Eq. (1.22). We carry out the Markov approximation and shift the upper bound of the integral into infinity, what yields

$$\begin{aligned}\left(\frac{\partial}{\partial t} \rho_{ab}\right)_{diss.} &= \sum_{cd} \int_0^\infty d\tau (M_{cd,db}(-\tau) e^{i\omega_{dc}\tau} \rho_{ac}(t) + M_{ac,cd}(\tau) e^{i\omega_{dc}\tau} \rho_{db}(t) \\ &\quad - [M_{db,ac}(-\tau) e^{i\omega_{db}\tau} + M_{db,ac}(\tau) e^{i\omega_{ca}\tau}] \rho_{cd}(t)).\end{aligned}\quad (1.33)$$

The dissipative part of the QME, or the operator acting on RDM here are complex quantities. Their real parts are responsible for the irreversible dynamics

of the density matrix. On the other hand the imaginary part only introduces some shift of transitional frequencies, what has often no qualitatively new contribution to the dynamics of the system. Therefore, one may get rid of the imaginary part and work with just the real one. Thus, we define the so-called *damping matrix*

$$\Gamma_{ab,cd}(\omega) = \text{Re} \int_0^\infty d\tau e^{i\omega\tau} M_{ab,cd}(\tau) \quad (1.34)$$

and the *relaxation matrix*

$$\begin{aligned} R_{ab,cd} = & \delta_{ac} \sum_e \Gamma_{be,ed}(\omega_{de}) + \delta_{db} \sum_e \Gamma_{ae,ec}(\omega_{ce}) \\ & - \Gamma_{ca,bd}(\omega_{db}) - \Gamma_{db,ac}(\omega_{ca}). \end{aligned} \quad (1.35)$$

The relaxation matrix (1.35) is usually called the *Redfield tensor* after [Red65]. Further details on Redfield tensor and the QME can be found in various textbooks like [MK99, Blu89].

To distinguish the standard Markovian QME from the QME with the dissipative part according to Eq. (1.30) the latter will be named the Markovian QME with *time-dependent Redfield-tensor*. A detailed comparison is given below of all three versions of the QME, i.e. of the standard Markovian QME, the non-Markovian QME, and of the Markovian QME with time-dependent Redfield-tensor.

1.3.3 Critical View on the Quantum Master Equation

Since the second order QME is only an approximative equation of motion for the RDO the validity of the general properties the time dependent RDO is expected to have has to be checked. Previously in section 1.2 we have mentioned that the asymptotic solution of the QME is the canonical thermal equilibrium density operator (1.23). Other important relation for $\hat{\rho}(t)$ which has to be fulfilled is the conservation of the trace $\text{tr}\{\hat{\rho}(t)\} = 1$. It can be easily show [MK99] that it is fulfilled by both Markovian and non-Markovian QME.

The real problem is encountered if considering the positivity of the RDO. Since in the state representation the diagonal elements of the density matrix $\rho_{aa}(t)$ represent probabilities they have to be non-negative. Unfortunately, it is not in general true for the QME that the $\rho_{aa}(t) \geq 0$. In seventies Lindblad [Lin74] derived the general form of the dissipation tensor entering equation of motion for density matrix which ensures the positivity of the probabilities in RDO. The so-called Lindblad form of the dissipation can be also derived from our non-Markovian QME under the assumption of the ultra-short correlation

times, so that we can write

$$C_{mn}(t) \approx C_{mn}\delta(t). \quad (1.36)$$

Provided the coefficients C_{mn} are real and diagonal the dissipative part of the Eq. (1.10) takes the form

$$\left(\frac{\partial}{\partial t}\hat{\rho}\right)_{diss.} = -\frac{1}{\hbar}\sum_m C_{mn} \{[K_m^2, \hat{\rho}]_+ - 2K_m\hat{\rho}K_m\} \quad (1.37)$$

which is the form derived by Linblad.

As this is the only known form of the QME generally preserving positivity of the RDO its breakdown has to be anticipated for finite memory times. The problem of the positivity of the density matrix within QME has lead to many studies trying to avoid the problem by different means [SSO92, GN99b]. In this work we assume that the break down of the positivity can be regarded as the breakdown of the second-order perturbation theory. Namely the factor $t|H_{S-R}|^2$ has to be small in order the second order approximation to be valid. Obviously, if the system-bath coupling (or the time t , or both) becomes too large QME is no more correct what can lead to different failures with respect to the general properties expected from RDO. To ensure the positivity we always use a reasonably weak coupling and short times in the following studies.

Chapter 2

Memory Effects and Ultrafast Optical State Preparation

The theoretical description of dissipative quantum dynamics using the RDO and leading to the formulation of QME has been particularly useful in the description of the relaxation phenomena in molecular systems. It enabled e.g. the quantum mechanical foundation of chemical reaction dynamics. The research done up to the eighties in optical experiments on electronic transitions and vibrational motion could be characterized by a clear separation of the time scales. To prepare a molecule in the excited state, picosecond or even nanosecond laser pulses have been used, whose durations are clearly much longer than the typical time nuclear DOF need to reach the equilibrium. This particular aspect enabled to justify coarse-graining approximations in the equation of motion for the relevant system and to disregard of the possible memory effects.

Meanwhile, optical pulses with a duration of less than 10fs are available what enables e.g. to detect the coherent nuclear dynamics [Zew94, MW95, Zew96, Sun98] and may possibly lead to the detection of the non-Markovian effects. This experimental achievements initiated a renaissance of dissipative quantum dynamics, putting emphasis on the description of ultrafast nuclear dynamics in polyatomic systems and systems in condensed phase.

Propagating the RDO on a time-scale of some tens of femtoseconds any time coarse-graining is forbidden and dissipative quantum dynamics asks for a proper incorporation of retardation effects between the active system and the environment (reservoir). The need for such a more sophisticated description becomes obvious if one imagines an experiment where (i) the nuclear oscillation period of the molecules lies in the range of 50fs up to 100fs , where (ii) the molecule is dissolved in a solvent with a correlation time again of about 100fs , and where (iii) the molecule is excited by a laser pulse with duration of some

10 fs (in similarity to experiments done, for example, at iodine in a solvent [SJF93] or in rare gas clusters [PLZ92]). Trying to simulate such an experiment one has to account for the interference of all three mentioned characteristic time-scales. It is the main aim of this chapter to study such an interference of (a) vibrational dynamics, (b) retarded coupling to the environment, and (c) ultrafast laser-pulse excitation. In the present work, emphasis will be put on the memory effects.

The main obstacle in the investigation of the non-Markovian effects lies in the difficulty of the solution of the non-Markovian QME. Its time non-local nature does not allow for the usage of a standard Runge-Kutta like numerical method to integrate Eq. (1.10). Also, methods developed to solve integro-differential equations such as Fourier-Laplace transform etc. are not general enough to provide a solution of the non-Markovian QME for all necessary cases. In the practical calculations throughout this thesis we use the so-called *Laguerre Polynomial Method* developed in [MBS98, MM00, MM01] and explained in detail in Appendix F. This method is suitable for solution of the non-Markovian QME in time domain if the external field is handled perturbatively, because it cannot treat the term $E(t)\hat{\rho}(t)$ in the equation of motion. Similar restrictions apply also the use of the Fourier transform method. The complete inclusion of the external fields within QME becomes possible with the method of artificial bath modes developed in [MT99]. Instead of the perturbative treatment of the external field we are faced here with the approximative treatment of the reservoir correlation function. The method is explained in Appendix E. It will be used to generalize the main topic of the Part III of this thesis for the case of non-Markovian dissipation.

In the following chapters, we will first try to get some analytical insight into how the memory effects and the initial correlation effects present themselves in the molecular dynamics and how the solution of the non-Markovian QME can be found. In section 2.2 the Fourier transform method to solve the non-Markovian QME is presented and used to analyze the memory effects in optical absorption coefficient. In section 2.3 we concentrate on the effects of initial correlation in case of the excitation of the relevant system by a short pulse of laser field. We derive a somewhat different form of QME which enable us to overcome the necessity to include the initial correlation term explicitly in QME. Another analytical result on QME can be obtained in the limit of very long correlation times. For such a case we solve in section 2.4 the problem of non-Markovian dynamics of the wavepacket on a harmonic PES. This result gives us some important hints for the identification of memory effects in time domain. In section 2.5 we present detailed calculation of the non-Markovian dynamics for a molecular system excited by a short laser pulse. Finally, a

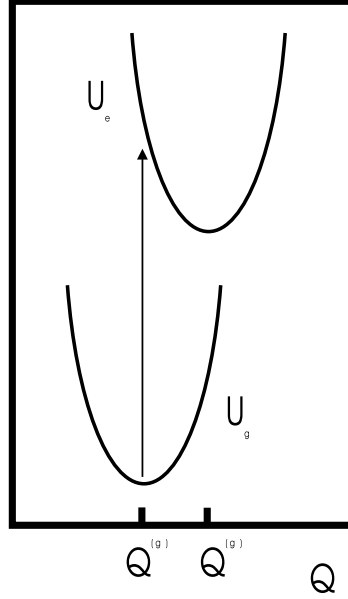


Figure 2.1: Scheme of the minimal model of two PES connected by an optical transition.

study concentrating on the non-Markovian effects in case of the non-linear system-bath coupling is presented in section 2.6.

2.1 The Molecular System

According to the introduction of active DOF our discussion will start with a respective separation of the complete Hamiltonian (1.1) which is standard in dissipative quantum dynamics and was introduced in Chapter 1.

The first part of the Hamiltonian describes the molecular system of interest (active system, Hamiltonian H_{mol}) together with its coupling to an external radiation field (Hamiltonian $H_{\text{field}}(t)$) $H_S(t) = H_{\text{mol}} + H_{\text{field}}(t)$. The part H_{S-R} accounts for the coupling of the active system to the reservoir, whereas the reservoir is described by H_R . The molecular contribution to H_S will be given by the expression

$$H_{\text{mol}} = \sum_a H_a(Q) |\varphi_a\rangle \langle \varphi_a|. \quad (2.1)$$

It corresponds to an expansion with respect to the adiabatic electronic states φ_a (with electronic quantum number a) and the neglect of any non-adiabatic coupling. The vibrational Hamiltonian $H_a = T_{\text{vib}} + U_a(Q)$ contains the kinetic

energy operator T_{vib} and the respective PES U_a defined with respect to the set $Q = \{Q_j\}$ of active vibrational DOF. The *eigenfunctions* of the various H_a will be denoted as $\chi_{aM}(Q)$, where M stands for the set of related vibrational quantum numbers.

The molecular Hamiltonian is general enough to carry out different considerations. Performing concrete numerical calculations it will be further reduced to the minimal model used in [SM97, SM98] for the simulation of ultrafast optical data obtained for a dissolved dye molecule. In particular, this model will serve as a reference system to study an interplay of the external field excitation of the molecule and the non-Markovian relaxation of the vibrational DOF in the excited electronic state. The minimal model consists of two electronic levels modulated by a single effective vibrational coordinate $Q = C^\dagger + C$, where C^\dagger and C are the vibrational quanta creation and annihilation operators, respectively. In this case the $H_a(Q)$ are vibrational Hamiltonian operators corresponding to the ground ($a = g$) as well as to the excited electronic states ($a = e$) and incorporating harmonic oscillator PES

$$U_a(Q) = U_a^{(0)} + \frac{\hbar\omega_{\text{vib}}}{4}(Q - Q_a)^2. \quad (2.2)$$

For the coupling to the radiation field we have in mind a description within the electric dipole approximation

$$H_{\text{field}}(t) = -\mathbf{E}(t)\hat{\mu}. \quad (2.3)$$

Here $\mathbf{E}(t)$ is the electric field-strength of a laser pulse (or a sequence of pulses). It reads in detail

$$\mathbf{E}(t) = \mathbf{n}A\mathcal{E}(t)e^{-i\omega_0 t} + \text{c.c.}, \quad (2.4)$$

where \mathbf{n} is the polarization unit vector, A the complex field amplitude, $\mathcal{E}(t)$ the normalized pulse envelope and ω_0 the carrier frequency. Furthermore, we introduced in Eq. (2.3) the molecular dipole operator

$$\hat{\mu} = \sum_{a,b} (1 - \delta_{a,b}) \mathbf{d}_{ab} |\varphi_a\rangle \langle \varphi_b|, \quad (2.5)$$

which only contains off-diagonal contributions connecting different electronic states. \mathbf{d}_{ab} is the related transition matrix element. In the concrete computations it will only connect the ground state φ_g with a single excited state φ_e .

The dissipative part of the QME to study non-Markovian effects in this model is taken in the form explained in section 1.2. The operator K in (1.9) will be taken to be equal to the dimensionless coordinate Q , so that the system-bath coupling takes a bilinear form.

2.2 Memory Effects in the Frequency Domain

Inspecting the general form of the QME, Eq. (1.10) the idea arises to use the Fourier–Laplace transformation method for the solution of the time non-local problem. Under certain additional conditions and for a few level systems one can obtain results by analytical calculations which are applicable, for example, to the computation of pump–probe spectra (see [GR92, LV91, VVL91, BMP94, GBF98]).

Omitting any field dependence ($H_S \equiv H_{mol}$), providing that the mean-field term, (see Eq. (1.10)) does not exist and setting $t_0 = 0$, one easily constructs the Fourier–Laplace transformed version of Eq. (1.10). Its solution reads

$$\hat{\rho}(\omega) = \{i\omega - i\mathcal{L}_{mol} - \mathcal{M}(\omega)\}^{-1}(\hat{I}(\omega) - \hat{\rho}(t=0)) , \quad (2.6)$$

where \mathcal{L}_{mol} denotes the Liouville superoperator corresponding to the commutator with H_{mol} and $\mathcal{M}(\omega)$ is the memory kernel, Eq. (1.12) transformed into the frequency domain. Choosing a concrete representation the respective Fourier–Laplace transformed density matrix can be determined, at least numerically. After a back transformation the time-dependence of the complete set of density matrix elements is available (see, e.g. [RM02]). But all those problems connected with the presence of a time-dependent external field cannot be treated in this manner. After the transformation into the frequency domain a convolution integral of the Fourier–Laplace transformed field and the density operator occurs. However, if a linearization with respect to the field can be carried out (or some higher-order expansions) the problem becomes tractable again. This will be demonstrated in the following for the case of the linear absorption coefficient.

We start with the time-dependent formulation of the frequency-domain absorption coefficient [MK99]

$$\alpha(\omega) = \frac{4\pi\omega n_{mol}}{3\hbar c} \text{Re} \int_0^\infty dt e^{i\omega t} C_{d-d}^{(-)}(t) , \quad (2.7)$$

where n_{mol} denotes the volume density of the absorbing molecules, and the dipole–dipole correlation function is given by $C_{d-d}^{(-)}(t)$. For the molecular systems under consideration the dipole operator should exclusively act on system DOF and should realize transitions from the electronic ground-state φ_g to the excited state φ_e (2.5). Accordingly, the dipole–dipole correlation function can be written as ($\text{tr}_{vib}\{\dots\}$ denotes the trace with respect to the active vibrational DOF)

$$C_{d-d}^{(-)}(t) = \mathbf{d}_{ge} \text{tr}_{vib} \{ \langle \varphi_e | \hat{\sigma}(t) | \varphi_g \rangle \}$$

$$+ \mathbf{d}_{eg} \text{tr}_{\text{vib}} \{ \langle \varphi_g | \hat{\sigma}(t) | \varphi_e \rangle \} . \quad (2.8)$$

The operator $\hat{\sigma}(t)$ is a solution of the non-Markovian QME but with the initial condition $\hat{\sigma}(0) = [\hat{\mu}, \hat{\rho}_{\text{eq}}]_-$ ($\hat{\rho}_{\text{eq}}$ is the vibrational equilibrium statistical operator in the electronic ground-state, see also [LM00]). Furthermore, since only electronic off-diagonal matrix elements of $\hat{\sigma}$ are needed the initial correlation term vanishes.

Eq. (2.8) together with (2.7) is a generalization of the well-known formula which gives the absorption coefficient at frequency ω via the Fourier transform of the vibrational wavepacket motion on the excited electronic state PES after an instantaneous transition from the ground-state at time $t = 0$ (see, for example [MK99]). In this picture the ultrafast wavepacket motion within a sub-picosecond time-region determines the cw-absorption. If the vibrational wavepacket motion on the excited state PES involves dissipation but without retardation effects (Markovian relaxation), or in other words if the coherences responsible for linear absorption decay according to an exponential law the frequency-domain line broadening appears to be of the Lorentzian type. Obviously, non-Markovian effects, i.e. non-exponential decay of the coherences will result in a deviation from the Lorentzian line-shape. This fact is well anticipated in semiconductor optics [ZW94], but has not been discussed in a similar clear fashion in chemical physics. Therefore, we shortly demonstrate the non-Lorentzian line-broadening of a vibrational progression corresponding to an electronic transition coupled to a single vibrational DOF (compare the Hamiltonian Eq. (2.1)).

To end up with an analytical formula we consider the special case where the coupling of the active vibrational DOF to the reservoir modes is much larger in the excited electronic state than in the ground-state, i.e. we set $K_g = 0$ in Eq. (1.10). A compact treatment is achieved if we introduce the Green's function type matrix $G_{MN}(t) = \Theta(t) \langle \chi_{eM} | \langle \varphi_e | \hat{\sigma}(t) | \varphi_g \rangle | \chi_{gN} \rangle$.

According to the initial value of $\hat{\sigma}$ we get $G_{MN}(t = 0) = \mathbf{d}_{eg} \langle \chi_{eM} | \chi_{gN} \rangle f(\hbar\omega_{gN})$, where f gives the thermal distribution versus the vibrational levels $E_{gN} = \hbar\omega_{gN}$ of the electronic ground-state. This Green's function enables us to rewrite the first electronic matrix element in Eq. (2.8). The second matrix element can be neglected since it leads to non-resonant (anti-resonant) contributions. Before giving the equation of motion for G_{MN} we note

$$\alpha(\omega) = \frac{4\pi\omega n_{\text{mol}}}{3\hbar c} \text{Re} \left\{ \mathbf{d}_{eg}^* \sum_{M,N} \langle \chi_{gN} | \chi_{eM} \rangle G_{MN}(\omega) \right\} . \quad (2.9)$$

Taking the general non-Markovian QME expanded with respect to electronic states and concentrating on a coupling to the reservoir DOF in the excited-

state only gives after a Fourier transform ($\omega_{eM,gN}$ are respective transition frequencies)

$$\begin{aligned} -i\omega G_{MN}(\omega) &= G_{MN}(t=0) - i\omega_{eM,gN} G_{MN}(\omega) \\ &- \sum_K \tilde{C}_{MK}(\omega + \omega_{gN}) G_{KN}(\omega) . \end{aligned} \quad (2.10)$$

The frequency-dependent correlation function has been introduced according to

$$\tilde{C}_{MK}(\omega) = \int_0^\infty dt C_{ee}(t) \langle \chi_{eM} | K_e(Q) U_e(t) K_e(Q) | \chi_{eK} \rangle . \quad (2.11)$$

The general absorption coefficient is obtained after inverting the matrix formed by the prefactor of G_{MN} in Eq. (2.10) [MAS99, RM00]. If one neglects the off-diagonal parts of \tilde{C}_{MK} one obtains

$$\begin{aligned} \alpha(\omega) &= \frac{4\pi\omega n_{\text{mol}} |\mathbf{d}_{eg}|^2}{3\hbar c} \times \\ &\sum_{M,N} f(\hbar\omega_{gN}) |\langle \chi_{gN} | \chi_{eM} \rangle|^2 \text{Re} \tilde{C}_{MM}(\omega + \omega_{gN}) \\ &\times \left((\omega - \omega_{eM,gN} + \text{Im} \tilde{C}_{MM}(\omega + \omega_{gN}))^2 \right. \\ &\left. + (\text{Re} \tilde{C}_{MM}(\omega + \omega_{gN}))^2 \right)^{-1} . \end{aligned} \quad (2.12)$$

The derived expression clearly shows that the correlation function (the quantity being responsible for non-Markovian effects) if transformed into the frequency domain, strongly influences the concrete line-shape of the optical absorption spectrum. The real part of \tilde{C}_{MM} is responsible for a line broadening of the transitions whereas the imaginary part shifts the position of the transitions. But the frequency dependence of both, i.e. $\text{Re} \tilde{C}_{MM}$ and $\text{Im} \tilde{C}_{MM}$ may result in strong deviations from a simple Lorentzian line shape [RM00].

2.3 Effects of Initial Correlations

Turning our attention back to the time domain and considering the laser pulses with short duration, the proper inclusion of the initial correlation term \hat{I}_{NZ} becomes necessary. The correlation term \hat{I}_{NZ} in Eq. (1.8) describes the decay of correlations present between the active system and the reservoir at the initial time t_0 . After starting the evolution these initial correlations tend to zero on a time-scale comparable to t_{mem} , and \hat{I}_{NZ} should be negligible for $t > t_0 + t_{\text{mem}}$. They compensate the incomplete description of the dynamics of

system S for initial times $t < t_0 + t_{\text{mem}}$. In a formulation of dissipative quantum dynamics where a time coarse-graining has been introduced which neglects a time-resolution comparable to t_{mem} (see Section 1.2) one can neglect initial correlations and can change to a Markov approximation of expression (1.10).

Obviously, in the contrary case of a time-resolution much below t_{mem} initial correlations together with retardation effects of the system-reservoir coupling (non-Markovian effects) have to be accounted for. The disregarding of the initial correlation is usually performed by setting initial density matrix of the compound system $S + R$ to $\hat{W}(t_0) = \hat{\rho}(t_0)\hat{R}_{eq}$ which yields $\hat{I}_{NZ} \equiv 0$. If retardation is considered but initial correlations are neglected the time-dependence of the density operator (its matrix elements) displays artificial oscillations for an initial time interval extending from t_0 to $t_0 + t_{\text{mem}}$ (or somewhat larger times). This has been recently demonstrated for the dissipative dynamics of a single molecular DOF moving in a double-well potential [MT99].

The situation changes if one considers (as it will be the case here) the action of field-pulses driving the system out of equilibrium. Now, it is not necessary to deal with initial correlations. According to their decay with the characteristic time t_{mem} one can arrange the presence of the field-pulses for times where the influence of initial correlations already vanished. For numerical simulations this means that one should let evolve the system freely without the action of the external field and without including the term \hat{I}_{NZ} for a time-interval large compared to t_{mem} . Therefore, if the field-pulse acts, a correct description of non-Markovian molecular dynamics has already been achieved.

The field influence on the system dynamics can be considered as establishing a new initial condition for $\hat{\rho}$ (this is best seen for a pulse short compared to t_{mem} as well as any other characteristic time of the active system). The act of the external field results in a sudden jump in the dynamics of the system breaking also the system-bath correlations. But, this takes place without contributions in the density matrix equations similar to the initial correlation terms $\hat{I}_{NZ}(t, t_0)$. Therefore, one can expect that the interplay of non-Markovian dynamics and short pulse excitations are similar to the time-evolution of $\hat{\rho}$ one observes for times just after starting the evolution with retardation accounted for but without the consideration of initial correlations. The following considerations are devoted to make this statement more clear.

We suppose that the external field starts to deviate from zero (arrival time of the pulse in the probe) at time t_{field} , where $t_{\text{field}} \gg t_0$. Thus, for any $t_0 \ll t < t_{\text{field}}$ the field-free version of Eq. (1.10) would be valid, and should describe the equilibrium situation between the active system and the reservoir. We will denote the respective equilibrium version of the reduced density operator by $\hat{\rho}_{eq}$. If the exact expression for the memory kernel is taken we expect

$\hat{\rho}_{\text{eq}} = \text{tr}_R\{\hat{W}_{\text{eq}}\}$, where \hat{W}_{eq} is the canonical equilibrium statistical operator of the active system plus reservoir, proportional to $\exp(-(H_{\text{mol}} + H_{\text{S-R}} + H_R)/k_B T)$. If the field-free memory kernel \mathcal{M}_0 is used in the second Born-approximation we get (see e.g. [MK99])

$$\hat{\rho}_{\text{eq}} = \exp(-H_{\text{mol}}/k_B T) / \text{tr}_S\{\exp(-H_{\text{mol}}/k_B T)\}, \quad (2.13)$$

i.e. the canonical statistical operator of the active system. Although the concrete computations presented in the following sections have been done in the framework of the second Born-approximation it is not necessary for the reasoning below to use this approximation.

Since equilibrium should be established for $t_0 \ll t < t_{\text{field}}$ we get from Eq. (1.10) (note the replacement of $t - t_0$, which is much larger than zero, by ∞)

$$0 = -i\mathcal{L}_{\text{mol}}\hat{\rho}_{\text{eq}} - \int_0^\infty d\tau \mathcal{M}(\tau)\hat{\rho}_{\text{eq}}. \quad (2.14)$$

For $t > t_{\text{field}}$, thus for times when the field already acts, the whole equation (1.10) (with $\hat{I}(t, t_0) = 0$) applies. To solve this equation for times $t > t_{\text{field}}$ we introduce a formal decomposition of the RDO according to

$$\hat{\rho}(t) = \Delta\hat{\rho}(t) + \hat{\rho}_{\text{eq}}, \quad (2.15)$$

where $\Delta\hat{\rho}(t)$ vanishes for times less than t_{field} . Inserting (2.15) into (1.10) we obtain for $t > t_{\text{field}}$

$$\begin{aligned} \frac{\partial}{\partial t}\Delta\hat{\rho}(t) &= -i\mathcal{L}_S(t)\Delta\hat{\rho}(t) \\ &- \int_0^{t-t_{\text{field}}} d\tau \mathcal{M}(t, t-\tau; \mathbf{E})\Delta\hat{\rho}(t-\tau) \\ &- i\mathcal{L}_{\text{field}}(t)\hat{\rho}_{\text{eq}} \\ &- i\mathcal{L}_{\text{mol}}\hat{\rho}_{\text{eq}} - \int_0^{t-t_0} d\tau \mathcal{M}(t, t-\tau; \mathbf{E})\hat{\rho}_{\text{eq}}. \end{aligned} \quad (2.16)$$

Here, the parts depending on $\hat{\rho}_{\text{eq}}$ (three last terms on the right-hand side) act as inhomogeneities. Indeed, one can interpret these inhomogeneities as terms replacing \hat{I} in Eq. (1.8).

If one neglects the less important effect of the field-influence on the memory kernel (and notes $t - t_0 \gg 0$) the last term in Eq. (2.16) is compensated by the foregoing one (compare Eq. (2.14)) and $i\mathcal{L}_{\text{field}}(t)\hat{\rho}_{\text{eq}}$ remains as the inhomogeneity. But in difference to \hat{I} this inhomogeneity substantially deviates from zero for the whole time the external field is present.

2.4 An Analytical Solution for the Case of Long Correlation Times

In the previous section we have transformed the initial correlation term \hat{I} into the inhomogeneity $i\mathcal{L}_{\text{field}}(t)\hat{\rho}_{eq}$. This transformation is very fruitful when considering the electronic excitation by a δ -pulse. Such a pulse just shifts the vibrational wavepacket from the ground state to the excited one. For all times $t > t_0$, where $t_0 = t_{\text{field}}$ is the time when the δ -pulse acts the inhomogeneity $i\mathcal{L}_{\text{field}}(t)\hat{\rho}_{eq}$ is zero and the equation

$$\frac{\partial}{\partial t}\Delta\hat{\rho}(t) = -i\mathcal{L}_S(t)\Delta\hat{\rho}(t) - \int_0^{t-t_0} d\tau \mathcal{M}(t, t-\tau)\Delta\hat{\rho}(t-\tau) \quad (2.17)$$

correctly describes the non-Markovian dynamics of the system for $t > t_0$. The initial condition of the equation is $\Delta\hat{\rho}(t = t_0) = |\xi_0\rangle\langle\xi_0|$ where $|\xi_0\rangle$ denotes the vibrational ground-state of the electronic ground-state PES, displaced by $Q = -(Q_e - Q_g)$ with respect to the vibrational ground state $|0\rangle$ of the excited electronic state. It means we assume an instantaneous transition of the wavepacket as it is depicted on Fig. 2.1. Q represents again the dimension-less oscillator coordinate.

We will focus on this situation and demonstrate that an analytical treatment of the non-Markovian QME, Eq. (2.16) is possible if the inequalities $t_{\text{mem}} > 1/\omega_{\text{vib}}$ and $t \gg t_{\text{mem}}$ are fulfilled. The first inequality corresponds to the case in which the internal motion of the oscillator (not disturbed by the environment) is faster than the retardation effect resulting from the environmental influence. The second inequality reduces the actual time on the interval from the beginning of the evolution up to times not larger than t_{mem} . Both inequalities enable us to replace the correlation functions $C(\tau)$ and $C^*(\tau)$ by the common and real value $C(\tau = 0)$. For the approximative description of the memory effects we write the dissipative term $\int_0^t d\tau \mathcal{M}(t-\tau)\Delta\hat{\rho}(\tau)$ as in Eq. (1.10). The time-integral can be removed by the definition of a new operator $\hat{\sigma}$. It follows the whole QME as

$$\frac{\partial}{\partial t}\Delta\hat{\rho}(t) = -\frac{i}{\hbar}[H_S, \Delta\hat{\rho}(t)]_- + i[\sqrt{C(0)}K, \hat{\sigma}(t)]_- , \quad (2.18)$$

with the definition

$$\hat{\sigma}(t) = i \int_0^t d\tau U_S(t-\tau)(\sqrt{C(0)}K, \Delta\hat{\rho}(t))_- U_S^\dagger(t-\tau) . \quad (2.19)$$

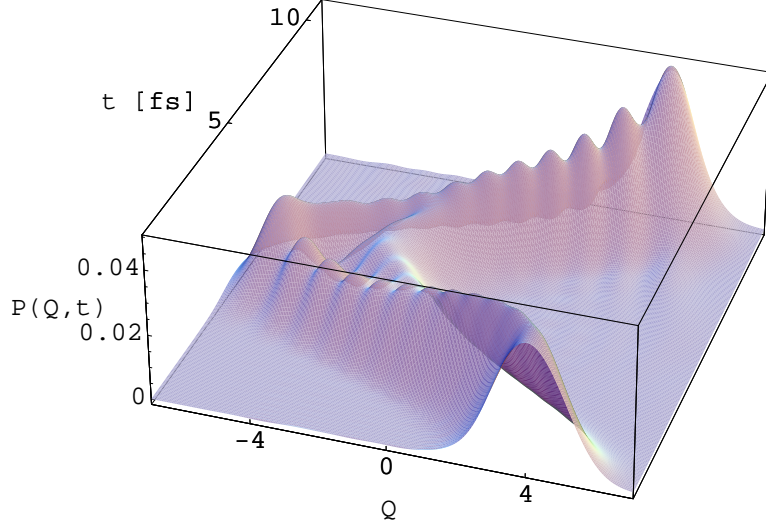


Figure 2.2: Wavepacket dynamics following from the solution of the non-Markovian QME for $t_{mem} = 100 fs$ and $J(\omega_{vib}) = 1.52 \times 10^{-12} fs$.

One easily verifies that the equation of motion for $\hat{\sigma}$ is obtained if we interchange $\Delta\hat{\rho}$ and $\hat{\sigma}$ in the given equation of motion for $\Delta\hat{\rho}$. Accordingly one can introduce the new density operators

$$\hat{w}^{(\pm)} = \Delta\hat{\rho} \pm \hat{\sigma} , \quad (2.20)$$

with initial conditions $\hat{w}^{(\pm)}(t=0) = \Delta\hat{\rho}(t=0)$ (note $\hat{\sigma}(t=0) = 0$). Furthermore, we note $\Delta\hat{\rho}(t) = (\hat{w}^{(+)}(t) + \hat{w}^{(-)}(t))/2$. Since the operator K which appears in the Eqs. (2.18) and (2.19) has been chosen be equal to the (dimensionless) oscillator coordinate Q (see section 2.1) the contribution $\sqrt{C(0)}Q$ resulting from non-Markovian dissipation can be incorporated into the oscillator Hamiltonian H_S by defining shifted potential energy functions

$$U^{(\pm)}(Q) = \frac{\hbar\omega_{vib}}{4}(Q \mp Q_c)^2 - \frac{\hbar C(0)}{\omega_{vib}} \quad (2.21)$$

The origin of the oscillator potential has been displaced to $Q_c = 2\sqrt{C(0)}/\omega_{vib}$.

The Hamiltonian $H_S^{(\pm)}$ following from the replacement of U by $U^{(\pm)}$ define dissipation-less equation of motions for $\hat{w}^{(\pm)}$ which solution is obtained as

$$\hat{w}^{(\pm)}(t) = \exp\left(-\frac{i}{\hbar}H_S^{(\pm)}t\right) \Delta\hat{\rho}(t=0) \exp\left(\frac{i}{\hbar}H_S^{(\pm)}t\right) . \quad (2.22)$$

Since $\Delta\hat{\rho}(t=0)$ describes a pure state, those states both density operators $\hat{w}^{(\pm)}$ describe at later times remain pure. In contrast, $\Delta\hat{\rho}(t)$ will describe a mixed state. The pure states corresponding to $\hat{w}^{(\pm)}$ are given by the propagation of the displaced vibrational ground-state $D^+(g)|0\rangle$ in the displaced oscillator potential $U^{(\pm)}$. Here $D^+(g)|0\rangle = \exp\{g(C - C^\dagger)\}$ with C and C^\dagger the oscillator annihilation and creation operators, is the well-known displacement operator [MK99]. Changing to the coordinate representation the solution follows as the moving wavepacket

$$\begin{aligned}\psi^{(\pm)}(Q, t) &= \langle Q | \exp(-\frac{i}{\hbar} H_S^{(\pm)} t) D^+(g) | 0 \rangle \\ &= \chi_0(Q^{(\pm)}(t)) e^{i\varphi^{(\pm)}(t)}.\end{aligned}\quad (2.23)$$

Here, $\chi_0(Q)$ denotes the oscillator ground-state wavefunction which reads in the present notation $(\mu_{\text{vib}}\omega_{\text{vib}}/\pi\hbar)^{1/4} \exp(-Q^2/4)$ (the phase $\varphi^{(\pm)}(t)$ can be found in [MK99]). The time-dependent coordinate $Q^{(\pm)}(t) = Q \mp Q_c + (2g \pm Q_c) \cos(\omega_{\text{vib}}t)$ leads to harmonic (but shape invariant) motion of the wavepacket. Again, we state that the non-Markovian dissipative dynamics discussed here is not described by a (coherent) superposition of the two types of wavefunctions $\psi^{(\pm)}(Q, t)$. There only appears a superposition of the related pure-state density operators. We introduce the respective coordinate distribution function as

$$\begin{aligned}P(Q, t) &= \langle Q | \Delta\hat{\rho}(t) | Q \rangle = \frac{1}{2} \langle Q | \hat{w}^{(+)}(t) + \hat{w}^{(-)}(t) | Q \rangle \\ &= \chi_0^2(Q^{(+)}(t)) + \chi_0^2(Q^{(-)}(t)).\end{aligned}\quad (2.24)$$

It give the (phase insensitive) superposition of two independent coordinate distribution functions. In contrast to the case of Markovian dissipation where a single wavepacket is moving the given superposition introduces a specific structure into coordinate distribution $P(Q, t)$. This can be seen in Fig. 2.2, where the numerical solution of the non-Markovian QME is displayed. The mentioned dip in $P(Q, t)$ disappears if the memory time is reduced.

For the time-dependence of the vibrational level populations $P_M = \langle M | \Delta\hat{\rho} | M \rangle$ one obtains

$$P_M(t) = |A_M^{(+)}(t)|^2 + |A_M^{(-)}(t)|^2 \quad (2.25)$$

where the transition amplitudes read

$$A_M^{(\pm)}(t) = \sum_N f_{FC}(M, N) \tilde{f}_{FC}(N, 0) \exp(-i\omega_{\text{vib}} N t). \quad (2.26)$$

The Frank-Condon factor $f_{FC} = \langle \xi_{eM} | \xi_N^{(\pm)} \rangle$ describes the overlap between

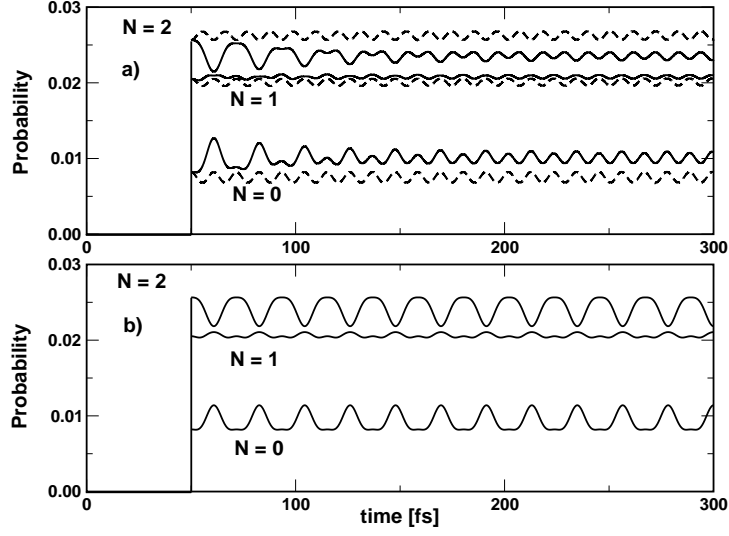


Figure 2.3: The population dynamics of the vibrational ground and the first two excited states in the case of a long correlation time $t_c = 50fs$ (part a) in comparison with the analytical result from Eq. 2.25 for the case of an infinitely long memory (part b). In part (a) the full non-Markovian calculation (full line) and the corresponding Markovian approximation (dashed line) are presented.

oscillator states belonging to U_e with quantum number M and those of the displaced oscillator with Hamiltonian $H_S^{(\pm)}$. The overlap between the state of $H_S^{(\pm)}$ and the electronic-ground state vibrational wavefunction $|\xi_{g0}\rangle$ is given by $\tilde{f}_{FC} = \langle \xi_N^{(\pm)} | \xi_{g0} \rangle$. Obviously, $P_M(t)$ should display constructive and destructive interferences among the various contributions stemming from the simultaneous presence of two different contributions $|A_M^{(\pm)}(t)|^2$. In Figure 2.3 the vibrational populations of the first three levels of the excited electronic states are presented. The analytical solution in part (b) of the figure is compared to the corresponding exact solution for the long correlation time and the Markovian solution (in part (a) of the figure). For the comparison with non-Markovian results we use the Markovian approximation introduced in section 1.3.1. More detailed discussion of the comparison between non-Markovian and Markovian results will be given later. For the time being one can analyze what we can learn about non-Markovian dynamics from the Figures 2.2 and 2.3.

In Figure 2.2 the whole one period of the wavepacket motion on the excited PES is presented. One notices the broadening of the wavepacket and creation of the dip in the middle of it. We find the wavepacket to be narrow when it is present on the one side of the harmonic PES and to be broad on the other

side. This movement is reflected by the population probabilities. The minima and maxima alternate after the half of the oscillator period $T = 2\pi/\omega_{vib}$ what can be clearly seen on Fig. 2.3 (b).

The situation for the Markovian dynamics described in terms of the wavepacket differs. On the time scales where the dissipation (described by the real part of the Redfield tensor) of the wavepacket energy is still negligible, the influence of the imaginary part of the Redfield tensor causes some changes of the wavepacket shape as it moves on the PES. In particular, the wavepacket broadens in the middle of the PES and becomes narrow when it hits the turning point on the PES. Similarly to the non-Markovian case this leads to the oscillations of vibrational populations. But now, the broadening and narrowing of the wavepacket happens twice in one period of the wavepacket motion. The Markovian vibration populations display the modulation by the frequency twice as high as the non-Markovian ones (compare Figs. 2.3 (a) and 2.3 (b)). The case with the finite memory time t_{mem} exhibits the non-Markovian frequency of the modulation in times just after the excitation which turns into Markovian one for times $t > t_{mem}$.

Another aspect differing Markovian and non-Markovian results is a clear separations of the overall course of the vibronic population. This separation happens immediately after the excitation with Markovian and non-Markovian populations heading opposite directions. This effect reminds the works suggesting the slippage of the initial conditions in Markovian equations to account for non-Markovian effect [SSO92, GN99b]. Indeed, in Fig. 2.3 (a) the change of the starting vibrational populations would be able to account for the difference between Markovian and non-Markovian dynamics in later times, but certainly not for time $t < t_{mem}$.

2.5 Interplay of Non-Markovian Relaxation and Ultrafast Optical State Preparation

In the previous sections we have already looked at the non-Markovian effects in the frequency domain, we have accounted for the initial correlation problem and obtained several hints on how to recognize the non-Markovian effects in the time domain via an analytical solution of the non-Markovian QME for certain special case. All the studies presented here so-far have assumed either a *cw*-field or an infinitely short pulse excitation. Now the case of the short pulse of the finite duration will be studied. Of basic interest for the following will be the study of the ultrafast laser-pulse action and its interplay with the non-Markovian dynamics of the vibrational DOF as well as the comparison of

the non-Markovian dynamics with the dynamic behavior present in the limit of the Markov approximation. This latter comparison can be carried out in different ways. First we can try to compare those types of non-Markovian dynamics which obey the same Markov-limit as a common feature. Inspecting Eqs. (1.33) and (1.35) it becomes obvious that the requirement for the same Markov-approximation is equivalent with the demand for the same Redfield-tensor. This can be translated to the requirement that the different types of correlation function $C(t)$ used in the comparison should have the same values $C(\omega)$ at certain frequencies. In the present case of a harmonic oscillator there remains only the single value $C(\omega_{\text{vib}})$ of $C(\omega)$ at which all correlation functions should coincide.

An alternative scheme to compare different types of non-Markovian dynamics could be based on the application of different correlation functions $C(t)$ with different extension along the time-axis, but with the same integral value. However, we found the first of these approaches to be more suitable for our purpose. In the Markov-limit and in so-called secular approximation (see e.g. [MK99]) the quantity $C(\omega_{\text{vib}})$, and in the present limit $T = 0$ $J(\omega_{\text{vib}})$ can be directly related to the inverse life-time of an oscillator level, i.e. we have $1/\tau_M = 2\pi M J(\omega_{\text{vib}})$. Thus, to compare non-Markovian results with different correlation functions we choose the coupling in such a way, that it corresponds in the Markovian limit to the same life-time of the first excited oscillator level.

2.5.1 Density Operator Equation

In the following we will consider the weak field case. The field-strength should be of such a low value that the following two approximations are allowed. First, we provide that it is sufficient to consider the excited-state population linear with respect to the intensity. This will enable us to reduce the description of the complete excited state dynamic to the computation of the electronic diagonal matrix element of the reduced density operator. Some details on the respective derivation can be found in Appendix D. Using the separation according to Eq. (2.15), we have exclusively to determine $\Delta\hat{\rho}_{ee}$, the density matrix operator corresponding to the excited electronic state (this is still an operator in the space of vibration states).

As a second consequence of the considered weak-field case we neglect the field-dependence of the memory kernel (cf. the discussion in [SM98]). It results the following density operator equation

$$\frac{\partial}{\partial t}\hat{\sigma}(t) = \frac{i}{\hbar}[H_e, \hat{\sigma}(t)]_-$$

$$- \hat{D}_{ee}(t - t_{\text{field}}; \hat{\sigma}) + \hat{F}_{ee}(t, t_{\text{field}}; \mathbf{E}) . \quad (2.27)$$

This equation directly follows from Eq. (D.15). Note the identification

$$\hat{\sigma} = \Delta \hat{\rho}_{ee} . \quad (2.28)$$

The dissipative part \hat{D}_{ee} is obtained from Eq. (D.5) in Appendix D, and the external-field dependent source term \hat{F}_{ee} is given in Eq. (D.16). In our calculation we use the following form of the quantity $J(\omega)$

$$J_{ee}(\omega) = \Theta(\omega) J_0 j(\omega) , \quad (2.29)$$

where $j(\omega)$ has been normalized to 1 in the frequency interval between 0 and ∞ , and $\Theta(\omega)$ denotes the unit-step function. Furthermore we use the following *ansatz* [SM98, WL93]

$$j(\omega) = \frac{\omega}{\omega_c^2} e^{-\omega/\omega_c} . \quad (2.30)$$

Here, we introduced a cut-off frequency ω_c , which corresponds to the characteristic memory time τ_{mem} on which the correlations of the reservoir DOF decay. The inverse of ω_c will be denoted as t_c and named correlation time.

2.5.2 Energy Representation

For the numerical determination of the density matrix we have to change from the operator expression $\hat{\sigma}$ to a concrete representation. In the present case it is most appropriate to take the harmonic oscillator like eigenstates of the vibrational Hamiltonian H_a which will be denoted by $|\chi_{aM}\rangle$. Then, the excited electronic state density matrix which elements will be calculated in the following reads

$$\sigma_{MN}(t) = \langle \chi_{eM} | \hat{\sigma}(t) | \chi_{eN} \rangle . \quad (2.31)$$

From Eq. (2.27) we directly obtain the following density matrix equation

$$\begin{aligned} \frac{\partial}{\partial t} \sigma_{MN}(t) &= -i\omega_{MN} \sigma_{MN}(t) \\ &- \sum_{K,L} \int_0^t d\tau \mathcal{M}_{MN,KL}(\tau) \sigma_{KL}(t - \tau) + F_{MN}(t) . \end{aligned} \quad (2.32)$$

Note the special choice $t_{\text{field}} = 0$, and the abbreviation $\omega_{MN} = (E_{eM} - E_{eN})/\hbar$, where the E_{eM} are the *eigenvalues* of H_e . The tetradic matrix $\mathcal{M}_{MN,KL}(\tau)$

following from the memory kernel superoperator reads in detail

$$\begin{aligned}
\mathcal{M}_{MN,KL}(\tau) &= \delta_{M,K} \sum_A M_{LA,AN}(-\tau) e^{i\omega_{AM}\tau} \\
&+ \delta_{N,L} \sum_A M_{MA,AK}(\tau) e^{i\omega_{NA}\tau} \\
&- M_{LN,MK}(-\tau) e^{i\omega_{NK}\tau} \\
&- M_{LN,MK}(\tau) e^{i\omega_{LM}\tau} ,
\end{aligned} \tag{2.33}$$

with

$$\begin{aligned}
M_{MN,KL}(\tau) &= \\
C_{ee}(\tau) \langle \chi_{eM} | K_e | \chi_{eN} \rangle \langle \chi_{eK} | K_e | \chi_{eL} \rangle .
\end{aligned} \tag{2.34}$$

The energy representation of the inhomogeneity is obtained as

$$\begin{aligned}
F_{MN} &= \frac{|\mathbf{d}_{eg}|^2}{\hbar^2} \sum_L \langle \chi_{eM} | \chi_{gL} \rangle \langle \chi_{gL} | \chi_{eN} \rangle f(E_{gL}) \\
&\times \mathcal{E}(t) \int_0^t d\bar{t} \mathcal{E}(\bar{t}) e^{-i(\omega_{ML} - \Delta\omega)(t - \bar{t})} + \text{h.c.} .
\end{aligned} \tag{2.35}$$

Here, $f(E_{gL})$ denotes the thermal distribution versus the electronic ground-state vibrational levels. To have a sufficient simple expression we neglected the contribution of the dephasing operator introduced in Eq. (D.14) of Appendix D. The field-pulse envelope \mathcal{E} has been introduced in Eq. (2.4). For the concrete computations we take the following form

$$\mathcal{E}(t) = \frac{A}{\tau_p} \sqrt{\frac{2}{\pi}} e^{-2(t - \tau_f)^2 / \tau_p^2} . \tag{2.36}$$

The time τ_f where the pulse reaches its maximum has to be chosen large compared to τ_p in order to get $\mathcal{E}(t = 0) \approx 0$. We set $\tau_f = 50$ fs. The field amplitude A (cf. Eq. (2.36)) together with the transition dipole moment is not specified explicitly. Instead, we choose $A \times \mathbf{nd}_{eg}$ in such a manner to achieve an excited state population sufficiently smaller than 1. For our computation this choice guarantees $\sigma_{NN}(t \rightarrow \infty) \approx < 10^{-3}$. Beside the envelope we introduced in Eq. (2.35) the quantity $\Delta\omega$ giving the detuning between the energetic distance of both PES and the photon energy, i.e

$$\Delta\omega = \Omega - (U_e^{(0)} - U_g^{(0)})/\hbar . \tag{2.37}$$

If we take the standard Markovian QME, Eq. (1.29) the dissipative part of Eq. (2.32) reads $\sum_{KL} \mathcal{R}_{MN,KL} \sigma_{KL}$ where the complex Redfield tensor reads

$$\begin{aligned} \mathcal{R}_{MN,KL} &= \delta_{M,K} \sum_A \hat{M}_{NA,AL}^*(-\omega_{AL}) \\ &+ \delta_{N,L} \sum_A \hat{M}_{MA,AK}(\omega_{KA}) \\ &- \hat{M}_{KM,NL}^*(-\omega_{NL}) - \hat{M}_{LN,MK}(\omega_{KM}) . \end{aligned} \quad (2.38)$$

Here, $\hat{M}_{MN,KL}(\omega)$ denotes the half-sided Fourier transform of the function introduced in Eq. (2.34) (note $\hat{M}_{MN,KL}(\omega) = \hat{M}_{KL,NM}^*(-\omega)$). The usual Redfield tensor is obtained as the real part of the above given expression [Blu89, MK99]. Finally, the time-dependent Redfield-tensor $\mathcal{R}_{MN,KL}(t, t_{\text{field}}; \mathbf{E} = 0)$ introduced in Eq. (1.30) follows from Eq. (2.38) in replacing $\hat{M}_{MN,KL}(\omega)$ by

$$\bar{M}_{KM,NL}(\omega, t) = \int_0^{t-t_{\text{field}}} d\tau e^{i\omega\tau} M_{KM,NL}(\tau) \quad (2.39)$$

The last two versions of the QME are local in time, so the solution can be found by a standard Runge-Kutta type method [PTVF92].

As we have already mentioned to solve the set of equations (2.32) the so-called *Laguerre-polynomial method* [MM00, MM01] is used in this work. The basic idea of the method is to expand the non-Markovian equations of motion with respect to some special functions [SB82, Men95]. Such an expansion will enable us to convert the respective integro-differential equations into algebraic ones. From earlier works [Man97, MBS98] it follows, that the most suitable set of special functions is given by the orthonormal set of Laguerre polynomials defined as

$$L_n(x) = \frac{1}{n!} e^x \left(\frac{d}{dx} \right)^n (x^n e^{-x}). \quad (2.40)$$

Besides other different properties explained in the Appendix F Laguerre polynomials obey the following important equation

$$\int_0^x d\bar{x} L_n(x - \bar{x}) = L_{n+m}(x) - L_{n+m+1}(x). \quad (2.41)$$

This represents the key relation to handle any type of time non-locality. If all ingredients of the non-Markovian density matrix equation are expanded with respect to the Laguerre polynomials the difficulty to treat the retardation effects has been overcome. The method is in detail explained in Appendix

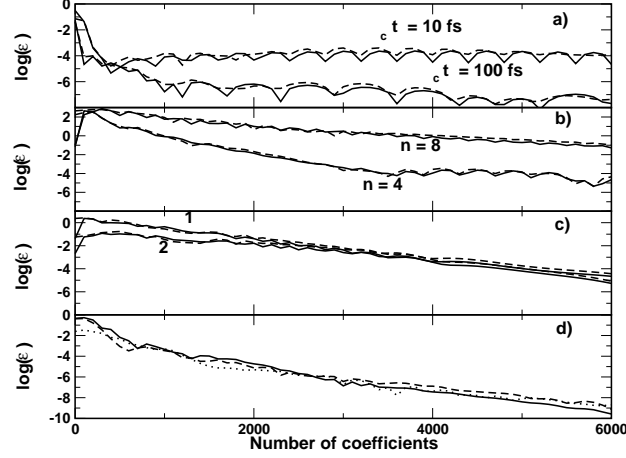


Figure 2.4: Accuracy of the Laguerre polynomial expansions. The measure $\epsilon(t_a = 0, t_b = 300 fs; N)$, Eq. 2.42 and $\Delta\epsilon(t_a = 0, t_b = 300 fs; N + 100, N)$, Eq. 2.43 are drawn versus the expansion order N . Part (a) ϵ (solid line) and $\Delta\epsilon$ (dashed line) determined for the correlation function $C_{ee}(t)$ with different t_c . Part (b) The same as in part (a) but for the function $C_{ee}(t)e^{in\omega_{vib}t}$, the single value $t_c = 10 fs$, and different n . Part (c) The same as in (a) but for the time-dependent part $\mathcal{E}(t) \int_0^t d\bar{t} \mathcal{E}(\bar{t}) \exp -i(n\omega - \Delta\omega)(t - \bar{t})$ of the field term, Eq. (2.35). Curve pair 1: $n = 0$, curve pair 2: $n = 8$. Part d) $\Delta\epsilon(t_a = 0, t_b = 300 fs; N + 100, N)$ versus N for the diagonal elements of the harmonic oscillator density matrix. Solid line: ρ_{00} , dashed line: ρ_{44} , dashed-dotted line: ρ_{88} .

F. Before the method will be used for actual calculations we try to test its accuracy.

A convenient way to proof the convergence of the expansion into Laguerre polynomials is to compute the contribution given by a few last terms in the expansion while enlarging the number of expansion coefficients. However, in a case where the function $f(t)$ to be expanded is known we can easily check the accuracy of the actual expansion $f_{\text{exp}}(t; N) = f_{\text{exp}}(t_{\text{char}}x; N) = \sum_{n=0}^N f^{(n)} L_n(x)$ of order N by introducing

$$\epsilon(t_1, t_2; N) = \frac{1}{t_2 - t_1} \int_{t_1}^{t_2} dt |f(t) - f_{\text{exp}}(t; N)|. \quad (2.42)$$

The expression gives the absolute value of the difference between the original function and its N th order expansion averaged with respect to the time interval $[t_1, t_2]$. Since we are mainly interested in the question how the Laguerre

polynomial expansion may be improved by enlarging the expansion order we will use the quantity $\epsilon(t_1, t_2; N)$ instead of an expression defining a relative deviation.

If the function $f(t)$ is not known one has to compare different orders N of the expansion, say N and $N + \Delta N$, ($\Delta N > 0$). For this reason one may introduce as a measure of accuracy

$$\Delta\epsilon(t_1, t_2; N + \Delta N, N) = \frac{t_{char}}{t_2 - t_1} \int_{t_1/t_{char}}^{t_2/t_{char}} dx \left| \sum_{n=N+1}^{N+\Delta N} f^{(n)} L_n(x) \right|. \quad (2.43)$$

In Fig. 2.4 we demonstrate the accuracy of the polynomial expansions of the correlation function, the density matrix elements and the field-term. The quantities $\epsilon(0, 300fs; N)$ and $\epsilon(0, 300fs; N + 100, N)$ (Eq. 2.42 and 2.43, respectively) are presented in part (a) of the Fig. 2.4 as a function of N for the correlation function $C_{ee}(t)$, ($1/\omega_c = t_c = 10fs$ and $100fs$). Both measures show a strong decay for N less than 10^3 . Afterwards a saturation appears if N is further increased. This behavior points out the fact that the accuracy of the expansion reaches its limit if it coincides with the accuracy of the spline approximation. Of course, this can be improved by shortening the step length of the spline approximation. Thanks to the smoother behavior of the $C_{ee}(t)$ with $t_c = 100$ fs as compared with $t_c = 10$ fs the corresponding spline approximation with the same step length is more accurate. This also leads to higher accuracy in the polynomial expansion.

According to Eq. (2.33) which determines the memory kernel terms of the type $C_{ee}(t) \exp(in\omega_{vib}t)$ have to be studied. In part (b) of Fig. 2.4 we again present ϵ and $\Delta\epsilon$ but defined for those expressions incorporating oscillating contributions with $n = 4, 8$ and $t_c = 10fs$. Now we are expanding highly oscillating functions what leads to the slower increase of the accuracy. However, in the case of $n = 4$, for example, we reach saturation at the same accuracy as in the case of $n = 0$ with some 4000 coefficients. As it has to be expected the accuracy of the term with $n = 8$ is lower. In the case of such a highly oscillating term we can, however, expect that their contribution is small and a less accurate expansion seems to be sufficient.

Next, in part (c) of Fig. 2.4 we show analogical picture for the expansion of the laser pulse. The field term does not show any dramatic oscillations and the functions dies out very fast far from the center of the pulse, so that the method explained in Appendix G enables us to evaluate actual infinite integrals determining the expansion coefficients of the laser pulse with a high accuracy using a small finite interval. Interestingly, in parts (a),(b) and (c) we could

observe that both quantities ϵ and $\Delta\epsilon$ are approximately of the same order. This indicates that they can be used alternatively.

Finally, the accuracy of the density matrix expansion is estimated where the only measure to be used is given by $\Delta\epsilon$, Eq. (2.43). The accuracy of this expansion is determined by the respective accuracy of the expansions of the memory kernel, the field-term, and the expansion of the free dynamics of the system. Different contributions may be expanded with different accuracies. For the highly oscillating terms of the memory kernel which do not contribute substantially to the dynamics low accuracy seems to be sufficient. The expansion of the free dynamics part is naturally involved in the algebraic equation (F.9). Thus, in part (d) Fig. 2.4 we display $\Delta\epsilon(0, 300fs; N + \Delta N, N)$ as a function of N for $\Delta N = 100$ and for the expansion of different matrix elements.

2.5.3 Numerical Results

In this section we present and analyze the numerical results on the model system presented in section 2.1. We use a short laser pulse excitation to populate the excited electronic state $|\varphi_e\rangle$ and study the subsequent evolution of the vibrational populations and the influence of the dissipation. We vary the excitation pulse length, the correlation time t_c and the strength of the dissipation. The latter is determined by the value of the spectral density $J(\omega)$ at the oscillator frequency ω_{vib} .

We start the presentation of numerical calculations by displaying the population $\sigma_{22}(t) = P_2(t)$ of the second excited vibrational level (which is the level positioned in resonance to the applied light field). Fig. 2.5 shows the time-development of $P_2(t)$ in its dependence on the length of the laser pulse. In part (a) we can identify three kinds of the non-Markovian effects. First, one can immediately notice that P_2 reaches somewhat lower values in the non-Markovian case. This behavior reflects the fact that the dynamics is determined by the preceding states of the system. Further we can observe that the fast oscillations of P_2 present in the Markov case become approximately twice slower in the non-Markovian case. After a certain time-interval this smaller oscillation frequency changes back to that of the Markov case, but with a smaller amplitude. Finally, an alternation of the decay rate of P_2 appears if one changes to the case of non-Markovian dynamics. (This latter effect can be seen more clearly in some other curves presented below.) Comparing the results of Fig. 2.5 valid for different pulse lengths one notices that the oscillating structures superimposed to P_2 disappear with pulses comparable or longer as the vibrational period $2\pi/\omega_{vib}$.

A similar behavior as in Fig. 2.5 is shown in Fig. 2.6, but now with a

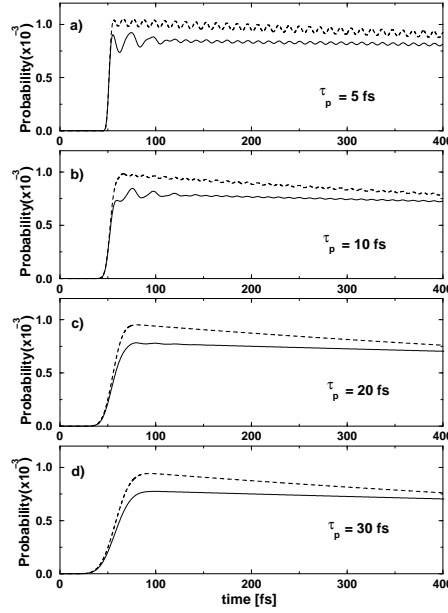


Figure 2.5: Population of the second excited vibrational level in dependence on the pulse-length τ_p based on the solution of the non-Markovian (full-line) and Markovian (dashed-line) QME. $t_c = 30\text{fs}$, $J(\omega_{vib}) = 1.9 \times 10^{-4}/\text{fs}$.

correlation time shorter than the vibrational period $2\pi/\omega_{vib}$. Using the same coupling strength as in Fig. 2.5 (upper curves) the situation change considerably since we observe only a very small deviation between the case of non-Markovian and Markovian dynamics. On the other hand while increasing the coupling strength j_0 we can again restore the situation from Fig. 2.5.

To further indicate the influence of the memory kernel decay-time, e.g. the correlation time t_c on the dynamics, we display in Fig. 2.7 the population of the first four vibrational levels for the two different correlation times of 20 fs and 30 fs. Using the coupling strength of Fig. 2.5 we found in the case of $t_c = 10\text{fs}$ a complete agreement between the Markovian and non-Markov dynamics (not shown). This coincidence is somewhat weakened for $t_c = 20\text{fs}$ (Fig. 2.7 a). But for $t_c = 30\text{fs}$ the characteristics of the non-Markovian effects as described above arise (part b).

A situation where the correlation time t_c is shorter than the vibrational period $2\pi/\omega_{vib}$ is considered in Fig. 2.8. Using the coupling strengths j_0 already applied in Figs. 2.5 and 2.7 we again find a complete agreement between the Markovian and non-Markovian type of dynamics. A small deviation between both cases can be observed in part b of Fig. 2.8. This part also shows that

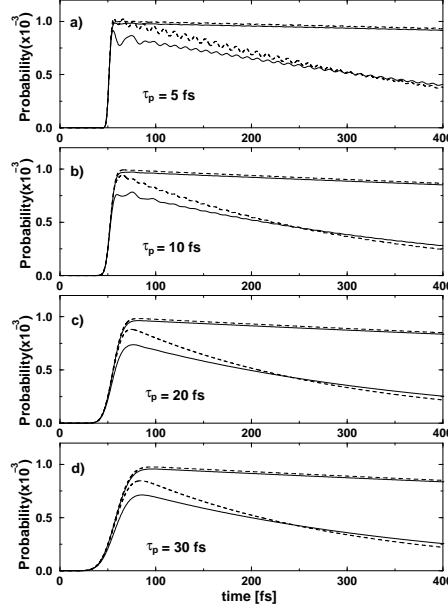


Figure 2.6: Population of the second excited vibrational level in dependence on the pulse-length τ_p based on the solution of the non-Markovian (full-line) and Markovian (dashed-line) QME. $t_c = 20\text{fs}$, $J(\omega_{vib}) = 1.9 \times 10^{-4}/\text{fs}$ (upper curves in graphs) and $J(\omega_{vib}) = 3.5 \times 10^{-4}/\text{fs}$.

a further increase of j_0 may cause some small deviations between the Markov and non-Markov case. In particular, in the case of non-Markovian relaxation the equilibrium value is reached slightly faster.

Let us summarize the phenomena which indicate a deviation of the non-Markovian type of relaxation from the Markovian case. First, we observed a change of the layout of the light-pulse induced vibrational levels population if non-Markovian relaxation is accounted for. And second, the retardation effect somewhat slows down the relaxation. Finally, as a third hint on non-Markovian effects we mention a reduction of the fast oscillations superimposed to the vibrational level populations. While the first two effects were found to be relatively unaffected by the pulse length, the oscillations are only present for pulse lengths sufficiently shorter than the oscillation period of the vibrational coordinate. Therefore, only the observation of these fast oscillations just after the pulse action can be considered as a sufficient clear hint on non-Markovian effects in the molecular dynamics. The results of the section 2.4 indicate that the irregular oscillations just after the external field action are really a pure memory effects.

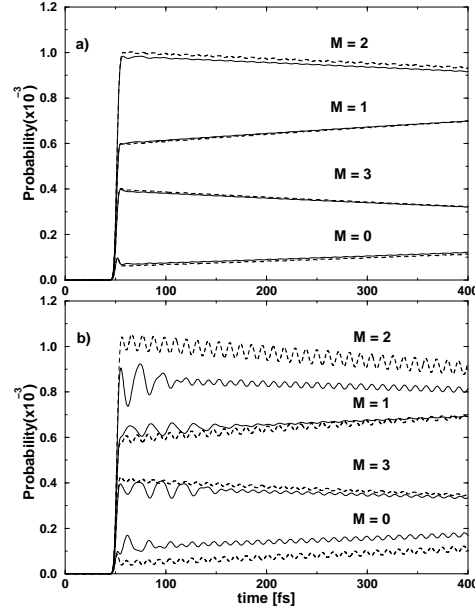


Figure 2.7: Influence of the correlation time t_c on the dynamics of the occupation probabilities of the first four vibrational levels. Parameters: $J(\omega_{vib}) = 1.9 \times 10^{-4}$, $\tau_p = 5fs$, $t_c = 20fs$ and $t_c = 30fs$ in parts a and b, respectively.

At the end of this section we will compare the given correct description of non-Markovian dynamics with the approximate one introduced in Section 1.3 via establishing the QME with a time-dependent Redfield-tensor. Since the non-equilibrium part $\Delta\hat{\rho}$ of the complete RDO obeys a QME starting at time t_{field} and having the same inhomogeneity whether non-Markovian dynamics or Markovian dynamics (including a time-dependent Redfield tensor) are considered, we expect that both approaches should give similar results. But a problematic issue of this comparison would be the choice of the time t_{field} .

In Fig. 2.9 we present respective results for the case of an impulsive excitation (infinitely short laser pulse). In such a case t_{field} can be identified with the center of the pulse, and the agreement between both types of dynamics is very good. Since the pulse is infinitely short the final population of the levels after the action of the pulse is the same for both, the Markovian as well as the non-Markovian case. However, details of the dynamics immediately after the pulse action differ in both case.

For a situation with laser pulses of finite duration one may expect a similar result as in the case of the impulsive excitation as long as the pulse length is shorter than the oscillation period of the vibrational coordinate. Indeed,

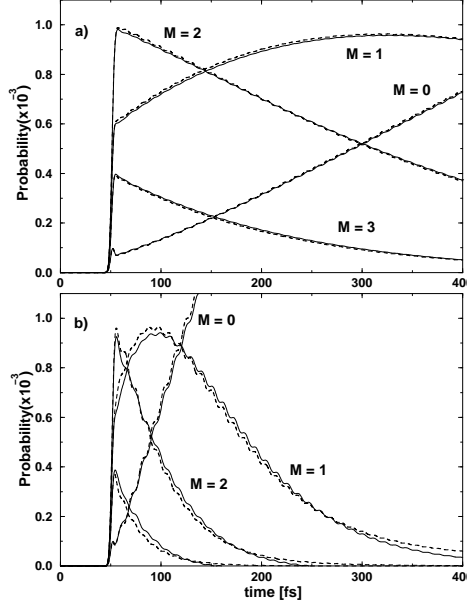


Figure 2.8: Influence of the system bath coupling on the population dynamics of the first four vibrational levels ($\tau_p = 5fs$, $t_c = 10fs$). Part a: $J(\omega_{vib}) = 3.5 \times 10^{-4}/fs$. Part b: $J(\omega_{vib}) = 2.3 \times 10^{-3}/fs$.

choosing an optimal time t_{field} one is able to reproduce the results of the non-Markovian case quite well (see Fig. 2.10 curve b). However, the agreement appears to be very sensitive on the choice of t_{field} . In particular, choosing t_{field} too close to the center of the pulse leads to an underestimation of the level populations created by the pulse (curve a in Fig. 2.10). The opposite choice leads to a fast convergence to the corresponding standard Markov results as demonstrated by curve c of Fig. 2.10.

To conclude we note that in the case of an instantaneous excitation, the time-dependent Markov approach reproduces some of the non-Markovian effects quite well. In particular, one is able within this approximation to account for the initial dynamics leading to the difference in the occupation probability after the action of the pulse and partly also for the initial change of the fast oscillations superimposed to the populations. Finally, we underline that the given evaluation of the approach based on the time-dependent Redfield-tensor justifies earlier studies on the field-pulse alternation of dissipation [SM98].

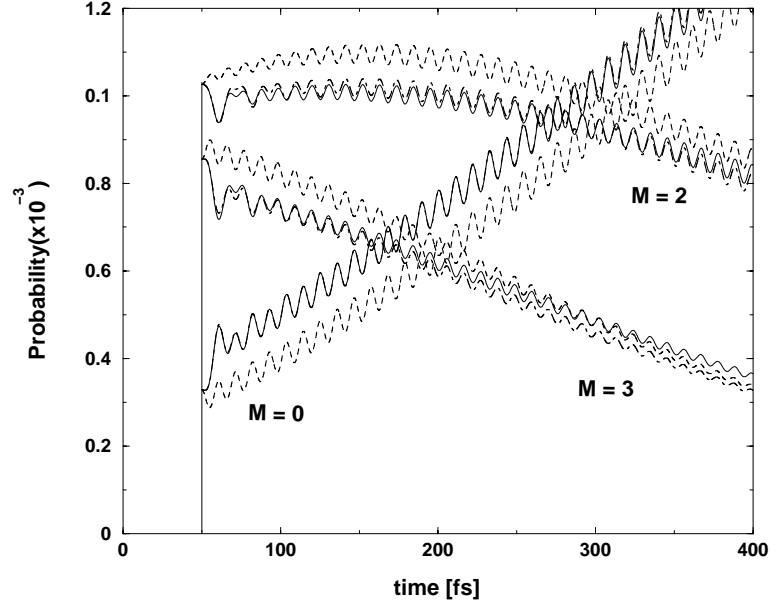


Figure 2.9: Population dynamics of some selected vibrational levels after impulsive excitation ($J(\omega_{\text{vib}}) = 3.5 \times 10^{-4}/\text{fs}$, $t_c = 20\text{fs}$). Full-line: solution of the non-Markovian QME, dashed-line: solution of the non-Markovian QME, dashed-dotted line; solution of Markovian QME with time-dependent Redfield tensor.

2.6 Non-Markovian Dissipation via Multi-Quantum Processes

The discussion of the non-Markovian effects has been so far limited to our bilinear system-bath coupling model with both system and bath coordinates appearing only linearly in the expression (1.14). Clearly, this represents the lowest order approximation of the general expression with respect to the system and bath coordinates and higher order interaction would be in principle possible.

The bilinear type of system reservoir coupling represented by formula (1.14) has been broadly used in dissipative quantum dynamics by additionally providing a normal-mode analysis with respect to the reservoir DOF (see for example [LCD⁺87, Wei93, MK99]). Consequently the bath coordinates Z_ξ , where ξ counts the bath modes, correspond to a thermal bath of decoupled harmonic oscillators. It has been demonstrated many times (see, e.g. [MK99] and references therein) that the used bilinear coupling results in a description

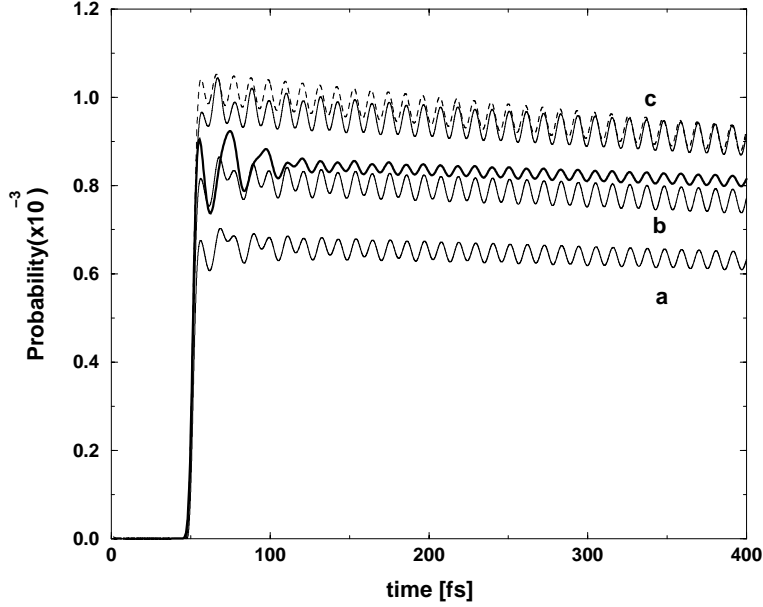


Figure 2.10: Population dynamics of the second excited vibrational level ($J(\omega_{\text{vib}}) = 1.9 \times 10^{-4}/\text{fs}$, $t_c = 30\text{fs}$, $\tau_p = 5\text{fs}$, $\tau_f = 50\text{fs}$). Thick full-line: solution of the non-Markovian QME, dashed-line: solution of the Markovian QME, thin full-lines; solution of Markovian QME with time-dependent Redfield tensor. The initial time t_0 for the propagation with the time-dependent Redfield tensor has been chosen in different ways. Curve a: $t_0 = \tau_f - 5\text{fs}$, curve b: $t_0 = \tau_f - 3.5\text{fs}$, curve c $t_0 = \tau_f - 2.5\text{fs}$.

of dissipation connected with the emission or absorption of a single reservoir oscillator quantum. Obviously, if the expansion of H_{S-R} with respect to Z_ξ is continued higher-order quantum processes may appear.

Anharmonic couplings among nuclear coordinates or normal-mode vibrations represent an ubiquitous phenomenon responsible for IVR, vibrational relaxation, and excitation energy dissipation. The discussion of such types of anharmonicities has a long tradition (see e.g. the more recent paper [KTF94] and references therein). Already in [OF89] some general relations for the incorporation into a density matrix description have been given.

It is the aim of the present section to study a modification of non-Markovian dynamics studied so far induced by such anharmonic couplings. For this reason we will deal with the first non-trivial example which goes beyond relation (1.14). This expression is given as the coupling of a single nuclear coordinate Q representing the system S (we use again dimension-less nuclear coordinate)

to the square of the passive reservoir coordinates, i.e. $H_{S-R} \sim QZ_\xi^2$.

The chosen type of anharmonic coupling can be justified as follows (see also [MK99]). Let us assume the existence of a PES which depends on the set of active-system coordinates R_S and on reservoir coordinates R_R . Then, an expansion of $U(R_S, R_R)$ with respect to the deviations ΔR_R from local equilibrium values $R_R^{(0)}$ can be carried out. The zeroth-order contribution gives the active-system PES. The second-order contribution if diagonalized (together with the kinetic energy part) leads to a harmonic oscillator PES of the reservoir. Using dimensionless normal-mode coordinates Z_ξ we obtain this PES as $\sum_\xi \hbar\omega_\xi(R_S)Z_\xi^2$, where the normal-mode frequencies depend on the active-system coordinates. Next let us reduce the set R_S to the single coordinate Q . Then, a power expansion of the respective $\omega_\xi(Q)$ yields in first order a system-reservoir coupling of type $\sim QZ_\xi^2$, whereas the zeroth order of this expansion leads to the unperturbed reservoir PES entering H_R . Finally, the first-order expansion of $U(R_S, R_R)$ gives a contribution linear with respect to Z_ξ . The given derivation can be put into the following type of system reservoir coupling (present in the excited electronic state φ_e)

$$H_{S-R}^{(e)} = K(Q)\Phi(Z) , \quad (2.44)$$

where $K(Q)$ is linear in Q and the second part reads as

$$\Phi = \sum_\xi \hbar\omega_\xi(g_I(\xi)Z_\xi + g_{II}(\xi)Z_\xi^2) . \quad (2.45)$$

The studies reported below are based on Eq. (2.44) for the system reservoir coupling and extend the investigations on non-Markovian nuclear dynamics in previous sections to the case where two-quantum processes govern the dissipative nuclear dynamics. In particular, we will demonstrate that the term proportional to Z_ξ^2 results in a correlation function which contains a time-independent part. The reasonableness of such a function which mainly determines the structure of the memory kernel entering the non-Markovian Quantum Master Equation (QME) is demonstrated and the breakdown of a Markovian Redfield-theory is shown. As the basic technique to solve the non-Markovian QME we use our Laguerre polynomial expansion method explained in Appendix F.

2.6.1 Non-Linear Coupling

In contrast to an expression where Φ depends linearly on the reservoir coordinates Eq. (2.45) results in a thermal averaged expectation value of Φ which

does not vanish but gives

$$\langle \Phi \rangle_{\text{R}} = \sum_{\xi} \hbar \omega_{\xi} g_{II}(\xi) (1 + 2n(\omega_{\xi})) \quad (2.46)$$

Here,

$$\langle \dots \rangle_{\text{R}} = \text{tr}_{\text{R}} \{ \hat{R}_{\text{eq}} \dots \} \quad (2.47)$$

denotes the thermal average with respect to the reservoir DOF. (\hat{R}_{eq} is the respective equilibrium statistical operator as in previous sections.) The non-vanishing $\langle \Phi \rangle_{\text{R}}$ leads to the appearance of the so-called mean-field term in the QME proportional to $\langle H_{\text{S-R}} \rangle_{\text{R}}$. To allow for excitation energy dissipation via a coupling to the reservoir of passive coordinates, we provide that initially the active coordinate has been prepared in a non-equilibrium state by a photo-excitation process into an excited electronic state. The complete QME governing the dynamics of the excited state the density operator $\hat{\sigma}$ (compare 2.27) ($\equiv \Delta \hat{\rho}_{ee}$) reads

$$\begin{aligned} \frac{\partial}{\partial t} \hat{\sigma}(t) &= -\frac{i}{\hbar} [H_e + \langle H_{\text{S-R}}^{(e)} \rangle_{\text{R}}, \Delta \hat{\sigma}(t)]_- \\ &\quad - \hat{D}(t - t_{\text{field}}; \Delta \hat{\sigma}) + \hat{F}(t, t_{\text{field}}; \mathbf{E}) , \end{aligned} \quad (2.48)$$

where the time argument t_{field} indicates the time region just before the action of the light-pulse. This time argument can be considered as the initial time of the density matrix propagation since we have $\hat{\sigma} = 0$ for $t < t_{\text{field}}$ (note that we will set $t_{\text{field}} = 0$ in the following). The light field enters Eq. (2.48) again via the source term \hat{F} introduced in Appendix D.

A straightforward calculation gives for the correlation function (compare also [OF89])

$$C(t) = C_I(t) + C_{II}(t) . \quad (2.49)$$

The first term on the right-hand side corresponds to the linear part of expansion (2.45) whereas the second term is originated by the quadratic contribution in Eq. (2.45). There is no mixing between both since expectation values of an odd number of reservoir coordinates vanishes. $C_I(t)$ can be written in the standard form [Wei93, MK99]

$$C_I(t) = \int d\omega \, \omega^2 \, e^{-i\omega t} (1 + n(\omega)) (J_I(\omega) - J_I(-\omega)) \quad (2.50)$$

with the Bose–Einstein distribution $n(\omega)$ and the spectral density $J_I(\omega) = \sum_{\xi} g_{\xi}^{(I)2} \delta(\omega - \omega_{\xi})$. For the second contribution to $C(t)$ we get

$$C_{II}(t) = C_{II}^{(1)}(t) + C_{II}^{(2)} . \quad (2.51)$$

The first time–dependent contribution is obtained as

$$\begin{aligned} C_{II}^{(1)}(t) &= \frac{1}{2} \int d\omega \, \omega^2 e^{-i\omega t} (1 + n(\omega/2))^2 \\ &\times (J_{II}(\omega) + J_{II}(-\omega)) , \end{aligned} \quad (2.52)$$

but with the new spectral density $J_{II}(\omega) = \sum_{\xi} g_{II}^2(\xi) \delta(\omega - 2\omega_{\xi})$. The frequency argument $2\omega_{\xi}$ indicates that the considered type of system–reservoir coupling results in relaxation processes where transitions within the spectrum of the active system are accompanied by the emission or absorption of two reservoir quanta. For the second, time–independent part of the correlation function, Eq. (2.51) one obtains

$$C_{II}^{(2)} = \int_0^{\infty} d\omega \, \omega^2 n(\omega/2) (1 + n(\omega/2)) J_{II}(\omega) . \quad (2.53)$$

The absence of any time–dependence shows that $C^{(2)}$, if inserted into the dissipative part of Eq. (2.48) (see Eq. (D.5)), results in a memory extending up to the beginning of the time–evolution. Consequently, such a retarded dissipation has to be considered within the non–Markovian version of the QME. Changing to the Fourier–transformed correlation function $C_{II}(\omega)$ the part $C_{II}^{(2)}$ would become proportional to $\delta(\omega)$. This singular frequency dependence, again, indicates that it cannot be described within a standard Markov approximation of the QME (Redfield theory).

However, the presence of a time–independent part in $C(t)$ does not mean that long–living correlations appear in the reservoir. This becomes obvious if one perturbs the reservoir with a coupling expression like that given in Eq. (2.44), where $K(Q)$, however, has to be understood as an external field and not as a quantum–mechanical operator. Asking for the linear response of the reservoir if the external field K has been applied one ends up with a generalized linear susceptibility (see, for example [MK99]). It is given as $-i\hbar\Theta(t)(C(t) - C(-t))$, where the unit step function $\Theta(t)$ takes notice of causality. Since the anti-symmetrized version of the correlation function enters the susceptibility any contribution of the time–independent part $C_{II}^{(2)}$, Eq. (2.53) is canceled, i.e. the susceptibility goes to zero for $t \rightarrow \infty$.

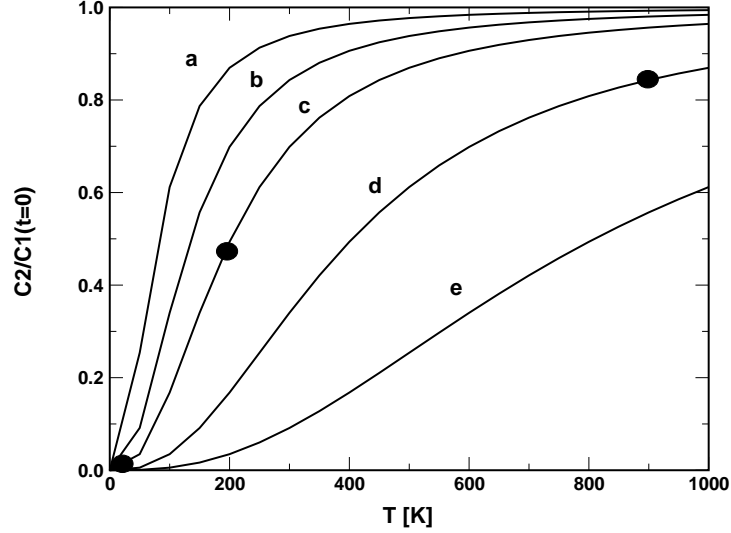


Figure 2.11: Ratio between the time-independent part $C_{II}^{(2)}$ of the correlation function and the time-dependent part $C_{II}^{(1)}(t)$ at time $t=0$ versus temperature and for different values of the correlation time $t_c = 1/\omega_c$: (a) $t_c = 50fs$, (b) $t_c = 30fs$, (c) $t_c = 20fs$, (d) $t_c = 10fs$ and (e) $t_c = 5fs$. Pairs of the correlation time and temperature taken to compute curves in further figures are indicated by a dot.

In the calculations, both spectral densities J_I and J_{II} are used in the common form $J(\omega) = \Theta(\omega)J_0j(\omega)$. The normalized quantity $j(\omega)$ is taken as $1/\omega_c^2 \times \exp(-\omega/\omega_c)$, and $\Theta(\omega)$ denotes the unit step function. The cut-off frequency ω_c mainly determines the memory time of the non-Markovian dynamics. We again denote the inverse of ω_c by t_c and call it correlation time.

Before presenting numerical results we will concentrate on the effect the time-independent part $C_{II}^{(2)}$ causes on the dissipative dynamics. Such a consideration would be most useful if $C_{II}^{(2)}$ dominates on $C_{II}^{(1)}$. According to Eqs. (2.52) and (2.53) this should be the case for higher temperatures. Fig. 2.11 shows the ratio $C_{II}^{(2)}/C_{II}^{(1)}(t=0)$ versus temperature for different $t_c = 1/\omega_c$. Indeed, for $k_B T \ll \hbar/t_c$ the dissipative dynamics are governed by the time-independent part of $C(t)$.

2.6.2 Numerical Results

In this section we calculate the non-Markovian dynamics of the system used also in previous sections i.e. the system consisting of two electronic states (see

Fig. 2.1). For the case where the time-independent part of the correlation function is predominant one can recall the analytical solution we have derived in section 2.4. For the analysis below we will orient on the results obtained on non-Markovian effects in the earlier chapters. There, the interplay has been discussed of optical state preparation, vibrational motion in the excited electronic state, and decay of reservoir coordinate correlations. It could be shown that the most pronounced deviation from non-retarded dynamics is obtained for the case of impulsive excitation. For such an excitation where the length of the light-pulse is short compared to the two other characteristic times the vibrational state populations P_M show characteristic oscillations modulating the redistribution of the probability among different vibrational levels. The doubling of the period characterizing the modulations of P_M just after the excitation process could be identified as a clear signature of retarded, i.e. non-Markovian dynamics. If the pulse length becomes larger or comparable to the vibrational period these modulations vanish but the overall time-dependence of the level populations show just a deviation from that of the Markovian case. In Fig. 2.2 in section 2.4 we have compared the full non-Markovian results for the case of a bilinear coupling and a long correlation time $t_c = 50fs$ with the corresponding Markovian results as well as the analytical solution for the case of an infinitely long correlation time. The system was excited by an infinitely short laser pulse at time $t = 50fs$ and the coupling with the bath in Fig. 2.2 part (a) is chosen so, that we cannot notice any considerable relaxation in our $300fs$ long time window. The non-Markovian results with finite memory show clearly both the features of the analytical solution with infinite memory and those of Markovian theory. Since the relaxation is negligible the differences are reduced to irregularities in the oscillation pattern of the non-Markovian population probabilities.

As already stated, the presence of a time-independent part $C_{II}^{(2)}$ of the correlation function leads to a breakdown of the Markov-approximation. Therefore, it is impossible to compare retarded with non-retarded dynamics. Instead, we use the irregular modulation of the level populations as an indication for the presence of retardation effects. If for a given parameter set temperature is increased we expect the dominance of the irregular modulation of the P_M since $C_{II}^{(2)}$ governs the whole dissipative dynamics.

Thus, in Fig. 2.12 we present the time-dependence of the vibrational level population. To meet conditions near an impulsive excitation we describe the excitation by a laser-pulse of $5fs$ duration, and the correlation time t_c is set equal to $20fs$. The magnitude J_0 of the spectral density (system reservoir coupling strength) has been chosen to observe non-Markovian effects in the dynamics even without the presence of the constant term $C_{II}^{(2)}$. Accordingly

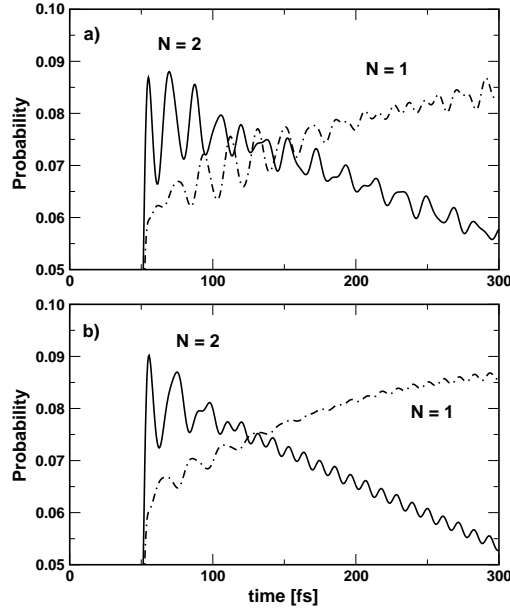


Figure 2.12: Vibrational population dynamics for the parameters: $C_I + C_{II}^{(1)} = 2.2 \times 10^{-41}/fs$ (Fourier-transformed correlation function), $\tau_p = 5fs$, and $t_c = 10fs$. Part (a): $T = 900K$ and Part (b): $T = 10K$. For the chosen parameters the linear coupling to the bath would result in population dynamics not showing any non-Markovian effects similarly to part (b). The modulation of the populations by a frequency $\omega \approx \omega_{vib}/2$ is clearly due to the constant contribution $C_{II}^{(2)}$.

the curves in Fig. 2.12 part (a) valid for the case $k_B T \ll \hbar/t_c$ show a typical non-Markovian behavior (irregular modulation of the populations) surviving up to large times. In contrast, at low temperature the irregular modulation of P_M is only present at an early part of the dynamics. After a sufficiently long time (say from $t \approx 150fs$) the low temperature dynamics in Fig. 2.12 part (b) exhibits the modulation with the frequency typical for Markovian dynamics. Consequently, this offers a clear distinction between Markovian and non-Markovian dynamics.

Another aspect of the given description is the fact that we can observe a non-Markovian behavior even for parameter sets for which the bilinear coupling, Eq. (1.14) or a description where $C_{II}^{(2)}$ has been removed would not show characteristic retardation effects. This indicates that the time-independent term $C_{II}^{(2)}$ is the only source of the non-Markovian effects in this case. In Fig. 2.13 we present respective results for a duration of the laser pulse of $5fs$,

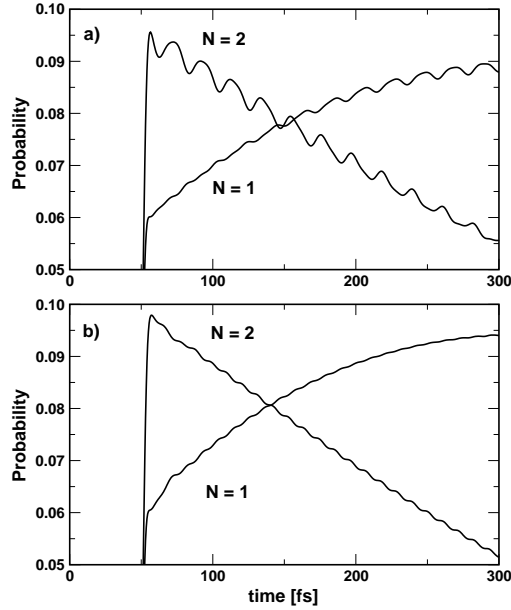


Figure 2.13: The vibrational population dynamics for the parameters $C_I + C_{II}^{(2)} = 2.2^{-41}/fs$ (Fourier-transformed correlation function), $\tau_p = 5fs$, and $t_c = 20fs$. Part (a): $T = 200K$ and Part (b): $T = 10K$. For the sake of clarity we only show the second and the first excited vibrational levels. Non-Markovian effects can also be observed for low temperature, but in the initial part of the dynamics only. The presence of the time-independent part of the correlation function prolongs these effects essentially.

and a correlation time $t_c = 10fs$. In part (a) of this figure, where the temperature equals $900K$ one can observe an irregular modulation of the level populations over the whole time. In the low temperature case ($T = 10K$) as displayed in part (b), however, any irregular modulation is absent and the time-dependence can be well reproduced by means of corresponding Markov-theory. The results obtained at $T = 900K$ while dropping $C_{II}^{(2)}$ (not shown) exhibit the same time-dependence as in the low temperature case. From what was written above we can draw the following general conclusion. Whenever an anharmonic coupling between active and passive coordinates becomes noticeably strong non-Markovian effects may become predominant. And, this would be even the case when a bilinear coupling with a comparable spectral density does not lead to any retardation effect in the course of the dissipative time-evolution.

2.7 Summary of Chapter 2

In Part II of this work we have dealt with the theory of open quantum systems with the particular emphasis on the memory effects. In Chapter 1 we have reviewed the well-known density matrix approach to the theory of open quantum systems, we have introduced the RDO and obtained the time non-local QME. We have also introduced the Markov approximation removing this time non-locality.

The central topic of the Chapter 2 was to study the memory effects in the photo-induced vibration dynamics of molecular systems. After discussing the necessary conditions for the memory effects to appear we introduced the molecular system in section 2.1 consisting of two electronic levels modulated by a single vibrational coordinate. With this model in mind we have shortly discussed the memory effects in frequency domain by deriving the *cw* absorption coefficient in section 2.2. Starting from the section 2.3 we concentrated exclusively on the time-domain memory effects.

In section 2.3 we derived a more convenient form of the QME getting explicitly rid of the initial correlation term. It was also argued that the non-Markovian dynamics after the ultra-fast optical preparation would be similar to the “artificial” dynamics which appears when neglecting the initial system-bath correlation term in the equation of motion involving memory. This is best seen while considering a δ -pulse. In order to see what kind of dynamics we could expect we solve a special case of an infinitely long memory time and excitation by δ -pulse analytically in section 2.4. We have observed an irregular wavepacket motion which can be described as a phase insensitive superposition of two independent wavepackets moving on effective potentials. More importantly, the wavepacket motion results in the oscillations of the vibrational populations which exhibit the frequency equal to the half of the vibrational frequency of the system.

The interplay of the memory effects and the optical state preparation by ultra-fast laser pulses has been studied in section 2.5. By means of the comparison of the results obtained from the full non-Markovian QME with the results following from the Markov approximation we have identified three main memory effects in the vibrational dynamics

- the different layout of the vibrational levels populations in times just after the excitation
- slight change in the life times of the vibrational levels
- change of the amplitude and the period of the oscillations modulating

the overall course of the vibrational level populations

Since in case of an experiment we do not have a comparison with Markovian dynamics only the change of the oscillation period can be taken a characteristics enabling to identify the memory effects independently. The irregular oscillation in the times just after the laser pulse excitation corresponds exactly to that one obtained from the analytical solution in section 2.4. The oscillation period tends to that one of the Markovian dynamics after the time roughly corresponding to the memory time.

Finally, the section 2.6 dealt with the extension of the QME to the case of the non-linear system-bath coupling. It was shown that the chosen form of the non-linearity leads to a constant part of the correlation function and thus to the survival of the memory effects to long times. The calculation suggested that in case of the strong non-linear system-bath coupling non-Markovian effects may become predominant.

The memory effects found in Chapter 2 are the most pronounced for the case of the impulsive excitation. For this case an alternative description using the time-dependent Redfield tensor has been found reproducing non-Markovian results quite well. For the finite laser pulses the correspondence of the results has been worse, but the memory effects become less pronounced, on the other hand. Thus, one may conclude, that unless there have to be large non-Markovian effects expected or the computational effort to solve non-Markovian equations is reduced the practical simulations of the photo-induced molecular dynamics may be successfully done within a (special type of) Markovian QME.

The memory effects identified in the dynamics of the studied system can be related to the effective redefinition of the initial state by the action of an ultrafast laser field. The effects appear as the reaction of the system on this sudden change which the system “remembers” at least for the memory time t_{mem} . In the regime of the weak system-bath interaction (which is the only valid here because of the usage of the second order perturbation theory with respect to the system-bath coupling in QME) such a sudden change cannot be induced by the dissipative part. Thus, one can conclude that in case of a weak dissipation the only non-Markovian effects possibly observable are those induced by ultra-fast external fields.

In the next part (Part III) of this work the optimal control theory is applied on the dissipative systems within the Markovian approximation. The generalization to include the memory effects is the next logical step in the construction of the theory and a corresponding formulation will be also done in Part III. The inclusion of the memory into the optimal control theory becomes necessary whenever the resulting optimal fields show ultrafast features.

Part III

External Field Control of Open Quantum Systems

Chapter 3

Laser Pulse Control of Molecular Dynamics

The suggestion to the control molecular dynamics by means of ultrashort laser pulses dates back to the middle of the eighties. First control schemes have been results of more or less completely theoretical considerations. A comprehensive overview on all attempts discussed so far has been given recently in [RZ00]. The effort invested into the laser pulse control of the molecular dynamics is mainly motivated by a prospect of the control of chemical reactions [RdVRMK00]. One expects to be able to selectively induce distinct channels of a chemical reaction to enhance the yield of special reaction products and to suppress unwanted ones. This goal should be achieved by means of specially tailored laser pulses. The idea is usually nicely depicted by a simple *ABC* model (Fig. 3.1). We start with the molecule consisting of a bond state of three components *A*, *B*, *C* and we aim to selectively induce a reaction yielding either a molecule *AB* and separate fragment *C* or a molecule *AC* and a fragment *B*.

Originally, several different approaches to the laser pulse control have been suggested, using several different mechanisms to achieve the control goal. In their pioneering work Tannor, Kosloff, and Rice [TKR86] suggested so-called *pump-dump* scheme. Here, the molecular system is first excited electronically by a short *pump* pulse. Such a short laser pulse has correspondingly broad frequency spectrum and enables to excite a coherent superposition of several vibrational levels in the excited electronic state. This yields a creation of a wavepacket in a non-equilibrium position on the PES of the excited electronic state and subsequent motion of the wavepacket on a given PES. The system evolves freely on the excited PES and after a particular delay t_d it is de-excited using a second (*dump*) laser pulse. The delay time t_d is chosen in such a manner, that the wavepacket has a convenient position in order to make a transition

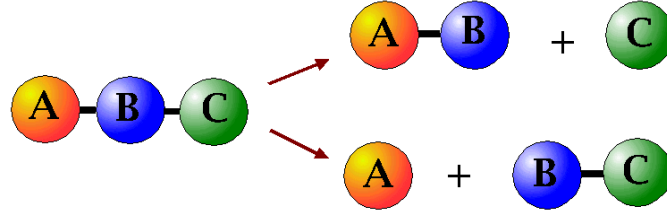


Figure 3.1: Example of the control of chemical reaction. The laser pulse should selectively drive the system into a given reaction channel.

into a desired reaction channel. On Figure 3.2 this mechanism is demonstrated for a one-dimensional PES.

A different control scheme this time using continuous lasers has been proposed by Brumer and Shapiro. It uses the phase relation between two laser fields to vary the population ratio between two energetically degenerated levels [BS86]. The basic idea is that if one finds two independent pathways that connect the same initial and final states of the system, one can modulate the probability of the population of a specific final state. This is possible because the probability of the transition from the initial to the final state is proportional to the square of the sum of the amplitudes associated with the individual transitions. As an example one can deal with a single- and three-photon excitation as it is depicted on Fig. (3.3). The control is performed by the laser pulse with frequency 3ω for the resonant excitation and the laser pulse with the frequency ω for three-photon excitation. The target states are denoted $|e\rangle$ and $|e'\rangle$. The probability of the transition from the initial state to the final state $|e\rangle$ with the energy E can be written as

$$W(e, E) = W_1(e, E) + W_3(e, E) + W_{13}(e, E). \quad (3.1)$$

Here, $W_1(e, E)$ and $W_3(e, E)$ represent the probabilities of the one-photon and three-photon transitions, respectively, and $W_{13}(e, E)$ represents an interference term rising from the simultaneous one-photon and three-photon transitions. In the weak field regime it can be shown [SB92] that $W_{13}(e, E)$ depends on the difference $\theta_3 - 3\theta_1$, where θ_1 and θ_3 are the phases of the radiation field of the one-photon and three-photon transitions, respectively. Because the interference term of the transition probabilities to the individual states depends on the mutual phase of the laser fields the ratio

$$R(e, e') = \frac{W(e, E)}{W(e', E)} \quad (3.2)$$

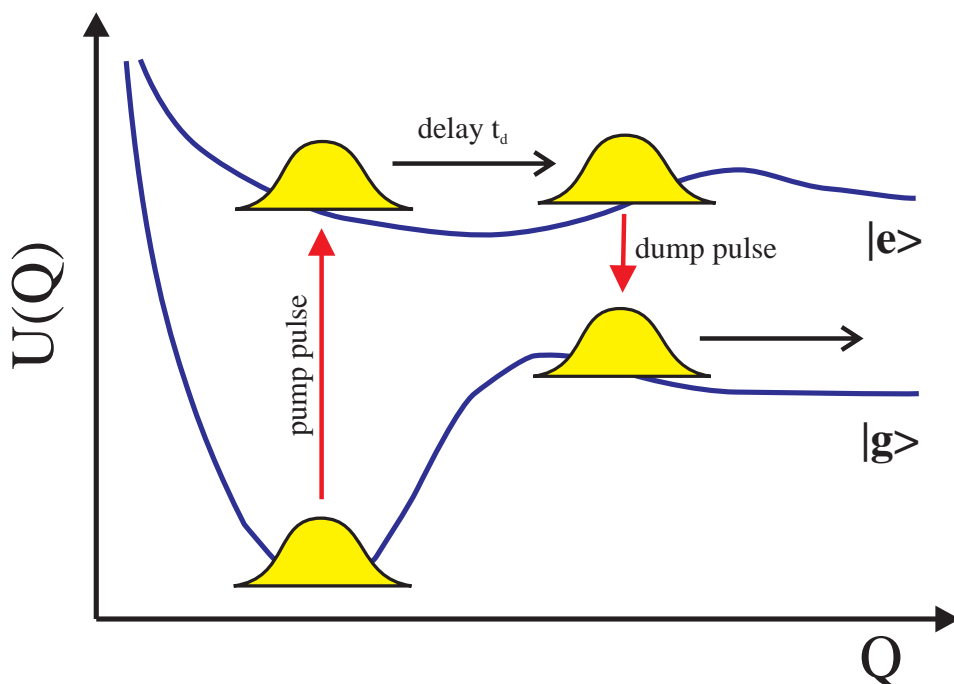


Figure 3.2: Example of the control by the *pump-dump* scheme. To dissociate the molecule one can use two transitions (red arrows) between the ground and the excited state. First, pump pulse creates a wavepacket on the excited PES. After a delay time t_d the position of the wavepacket is suitable for the second transition accomplished by the dump pulse. It results in a non-equilibrium position of the wavepacket on the ground state PES leading to the dissociation of the molecule.

may be changed within some interval by shifting those phases.

Both above discussed schemes have been developed theoretically and require the knowledge of the PES of the molecular system to be controlled. They are characterized by a small number of control parameters which may be varied to optimize the probability of the formation of the desired product of the reaction. Indeed, both Tannor–Rice and Brumer–Shapiro schemes have been verified experimentally [HCP⁺00] (or see [RZ00] and references therein).

The theory of laser–pulse control has been finally put into a universal frame in suggesting the so-called Optimal Control (OC) theory by Rabitz and coworkers [PDR88, SWR88]. The OC theory is based on a certain functional which extremum has to be found. Once this extremum has been calculated the shape is known of the laser pulse which drives the system in a desired manner. The

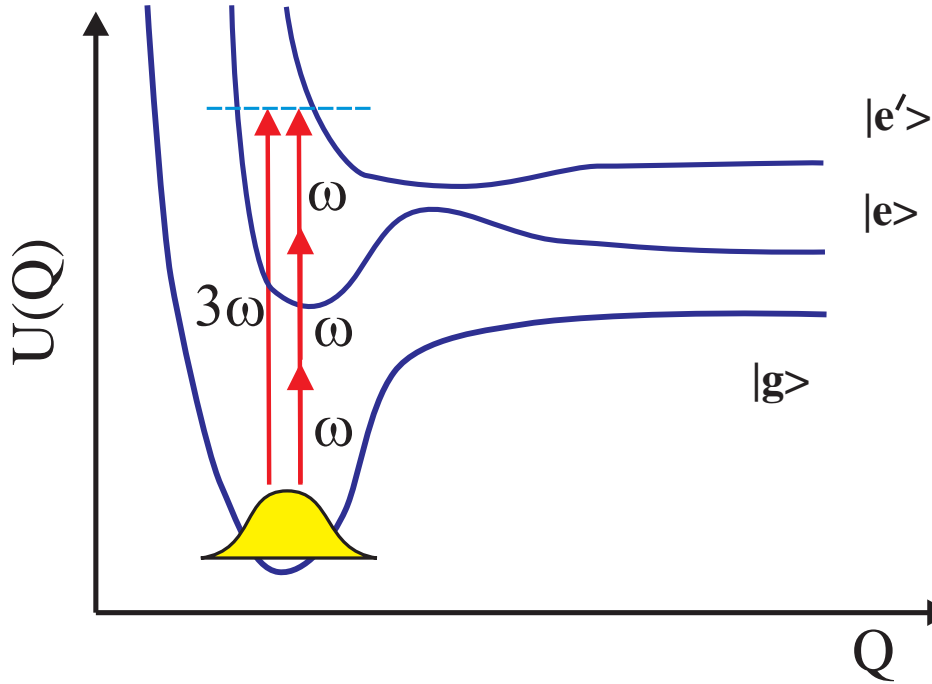


Figure 3.3: Control of dissociation into two different product states.

functional consists of the expectation value of the observable one wants to maximize (e.g. the population of a particular state) at a certain time, and a constrain which restricts the pulse energy to a finite value. It is believed that the above discussed direct control schemes can be reproduced by the OC theory when applying suitable constrains on the laser field. It will be demonstrated in this work for the case of Tannor-Rice scheme [TKR86].

Originally, the OC theory has been formulated for gas-phase systems which dynamics are governed by the time-dependent Schrödinger equation [PDR88, SWR88]. A formulation for mixed states could be already achieved in Ref. [YGW⁺93]. The extension to reduced state dynamics of an open quantum system has been given in [BKT93], and recently in [YOR99] by extending the efficient iteration scheme of Refs. [ZBR98, ZR98].

Also the experiments on femtosecond laser-pulse control of molecular dynamics became a subject of an active physico-chemical research [BG95, Zew97, Wil99]. Most of the work has been concentrated on the central idea of controlling chemical reactions resulting in a destruction or formation of a selected chemical bound. And indeed, a number of promising examples already exists even in the condensed phase [BDNG00]. While direct strategies according to

the above discussed schemes to achieve the control goal have been applied in an earlier state of this research (see [RZ00] and references therein) it was an experimental breakthrough to use highly flexible optical pulse shaping systems combined with self-learning algorithms as suggested in [JR92b]. Such techniques have been used for a broad variety of problems, among others for the control of fluorescence yields in dye molecules [BYW⁺97], to control yield of molecular photodissociation reactions [ABB⁺98, BBK⁺99, DFG⁺01], to control atomic two-photon transitions [MS98], to tailor atomic wavefunctions [WAB99], to excite selective molecular vibrations [WWB99] or to increase the efficiency of high-harmonic generation [BBz⁺00]. Beside the applications on the field of OC, the techniques developed to shape laser pulses and to use them for automatic optimal control experiments found also technological applications in telecommunications [WK98], in automated compression of ultrashort laser pulses [YMS97, BBS⁺97, EMB⁺98] or in multi-photon imaging techniques [BYS⁺99].

Although this type of approach found a widespread experimental application the use of self-learning algorithms in theory would remain on a preliminary level. This is because of the enormous amount of computational time necessary for carrying out the multitude of dynamic propagations. Consequently, it is much more appropriate to apply the OC theory whenever a control experiment has to be simulated.

The optimal laser fields obtained from the OC theory are usually characterized by a high complexity in contrast to the direct strategies as e.g. the pump-dump scheme. They may appear in the form of a complicated train of pulses with single features as short as few femtoseconds. It is almost certainly a difficult task to create such pulses experimentally. Clearly, there is a lack of any restriction on the form of the optimal pulse in the standard formulation of OC theory we will present in the next section. This is an advantage against the experimental approach with self-learning algorithms while searching for new control pathways but creates a significant obstacle for the application of the theoretical results in the experiments. Thus, the theory and experiment could not easily benefit from the advances of each other and their developments proceeded relatively independently in the past. This resulted in a significant incompatibility between both approaches. Namely, due to the different methodology the conditions put on the optimal search in the experiment and the theoretical considerations differ substantially. While in the initial stage the research on the OC of molecular dynamics has concentrated on developing the methods of control and proving the controllability as such, recently efforts have been done to bring the experimental and theoretical approaches into closer cooperation [HMdVR01, HMdVR02, MM02].

It will be the aim of the following sections to formulate a general OC theory for the systems exhibiting dissipative dynamics and to study the possibility of their control by means of short laser pulses. Concerning the applicability of the theoretical results in OC experiments we will also discuss a standard experimental set-up for OC experiments and the ways of adapting the OC theory to the experimental conditions. First, in Chapters 3, 4 we concentrate on the prospects of the OC of electron transfer (ET) reactions also including the dissipative influence of the environment on the controlled dynamics. To this end we formulate the general OC for density matrix in Chapter 3 and apply it on diverse ET systems in Chapter 4. In Chapter 5 we introduce several generalizations of the OC and in Chapter 5 we discuss an example of the experimental set-up for OC experiments and its theoretical description and also formulates the OC theory in order to meet the requirements for the successful simulation of the OC experiments. In particular we address the problem of static disorder in the molecular ensemble and the optimization of the probe signal in the pump-probe experiment. The discussion from Chapter 5 enables us to define certain notion of the complexity of the control task presented in section 5.2. Finally, to connect the OC theory for dissipative dynamics with Part II of this work we formulate the OC theory for non-Markovian dynamics in section 5.4.

3.1 Optimal Control Scheme for Dissipative Molecular Dynamics

The aim of this section is to derive an effective optimal control scheme valid for the optimization of the the control yields in open quantum systems. To this end we start with the most general type of OC theory, i.e. the formulation for a density operator [YOR99]. A reduction to mixed or pure state dynamics of closed system is straightforward and will be presented in the next section.

The time evolution of the density matrix has been discussed in detail in section (1.2). There, several types of dissipative dynamics have been studied with particular emphasis on memory effects. It was show there that these effects really induce different dynamics for the case of the system interaction with short laser pulses. On the other hand it became clear that in many cases their influence is not dramatic and some of them can be even reproduced by a certain corrections within the Markov theory. Also, to include memory effects proofed to be a very difficult task. Therefore, we will concentrate on the Markovian dynamics and thus omit the memory effects as well as the influence of the laser field on the dissipative part of the equation of motion. A possible

generalization of the OC theory for the case of the non-Markovian dynamics will be given in section 5.4.

Thus, the equation of motion for the reduced density matrix of the system to control reads

$$\frac{\partial}{\partial t}\hat{\rho}(t) = -i\mathcal{L}_{\text{mol}}\hat{\rho}(t) - i\mathcal{L}_{\text{F}}(t)\hat{\rho}(t) - \mathcal{D}\hat{\rho}(t) . \quad (3.3)$$

Here, we comprised the whole dissipative influence of the thermodynamic reservoir into a superoperator \mathcal{D} . Its concrete form follows from the QME formulation in the Markov approximation (see section 1.3 and Appendix I. The system Hamiltonian is divided into a part describing the molecular system itself H_{mol} and its interaction with the radiation field $H_{\text{F}}(t)$. The \mathcal{L}_{mol} and \mathcal{L}_{F} are the Liouville superoperators corresponding to the commutators with H_{mol} and $H_{\text{F}}(t)$, respectively. The time evolution of the reduced density operator can be expressed using the time evolution superoperator $\mathcal{U}(t, t_0, \mathbf{E})$ as

$$\hat{\rho}(t) = \mathcal{U}(t, t_0; \mathbf{E})\hat{\rho}(t_0) . \quad (3.4)$$

As we have already mentioned in the introduction to this chapter, the OC of molecular dynamics is usually formulated as the task to realize at a certain final time t_f the expectation value

$$O(t_f) = \text{tr}_S\{\hat{O}\hat{\rho}(t_f)\} \quad (3.5)$$

of the observable described by the (hermitian) quantum mechanical operator \hat{O} . To get $O(t_f)$ one applies a field pulse $\mathbf{E}(t)$ which should drive the system in the required manner (the optimal pulse). According to [YGW⁺93] the optimal pulse is defined as the extremum of the following functional

$$J(t_f; \mathbf{E}) = O(t_f; \mathbf{E}) - \frac{1}{2} \int_{t_0}^{t_f} dt \lambda(t) \mathbf{E}^2(t) , \quad (3.6)$$

where the second term on the right-hand side guarantees an upper limitation of the field intensity. (The penalty factor $\lambda(t)$ has been taken time-dependent to avoid a sudden switch on and switch off of the control field [SdVR99].) A slightly different version of the functional has been suggested by Rabitz [ZBR98, ZR98, YOR99], who used a somewhat larger expression which ensures the use of the correct dynamic equations. In the present approach, however, the concrete dynamic equation to be used is already fixed by the demand how to determine $O(t_f)$, Eq. (3.5).

In order to determine the extremum one sets the functional derivative of J with respect to \mathbf{E} equal to zero. One obtains (details of the derivation are given in the Appendix H)

$$\mathbf{E}(t) = \frac{1}{\lambda(t)} \frac{\delta O(t_f)}{\delta \mathbf{E}(t)} = \frac{\mathbf{K}(t_f, t; \mathbf{E})}{\lambda(t)}. \quad (3.7)$$

This expression has to be understood as a self-consistency relation for the optimal field. The actual value of the field at time t becomes proportional to the change of $O(t_f)$ with respect to the field-strength at this time. The quantity

$$\mathbf{K}(t_f, t; \mathbf{E}) = \frac{i}{\hbar} \text{tr}_S \{ \hat{O} \mathcal{U}(t_f, t; \mathbf{E}) \mathcal{M} \mathcal{U}(t, t_0; \mathbf{E}) \hat{\rho}(t_0) \} \quad (3.8)$$

is called the (vectorial) control kernel and depends on \mathbf{E} in a highly nonlinear manner. The kernel is obtained by propagating in a first step the reduced density operator (under the presence of the external field) from the initial time t_0 up to an intermediate time $t \leq t_f$. Then, the commutator with respect to the dipole operator is calculated (abbreviated here by the action of the dipole superoperator $\mathcal{M} \dots = (\hat{\mu}, \dots)_-$). Afterwards, the result has to be propagated from t to the final time t_f where the operator \hat{O} acts. According to Eq. (3.7) the control kernel has to be calculated in such a manner that it coincides (despite the prefactor $1/\lambda$) with the field. If this became possible the optimal field has been determined.

Obviously, one needs a certain iteration procedure to solve Eq. (3.7). A direct iteration of Eq. (3.7) has been proposed in [YGW⁺93]. Its inconvenience and sometimes inability to achieve convergency has been discussed in literature [ZBR98, ZR98, YOR99]. In these works the theory has been used to investigate just a few level systems. The approach has been generalized for larger systems in [MM01] and applied for electron transfer problems in [MKM02].

For this reason the control kernel is rewritten as

$$K(t_f, t; \mathbf{E}) = \frac{i}{\hbar} \text{tr}_S \{ \hat{\sigma}(t; \mathbf{E}) \mathcal{M} \hat{\rho}(t; \mathbf{E}) \}, \quad (3.9)$$

where the two time-dependent operators $\hat{\sigma}(t; \mathbf{E})$ and $\hat{\rho}(t; \mathbf{E})$ are propagated separately up to the intermediate time t . The operator at the left part of the trace is given as

$$\hat{\sigma}(t; \mathbf{E}) = \tilde{\mathcal{U}}(t_f, t; \mathbf{E}) \hat{O}. \quad (3.10)$$

It comprises a reverse propagation from the final time t_f up to the intermediate time starting with \hat{O} at $t = t_f$. The time-evolution superoperator $\tilde{\mathcal{U}}$ is discussed in some more detail in Appendix I.

This separate propagation of $\hat{\sigma}$ and $\hat{\rho}$ is used to establish an efficient iteration procedure [YOR99]. Therefore, the explicit appearance of the control field \mathbf{E} via the term proportional to $\mathcal{L}_F(t)$ is removed in the equations for $\hat{\rho}$ and $\hat{\sigma}$ in using Eqs. (3.7) and (3.9) for the control kernel. As a result a coupled set of nonlinear equations of motion is obtained

$$\begin{aligned} \frac{\partial}{\partial t} \hat{\rho}(t) &= -i\mathcal{L}_{\text{mol}}\hat{\rho}(t) - \mathcal{D}\hat{\rho}(t) \\ &- \frac{1}{\hbar^2\lambda(t)} \text{tr}_S\{\hat{\sigma}(t)\mathcal{M}\hat{\rho}(t)\} \mathcal{M}\hat{\rho}(t) , \end{aligned} \quad (3.11)$$

and

$$\begin{aligned} \frac{\partial}{\partial t} \hat{\sigma}(t) &= -i\mathcal{L}_{\text{mol}}\hat{\sigma}(t) + \tilde{\mathcal{D}}\hat{\sigma}(t) \\ &- \frac{1}{\hbar^2\lambda(t)} \text{tr}_S\{\hat{\sigma}(t)\mathcal{M}\hat{\rho}(t)\} \mathcal{M}\hat{\sigma}(t) . \end{aligned} \quad (3.12)$$

Here, the coupling via the field \mathbf{E} is replaced by Eq. (3.7) i.e by a coupling via the terms being nonlinear in both density operators. These nonlinearities ensure a feedback of the dynamics of $\hat{\rho}$ as well as $\hat{\sigma}$ via the field-term on itself. Since the equation for $\hat{\sigma}(t)$ has to be propagated in reverse time order, i.e. from t_f to earlier times t a simultaneous solution of the Eqs. (3.11) and (3.12) is not possible. The iteration procedure [ZBR98, ZR98, YOR99] is based on the idea to determine, e.g. $\hat{\sigma}(t)$ appearing in Eq. (3.11) for $\hat{\rho}(t)$ separately. Then, Eq. (3.11) for $\hat{\rho}(t)$ is closed and an approximate version for $\hat{\rho}(t)$ can be computed. Inserting this $\hat{\rho}(t)$ together with the used form for $\hat{\sigma}(t)$ into Eq. (3.7) an approximate form of the optimal field has been obtained, too. (Note that the role of $\hat{\sigma}(t)$ and $\hat{\rho}(t)$ can be interchanged in the present scheme.)

The given procedure is based on the following n'th order iteration step for $\hat{\rho}$ ($n > 0$)

$$\begin{aligned} \frac{\partial}{\partial t} \hat{\rho}^{(n)}(t) &= -i\mathcal{L}_{\text{mol}}\hat{\rho}^{(n)}(t) - \mathcal{D}\hat{\rho}^{(n)}(t) \\ &- \frac{1}{\hbar^2\lambda(t)} \text{tr}_S\{\hat{\sigma}^{(n-1)}(t)\mathcal{M}\hat{\rho}^{(n)}(t)\} \mathcal{M}\hat{\rho}^{(n)}(t) , \end{aligned} \quad (3.13)$$

where $\hat{\sigma}^{(n-1)}(t)$ is the result of the foregoing iteration step. In a similar manner we obtain for $\hat{\sigma}^{(n)}(t)$

$$\begin{aligned} \frac{\partial}{\partial t} \hat{\sigma}^{(n)}(t) &= -i\mathcal{L}_{\text{mol}}\hat{\sigma}^{(n)}(t) + \tilde{\mathcal{D}}\hat{\sigma}^{(n)}(t) \\ &- \frac{1}{\hbar^2\lambda(t)} \text{tr}_S\{\hat{\sigma}^{(n)}(t)\mathcal{M}\hat{\rho}^{(n)}(t)\} \mathcal{M}\hat{\sigma}^{(n)}(t) . \end{aligned} \quad (3.14)$$

The zero-order approximation for $\hat{\rho}$ follows by replacing the optimal field term by a concrete field expression

$$\begin{aligned} \frac{\partial}{\partial t} \hat{\rho}^{(0)}(t) &= -i\mathcal{L}_{\text{mol}} \hat{\rho}^{(0)}(t) - \mathcal{D} \hat{\rho}^{(0)}(t) \\ &+ \frac{i}{\hbar} \mathbf{E}(t) \mathcal{M} \hat{\rho}^{(0)}(t) , \end{aligned} \quad (3.15)$$

Every iteration step produces two approximation of the optimal field. The first reads

$$\mathbf{E}^{(n)}(t) = \frac{i}{\hbar \lambda(t)} \text{tr}_S \{ \hat{\sigma}^{(n-1)}(t) \mathcal{M} \hat{\rho}^{(n)}(t) \} . \quad (3.16)$$

If $\hat{\sigma}^{(n-1)}(t)$ is replaced by the n'th iteration $\hat{\sigma}^{(n)}(t)$ the second approximation for the field is obtained. The fast convergence of this iteration could be demonstrated in [YOR99].

3.2 Restriction to Mixed and Pure-State Dynamics

The control scheme explained in the foregoing section provides the introduction of a RDO and is based on dynamic equations including dissipation. Neglecting any coupling to the environment the scheme can be easily specified to closed system dynamics characterized by pure or mixed states. Therefore, the reduced density operator will be identified with the complete statistical operator $\hat{W}(t)$ of a closed system. In such a case the time evolution superoperator introduced in Eq. (3.4) is reduced to

$$\hat{W}(t) = \mathcal{U}(t, t_0; \mathbf{E}) \hat{W}(t_0) \equiv U(t, t_0; \mathbf{E}) \hat{W}(t_0) U^\dagger(t, t_0; \mathbf{E}) \quad (3.17)$$

with the ordinary time-evolution operator $U(t, t_0; \mathbf{E})$ defined via the system Hamiltonian $H_S = H_{\text{mol}} + H_F(t)$. For the initial value of the statistical operator we use the canonical equilibrium form written here via an expansion with respect to the *eigenstates* $|\psi_\alpha\rangle$ of H_{mol} (f is the thermal distribution versus the *eigenenergies* E_α)

$$\hat{W}(t_0) = \hat{W}_{\text{eq}} = \sum_{\alpha} f(E_\alpha) |\psi_\alpha\rangle \langle \psi_\alpha| . \quad (3.18)$$

The pure state version of $\hat{W}(t_0)$ is given by $|\psi_{\text{ini}}\rangle \langle \psi_{\text{ini}}|$, where $|\psi_{\text{ini}}\rangle$ is the state vector of the initial pure state.

The reduction of \mathcal{U} to the action of ordinary time-evolution operators enables a rearrangement of the various terms in Eq. (3.8) with the following result

$$\begin{aligned} \mathbf{K}(t_f, t; \mathbf{E}) = & \\ - \frac{2}{\hbar} \text{Im} \text{tr} \{ & U^+(t_f, t_0; \mathbf{E}) \hat{O} U(t_f, t; \mathbf{E}) \hat{\mu} U(t, t_0; \mathbf{E}) \hat{W}(t_0) \} . \end{aligned} \quad (3.19)$$

Introducing Eq. (3.18) and carrying out the trace gives

$$\mathbf{K}(t_f, t; \mathbf{E}) = -\frac{2}{\hbar} \sum_{\alpha} f(E_{\alpha}) \text{Im} \{ \langle \Theta_{\alpha}(t) | \hat{\mu} | \psi_{\alpha}(t) \rangle \} , \quad (3.20)$$

where we defined

$$| \psi_{\alpha}(t) \rangle = U(t, t_0; \mathbf{E}) | \psi_{\alpha} \rangle , \quad (3.21)$$

and

$$| \Theta_{\alpha}(t) \rangle = U(t, t_f; \mathbf{E}) \hat{O} | \psi_{\alpha}(t_f) \rangle . \quad (3.22)$$

The state $| \psi_{\alpha}(t) \rangle$ is obtained as the propagation according to the time-dependent Schrödinger equation of one of the states $| \psi_{\alpha} \rangle$ (but, as indicated, with the inclusion of the radiation field). The index α gives a hint on the particular initial state. In contrast, the state $| \Theta_{\alpha}(t) \rangle$ is the result of a reverse propagation from t_f to the earlier time t starting with $\hat{O} | \psi_{\alpha}(t_f) \rangle$ as the initial state. Therefore, this propagation requires the complete propagation of $| \psi_{\alpha}(t) \rangle$ up to $t = t_f$.

In similarity to the general scheme given in the forgoing section we introduce the iteration procedure to determine the optimal pulse. We start with a zero-order solution for $| \psi_{\alpha}(t) \rangle$ in solving the time-dependent Schrödinger equation corresponding to Eq. (3.21) with an arbitrary chosen field pulse $\mathbf{E}(t)$. Having this zero-order solution one can determine the n 'th order ($n > 0$) solution by an iteration procedure where the n 'th iteration step is given by (mixed state version of Eqs. (3.13) and (3.14))

$$\begin{aligned} i\hbar \frac{\partial}{\partial t} | \psi_{\alpha}^{(n)}(t) \rangle &= H_{\text{mol}} | \psi_{\alpha}^{(n)}(t) \rangle + \frac{2}{\hbar \lambda(t)} \sum_{\beta} f(E_{\beta}) \\ \text{Im} \{ \langle \Theta_{\beta}^{(n)}(t) | \hat{\mu} | \psi_{\beta}^{(n)}(t) \rangle \} \hat{\mu} &| \psi_{\alpha}^{(n)}(t) \rangle , \end{aligned} \quad (3.23)$$

and

$$\begin{aligned} i\hbar \frac{\partial}{\partial t} | \Theta_{\alpha}^{(n)}(t) \rangle &= H_{\text{mol}} | \Theta_{\alpha}^{(n)}(t) \rangle + \frac{2}{\hbar \lambda(t)} \sum_{\beta} f(E_{\beta}) \\ \text{Im} \{ \langle \Theta_{\beta}^{(n)}(t) | \hat{\mu} | \psi_{\beta}^{(n-1)}(t) \rangle \} \hat{\mu} &| \Theta_{\alpha}^{(n)}(t) \rangle , \end{aligned} \quad (3.24)$$

m	$U_m^{(0)} - U_g^{(0)}$	$\hbar\omega_{\text{vib}}$	$Q^{(m)}$
g	0	0.1 eV	0
e	2 eV	0.1 eV	2.1

Table 3.1: Parameters of the PES of the diatomic model molecule used to test the appearance of the pump-dump scheme in OCT.

with

$$|\Theta_\alpha^{(n)}(t_f)\rangle = \hat{O}|\psi_\alpha^{(n-1)}(t_f)\rangle. \quad (3.25)$$

Since for $n = 1$ the zero-order solution $|\psi_\alpha^{(0)}(t)\rangle$ already exists the initial value, Eq. (3.25) for the first iteration of $|\Theta_\alpha(t)\rangle$ is well defined, and Eq. (3.23) (for $n = 1$) can be solved, too. Proceeding in this manner fast convergency can be achieved [YOR99]. For every iteration step two approximations for the optimal field can be given, either

$$\mathbf{E}^{(n)}(t) = -\frac{2}{\hbar\lambda(t)} \sum_\alpha f(E_\alpha) \text{Im}\langle\Theta_\alpha^{(n)}(t)| \hat{\mu} |\psi_\alpha^{(n-1)}(t)\rangle, \quad (3.26)$$

and a somewhat improved expression with $|\psi_\alpha^{(n)}(t)\rangle$ instead of $|\psi_\alpha^{(n-1)}(t)\rangle$.

3.3 Reappearance of the *Pump-Dump* Scheme in the Optimal Control Theory

In order to demonstrate the compatibility of the OC equations derived in the previous section with the control schemes discussed at the beginning of this chapter, we apply them to a simple control problem in a diatomic molecule. The control task will be to create a wavepacket in a non-equilibrium position on the ground state PES at a certain time t_f . According to our previous discussion, this should lead to the *pump-dump* scheme of [TKR86].

We employ the simplest model of a diatomic molecule assuming only the ground and the first excited electronic states $|\varphi_g\rangle$ and $|\varphi_e\rangle$, respectively, with corresponding electronic energies E_g and E_e to be of importance. The PES corresponding to each electronic level are supposed to be harmonic with the same frequency ω . Thus, the system Hamiltonian can be taken in the form (2.1) and (2.2). We use again the well-known dimensionless coordinates Q (see [MK99]) for the harmonic PES. The coupling to the laser field is realized via

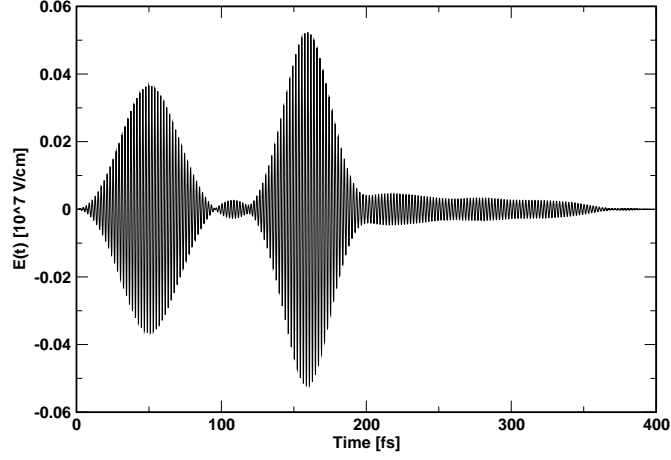


Figure 3.4: The optimal pulse as a solution of the control task from the section 3.3. One immediately notices the double pulse structure characteristic for the *pump-dump* control scheme.

the term (2.3). In the present calculations we set the transition dipolemoment between the states $|\varphi_g\rangle$ and $|\varphi_e\rangle$ to be equal $1D$. The parameters used in our calculation are summarized in Table 3.3.

We assume that the molecule is initially in the electronic and vibrational ground state. The control task will be now to shift the ground state wavepacket (having the Gaussian form) from its equilibrium position at $Q = 0$ into a new position on the electronic ground state PES. For our example we choose $Q_{\text{shift}} = 4.2$. The wavepaket should arrive at the target position at some time t_f . Since the coupling between the laser field and the molecule connects the ground- and excited electronic level the population transfer will certainly proceed over the excited electronic state. In other words, we work with the optical laser fields, so that any possible coupling among the vibrational levels is irrelevant for the control task. But notice that in this formulation of the OC theory there is no limitation on the resulting optimal field to the optical region. If our Hamiltonian would include coupling to the laser field connecting the vibrational levels within the same electronic level the optimal field would include the corresponding infra-red transition frequencies. The absence of such a coupling can be understood as the additional restriction of the OC to the optical fields.

Working with the optical fields the conditions for obtaining the optimal pulse in form of the *pump-dump* scheme are fulfilled. Indeed, in Figure 3.4 we observe the desired pattern of two pulses and also the electronic populations

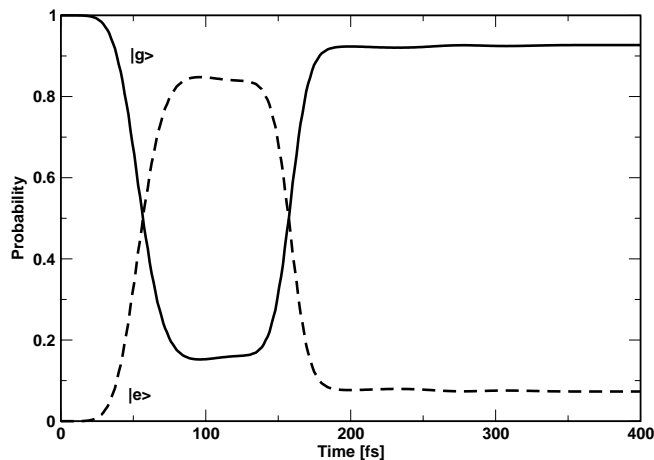


Figure 3.5: Electronic populations corresponding to the Fig. 3.4. The time dependence of the populations confirms the *pump-dump* nature of the control mechanism.

on Figure 3.5 display a characteristic time evolution which also confirms the character of the first pulse as *pump* and the second one as *dump* pulse, respectively. The yield of the reaction is in this case about 60% which is less than one may expect. The reason is the chosen value of the target time t_f . We have chosen t_f to correspond to the oscillation frequency of the wavepacket on the excited PES in order to allow for no more than one cycle of the wavepacket on the excited PES and thus also for no more than one cycle of the *pump-dump* scheme.

Similarly, it should be possible to obtain also other previously discussed direct control schemes from the OC theory using a proper molecular model and a proper restriction of the OC algorithm. Moreover, if these schemes do not appear in OC calculation it may also mean that in the case they have been previously used, other more effective ways of controlling the system exist. These should of course be found by OC theory. In this way we have demonstrated (at least for one predicted control scheme) that the previous development towards controlling the molecular dynamics is consistent with the OC theory.

For the same target state to be reached and the same arrangement with the relative shift $Q_{shift} = 4.2$ but with the target time 10 times longer the optimal field changes dramatically. The result is plotted in Fig. 3.6. Here, the pulse consists of many repeating cycles of the previous scheme. This can be also confirmed by looking at the populations of the electronic states presented of Fig. 3.7. This suggests that for different control schemes the characteristic

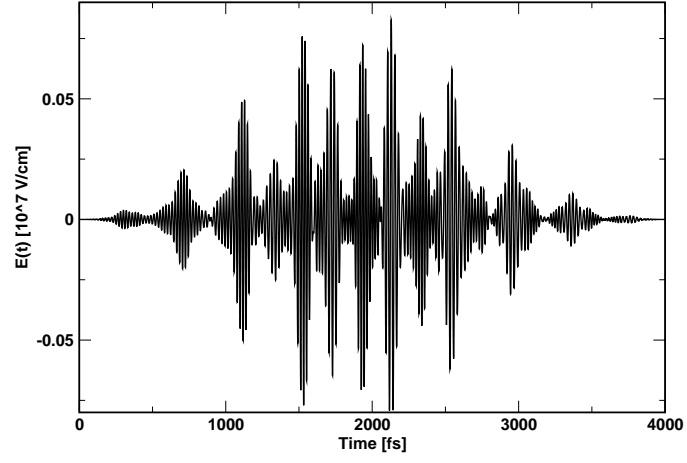


Figure 3.6: *Pump-dump* scheme for large target times t_f . The OC field consists of many cycles similar to those on Fig. 3.4.

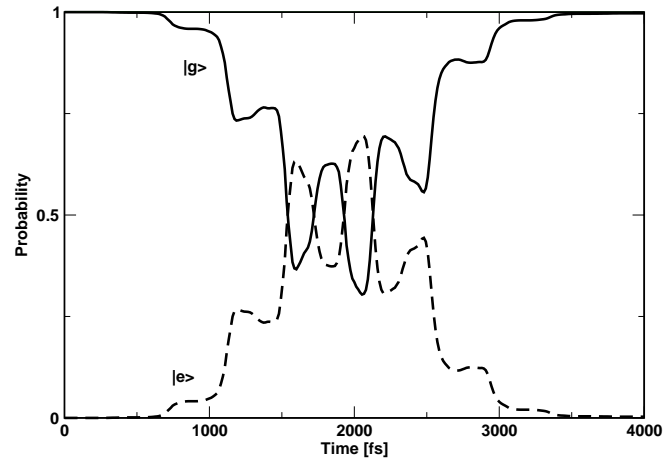


Figure 3.7: Populations in the *pump-dump* scheme for large target times t_f . Repeating of many *pump-dump* cycles is clearly visible.

times exist. If the target time exceeds this characteristic time the scheme is iteratively repeated to achieve higher yield of the control.

The results obtained in this section underline the importance of the time t_f in the OC algorithm. It shows also that the optimal laser pulse resulting from the OC algorithm (and generally also from other optimum searching methods) may depend drastically on the external parameters of the optimization, which are not properties of the optimized molecular system.

Chapter 4

Optimal Control of Electron Transfer

After demonstrating the capabilities of the OC theory on a rather simple two electronic state system in previous chapter, we will now concentrate on a more complicated problem. Namely, the photo-induced electron transfer (ET). There is a certain amount of theoretical literature on the external field control of ET [Dak94, DC95, DEKC95, GPM96, GPM97, GH98, YD01]. These studies, however, do not deal with photoinduced ET reactions but with a type of external field control characterized by the action of a high-frequency electric field which modulates the energetic distance between the donor and acceptor level. In contrast in the following we will demonstrate the control of ET reactions by another mechanism using external fields in the optical region. In particular, we are going to study bridge mediated ET on a simple donor-bridge-acceptor (DBA) system. Although it only represents a generalization of the standard curve-crossing problem by an additional level it allows to describe different new aspects of ET [JB99]. Here, first the dissipation-less control of ET will be considered to test the feasibility of the control and to find the underlying control mechanisms. The OC of the systems under the influence of the dissipation is also studied in the this chapter for a slightly reduced molecular system consisting of just donor and acceptor states. The main questions to be answered are whether and to which extent the control of the molecular systems under the influence of the dissipation becomes possible.

4.1 The Electron Transfer Model

A common model for the description of ultrafast photo-induced ET is given by a set of electronic levels which are defined versus a small set of vibrational (reaction) coordinates (see e.g. [MK99]). Often it is sufficient to consider one or two vibrational coordinates, but in case one needs to account for dephasing and energy dissipation a coupling to environmental vibrational modes becomes necessary. In similarity to the section 3.3 the relevant system Hamiltonian H_S includes the molecular part H_{mol} and the coupling to an external field $H_F(t)$. Using the diabatic electronic states $|\varphi_a\rangle$ of the molecular system the first contribution can be written as

$$H_{mol} = \sum_{a,b} (\delta_{a,b} H_a + (1 - \delta_{a,b}) V_{ab}) |\varphi_a\rangle \langle \varphi_b|. \quad (4.1)$$

The electronic quantum number a comprises the ground-state contribution $a = g$ as well as the donor, bridge and acceptor states $a = D, B, A$. The coupling terms V_{ab} concern only the donor, bridge and acceptor states. The vibration Hamiltonian H_a written with dimensionless coordinates $Q = \{Q_j\}$ reads

$$H_a = T_{vib} + U_a^{(0)} + \sum_j \frac{\hbar \omega_j}{4} (Q_j - Q_j^{(a)})^2. \quad (4.2)$$

The minima and the mutual displacement of the respective PES are denoted by $U_a^{(0)}$ and $Q_j^{(a)}$, respectively. The coordinates Q_j can be expressed via the harmonic oscillator creation and annihilation operators C_j and C_j^+ according to $Q_j = C_j^+ + C_j$. Respective vibrational eigenfunctions of the Hamiltonian H_a read $|\chi_{aM}\rangle$ where M denotes the set of vibrational quantum numbers. Consequently, the complete electron-vibrational states are given by $|\chi_{aM}\rangle |\varphi_a\rangle$. The external field part of the system Hamiltonian H_s is given by

$$H_F(t) = -\mathbf{E}(t) \hat{\mu} \quad (4.3)$$

similarly to the section 2.1. The dipole operator reads

$$\hat{\mu} = \mathbf{d}_{Dg} |\varphi_a\rangle \langle \varphi_g| + h.c., \quad (4.4)$$

and is assumed to be independent of the Q_j (Condon approximation).

For the present calculation we use a three level model versus a single vibrational coordinate which is depicted on Fig. 4.1. Such a model has been already successfully used for the simulations of an ultrafast ET in dye molecules [RWM00].

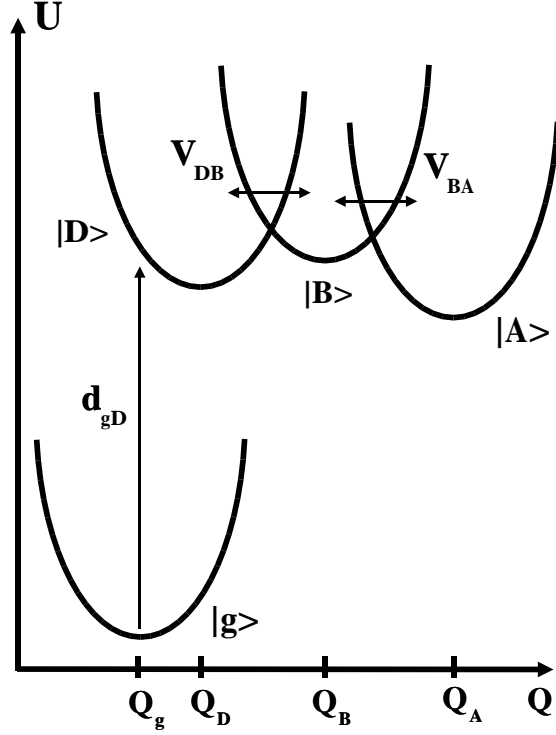


Figure 4.1: PES of the Donor-Bridge-Acceptor system. The laser field excitation from the ground state $|g\rangle$ is possible due to the existence of the molecular dipole moment d_{gD} . The transfer integrals V_{DB} and V_{BA} couple the donor, bridge and acceptor states and enable the ET in the excited state.

4.2 Optimal Control of Dissipation-Less Electron Transfer

For the subsequent discussion, which should serve as simple reference case for more involved further computation, we additionally neglect any coupling of the reaction coordinate (active coordinate) to a thermal reservoir of passive molecular DOF. Furthermore, we start with the electronic and vibrational ground state as the initial state (zero-temperature case). Therefore, the set of *eigenstates* $|\psi_\alpha\rangle$ appearing in the scheme of the section 3.2 has to be replaced by the electron-vibrational ground state $|\chi_{g0}\rangle|\varphi_g\rangle$ of the ET system. It enters Eq. (3.21) where it acts as a single initial state for the single wavefunction $|\psi(t)\rangle$ to be determined. To solve Eq. (3.22) where a backward time propagation has to be carried out, first we have to fix the observable represented by the operator

m	$U_m^{(0)} - U_g^{(0)}$	$\hbar\omega_{\text{vib}}$	$Q^{(m)}$
g	0	0.1 eV	- 4
D	2 eV	0.1 eV	- 1.172
B	2 eV	0.1 eV	1.414
A	2 eV	0.1 eV	4

Table 4.1: Parameters of the single-mode version of the ET model introduced in Section 4.1. The transfer integrals among the three PES responsible for the ET have been taken as $V_{DB} = V_{BA} = 0.03$ eV, and $V_{DA} = 0$. The transition dipole moment d_{Dg} has been set equal to 12 D.

\hat{O} . Since dynamical electron localization at a single electron–vibrational state (or a superposition of such states) will be of main interest we identify \hat{O} with a projector on a certain state $|\psi_{\text{target}}\rangle$ (target state).

To carry out the iteration of the Eqs. (3.23) and (3.24) we change to a representation using the diabatic electron–vibrational states $|\chi_{mM}\rangle|\varphi_m\rangle$ and use the type of penalty function $\lambda(t)$, Eq. (3.6) suggested in [SdVR99]. As the zero-order approximation for the field we took a Gaussian shaped pulse of 20 fs duration, with maximum at 50 fs, and with carrier frequency in the Frank–Condon region of the donor excitation. The parameters of the Hamiltonian for these calculations are summarized in Table 4.2.

In order to observe the ET unaffected by the external field we first compute a reference case with the ET dynamics after an impulsive (instantaneous) and complete excitation of the donor level i.e. after the action of an infinitely short pulse. Here obviously, the structure of the pulse cannot play any role. This results in a propagation of the Schrödinger equation for the ET system in the absence of an external field but with an initial condition determined by the field. The latter is given by $|\psi(0)\rangle = |\chi_{g0}\rangle|\varphi_D\rangle$ and corresponds in the scheme of PES, Fig. 4.1 to a vertical displacement of the electronic ground-state vibrational wavefunction $|\chi_{g0}\rangle$ into the (excited) donor state $|\varphi_D\rangle$.

To visualize the dynamics we draw in the following the complete diabatic electronic level populations

$$P_m(t) = \sum_M P_{mM}(t) , \quad (4.5)$$

where P_{mM} is the electron–vibrational state population. The respective $P_m(t)$

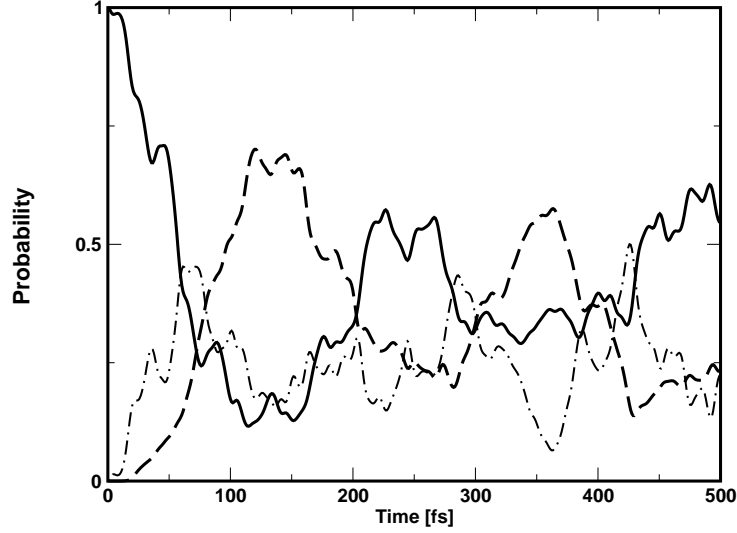


Figure 4.2: Reference dynamics in the DBA-system (parameters see Tab.4.2) after an impulsive excitation at $t = 0$. The excitation process results in a complete probability transfer into the donor level. The total populations P_m of the donor level (solid line), the bridge-level (dot-dashed line), and the acceptor level (dashed-line) are plotted .

($m = D, B, A$) valid for the case of impulsive action of the external field are displayed in Fig. 4.2 for the first 500 fs. The transferred electron starting with 100% population of the donor state reaches a maximum population of about 70% at the acceptor after $t \approx 120$ fs. Since any dissipation is absent the populations show a coherent oscillatory behavior. Changing to the corresponding wavepacket motion (in the coordinate representation, not shown here) one notices a fast spread out of the initial wavepacket over a broad range on the Q -axis.

It is the question we try to answer whether or not it is possible to control (guide) the ET dynamics in such a manner to reach a chosen state at a chosen time. A first example for the application of OC approach is shown in Fig. 4.3. Here, the second excited vibrational state of the acceptor electronic state $|\chi_{A2}\rangle|\varphi_A\rangle$ has been chosen as the target state which should be reached at time $t_f = 500$ fs. One notices that the population dynamics under the action of the control pulse turns out to be rather regular and finally the system reaches the desired state with a probability of about 95%. To obtain this result less than 20 iterations of the Eqs. (3.23) and (3.24) have been necessary. In Fig. 4.3 we also presented the optimal pulse. It increases up to a time (about 130 fs) at

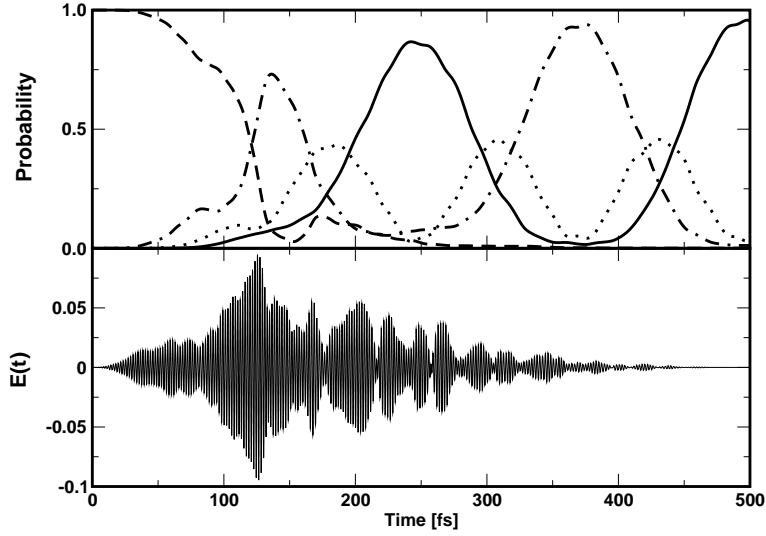


Figure 4.3: Laser pulse control of photoinduced ET in DBA-system. Optical excitation proceeds in the Frank-Condon transition region of the donor level. The second excited vibrational state of the acceptor level $|\chi_{A2}\rangle|\varphi_A\rangle$ has been chosen as the target state. Upper part: populations P_g of the ground state of the ET-system (dashed line), P_D of the donor level (dot-dashed line), P_B of the bridge level (dotted line) and P_A of the acceptor level (solid line). Lower part: shape of the optimal laser pulse field in units of $10^7 V/cm$.

which the ground-state population is nearly completely removed. Afterwards the pulse kicks the ET dynamics (with decreasing amplitude) in such a manner to achieve the required population of the acceptor level. If one takes a look on the related moving wavepacket the regular behavior of the external-field guided ET can be observed, too. The quantity drawn in Fig. 4.4 is the time-dependent probability distribution $P(Q, t)$ of the reaction coordinate. It is obtained via the expectation value of the projector on the coordinate operator *eigenstates*

$$P(Q, t) = \langle \psi(t) | Q > < Q | \psi(t) \rangle . \quad (4.6)$$

Introducing an expansion of $|\psi(t)\rangle$ with respect to the diabatic electron-vibrational states one obtains $P(Q, t) = \sum_{m,M,N} c_{mM}^*(t) c_{mN}(t) \chi_{mM}^*(Q) \chi_{mN}(Q)$ where the $c_{mM}^*(t)$ and $c_{mN}(t)$ denote the related time-dependent expansion coefficients. Thus, the expansion is diagonal with respect to the diabatic electronic states but off-diagonal with respect to the vibrational wavefunctions. The oscillatory behavior which is shown by $P(Q, t)$ nicely corresponds to the oscillations of the level populations in Fig. 4.3.

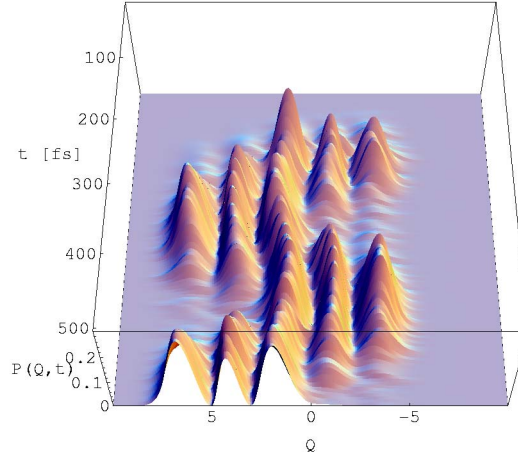


Figure 4.4: Wavepacket motion (probability distribution $P(Q, t)$ of the vibrational coordinate) related to the controlled ET dynamics shown on Figure 4.3 (Note that time increases from the backward part of the figure to the foreground.) The shape of the probability distribution corresponds mainly to a wavepacket with two nodes indicating that the corresponding target state $|\chi_{A2}\rangle|\varphi_A\rangle$ has been reached.

Besides the population of a single electron–vibrational state we can, of course, design pulses which lead to the formation of a wavepacket of Gaussian (or any other) form. To that end, we introduce the target state as the displaced vibrational ground state of the acceptor level. Using the coordinate representation with respect to the vibrational coordinate it reads $\langle Q - Q_{\text{dis}} | \chi_{A0} \rangle | \varphi_A \rangle$. The quantity Q_{dis} ($= 2.4$, compare Fig. 4.5) denotes the actual displacement with respect to acceptor equilibrium position $Q^{(A)}$. As shown in Fig. 4.5 the optimization procedure results in a 91% population of the target state. Although the pulse extends over more than 300fs the main portion of the excitation is achieved in the time period just after $t = 100\text{fs}$ (compare the population P_g of the electronic ground state). Between $t \approx 150\text{fs}$ and $t \approx 350\text{fs}$ there is no further probability transfer from the ground–state. The corresponding wavepacket motion (Fig. 2.8) shows again an oscillatory behavior corresponding to the electronic population dynamics and finally the formation of the required wavepacket.

Next we chose the population of the vibrational ground–state of the bridge state $|\chi_{B0}\rangle|\varphi_B\rangle$ as the target state. The results of the OC approach are dis-

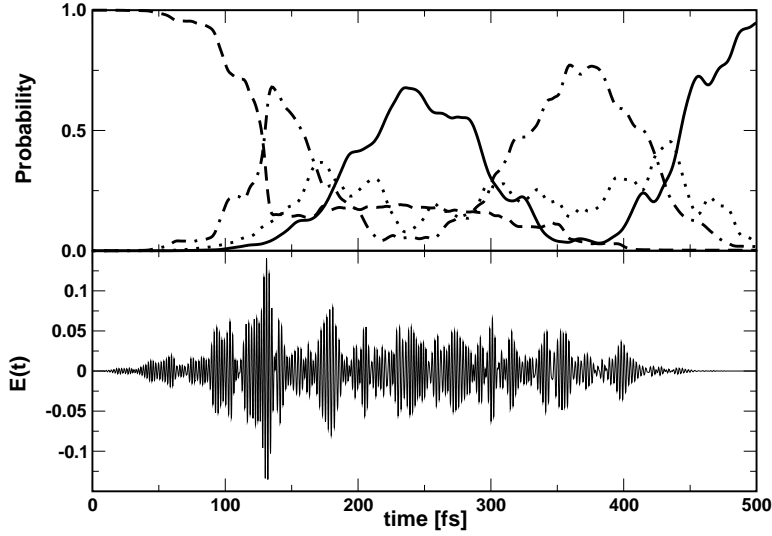


Figure 4.5: Laser pulse control of photoinduced ET in DBA-system. Optical excitation proceeds in the Frank-Condon transition region of the donor level. The target state is given by the vibrational ground-state of the acceptor level but displaced from $Q^A = 4$ to a new position 6.4. Upper part: populations P_g of the ground state of the ET-system (dashed line), P_D of the donor level (dot-dashed line), P_B of the bridge level (dotted line) and P_A of the acceptor level (solid line). Lower part: shape of the optimal laser pulse field in units of $10^7 V/cm$.

played in Fig. 4.7. In the DBA configuration introduced for the ET transfer system the bridge PES lies symmetrically between donor and acceptor PES. Therefore, the field tries to synchronize the population of the donor and acceptor level. If the respective oscillations of P_D and P_A reach their minimum the bridge population achieves its maximum with a higher and higher population up to the nearly 100% population of the target state at $t_f = 0.5$ ps.

The above given results demonstrate the possible laser pulse control of ET reactions. For all the chosen target states we have been able to achieve an optimal laser pulse yielding more than 90% population of the desired target state. In the Figures of this section only the electronic populations have always been presented, but the detailed analysis of the vibrational populations (not presented here) in case of targeting a single vibrational level shows that the whole population of the target electronic state is concentrated in the target vibrational state.

To conclude the investigations made in this we may state that indeed the

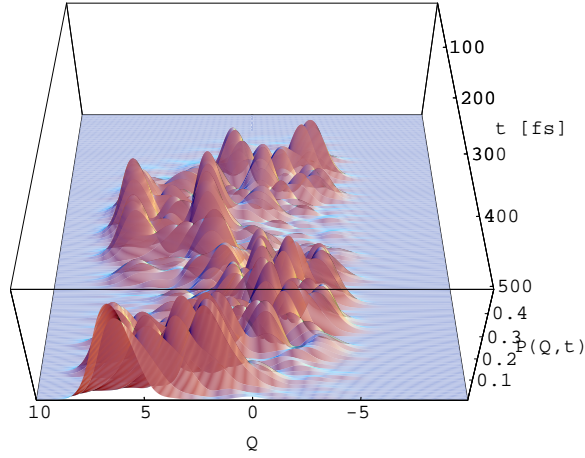


Figure 4.6: Wavepacket motion (probability distribution $P(Q, t)$ of the vibrational coordinate) related to the controlled ET dynamics shown on Figure 4.5 (Note that time increases from the backward part of the figure to the foreground.)

control of the bridge mediated electron transfer becomes possible. We have found the OC theory to suggest pulses which use a special timing to synchronize the movement of the wavepacket on the DBA system to fulfill a given control task. The population of targeted vibrational levels as well as the preparation of precisely located wavepackets has been demonstrated.

4.3 Electron Transfer and Vibrational Relaxation

After the encouraging results of both theory and experiment on the laser pulse control of the molecular dynamics of small systems in gas-phase the next step is to apply control methods on systems exhibiting dissipative dynamics [Ger01]. In the present section we use a slightly simplified (in comparison to the previous section) molecular system to study the feasibility of the OC in presence of the dissipation. We first perform some calculations with absence of the coupling to the reservoir to have a reference case. The subsequent calculations with increasing strength of the coupling to the dissipative reservoir will be compared to this reference case and some conclusions on the controllability of the dissipative dynamics will be drawn.

We decided to reduce the number of the excited electronic states to donor

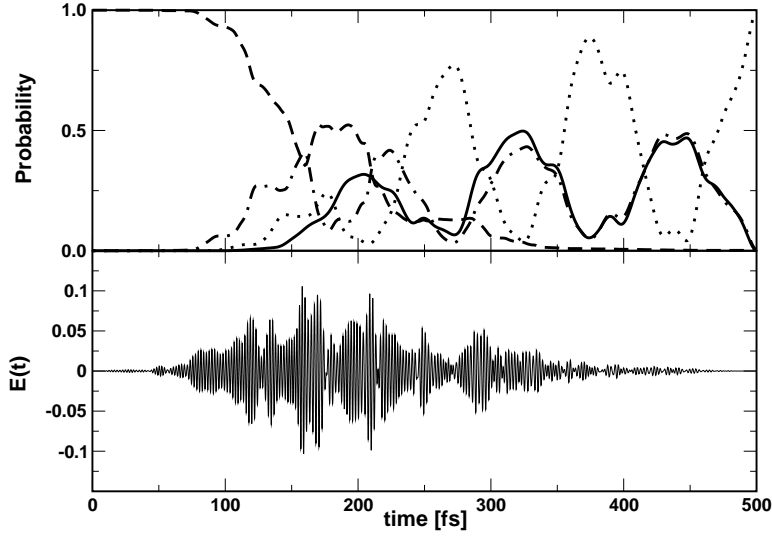


Figure 4.7: Laser pulse control of photoinduced ET in DBA-system. Optical excitation proceeds in the Frank-Condon transition region of the donor level. The target state is given by the vibrational ground-state of the bridge level. Upper part: populations P_g of the ground state of the ET-system (dashed line), P_D of the donor level (dot-dashed line), P_B of the bridge level (dotted line) and P_A of the acceptor level (solid line). Lower part: shape of the optimal laser pulse field in units of $10^7 V/cm$.

and acceptor only, in order to reduce the size of the model system and thus reduce the amount of the computational time necessary for carrying out the density matrix calculation. We denote this particular model Hamiltonian as model *I*. For the later use in this section we also introduce a different kind of ET model Hamiltonian allowing to study the OC in the system exhibiting an interplay of the vibrational relaxation and internal conversion. This Hamiltonian corresponds to model *II*. The particular parameters of the models are summarized in the corresponding tables 4.3, 4.3 and 4.4. We use two different parameters sets denoted as *I* – 1 and *I* – 2 for model *I* and one parameter set for the model *II*. Both model systems are depicted on Figure 4.8.

First of all we will concentrate on the controllability of the ET in dependence on the control pulse length. It is obvious that ET spontaneously proceeds between the donor and the acceptor if initially electron–vibrational state has been prepared in the donor PES (probably by a laser excitation). And it depends on the degree of dissipation whether the electron remains at the acceptor after the ET took place or whether it moves different times back and

m	$U_m^{(0)} - U_g^{(0)}$	$\hbar\omega_{\text{vib}}$	$Q^{(m)}$
g	0.00	0.1 eV	0.0
D	2.00 eV	0.1 eV	3.2
B	1.85 eV	0.1 eV	7.0

Table 4.2: Model I-1. Parameters of the single-mode version of the ET model introduced in Section 4.1 reduced to only donor-acceptor system. The transfer integrals have been taken as $V_{DB} = V_{BA} = 0.03$ eV, and $V_{DA} = 0$. The transition dipole moment d_{Dg} has been set equal to 12 D.

m	$U_m^{(0)} - U_g^{(0)}$	$\hbar\omega_{\text{vib}}$	$Q^{(m)}$
g	0.00	0.1 eV	0.0
D	2.00 eV	0.1 eV	3.2
B	1.89 eV	0.1 eV	7.0

Table 4.3: Model I-2. Parameters of the single-mode version of the ET model introduced in Section 4.1 reduced to only donor-acceptor system. The transfer integrals have been taken as $V_{DB} = V_{BA} = 0.03$ eV, and $V_{DA} = 0$. The transition dipole moment d_{Dg} has been set equal to 12 D.

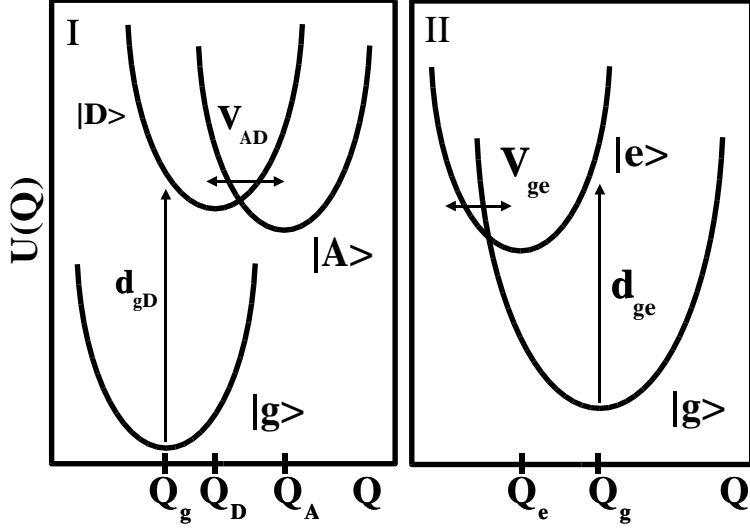


Figure 4.8: PES of the studied model systems. ET model I: a donor-acceptor system typical for photo-induced ET. ET-model II: a system showing ET in the inverted regime after photo-induced charge separation into an excited state. The electronic transfer coupling (non-adiabatic coupling) and the optical transition are indicated by horizontal and vertical arrows, respectively.

forth between the donor and the acceptor. In both cases the ET can be controlled by a particular shaping of the initial electron-vibrational wavepacket. For weak dissipation a continuous formation of the electron-vibrational wave packet through the Frank-Condon window of the optical transition would control the ET. And in any case the target time t_f at which the electron should arrive at the target state must be comparable or longer than the time t_{ET} the electron needs to reach the acceptor without an external field influence. If $t_f > t_{ET}$ and if dissipation is weak enough or completely absent the laser pulse may act within different cycles of the electron motion between the donor and the acceptor.

To have a reference case for a comparison with more involved calculation including dissipation, we still work in the absence of the dissipation here (or assume it to be so weak that it does not play any role in the dynamics on our time scale). Fig. 4.9 demonstrates that for $t_f > t_{ET}$ the OC yield can be increased if the number of the forth and back motion of the electron, i.e. if t_f is increased. Note, that the first excited vibrational state $|\varphi_A\rangle|\chi_{A1}\rangle$ at the acceptor PES has been taken as the target state. Besides the structure of the optimal pulse Fig. 4.9 also shows the yield of the laser pulse control in

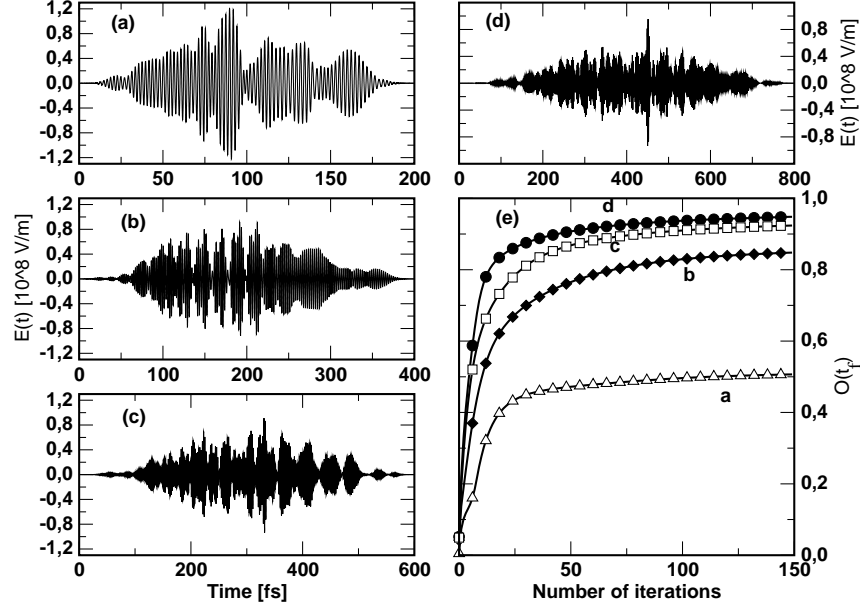


Figure 4.9: Laser pulse control of ET in the absence of dissipation (system parameters according to Tab. 4.3, target state: $|\phi_A\rangle|\chi_{A1}\rangle$). The optimal pulse is shown for control tasks which differ with respect to their target time t_f . Panel a: $t_f = 200\text{fs}$, panel b: $t_f = 400\text{fs}$, panel c: $t_f = 600\text{fs}$, panel d: $t_f = 800\text{fs}$. The convergency behavior of the OC algorithm is shown in panel e.

dependence on the number of iteration steps within the OC algorithm. Here and in the following the yield (control efficiency) is given by $O(t_f)$, Eq. (3.5), i.e. the degree to which the control task has been solved. The OC algorithm leads to a fast convergency into regions where more than 90 % of the final value of $O(t_f)$ have been realized. This behavior may indicate that the chosen iteration procedure drives the solution of the optimization problem into a local minimum. If the "surrounding" of the local minimum is reached the convergency becomes weak. Furthermore we emphasize the strong dependence of the control yield on details of the control task, here in particular on the chosen target time. A similar dependence on the target state could be also observed within other control tasks. This indicates again (compare section 3.3) that beside the specificity of the molecular system also details of the control task can strongly affect the completeness the task may be solved by OC theory. The fast convergency of the iteration as reported in literature (see, for example [ZBR98, ZR98, YOR99, SdVR99]) can be confirmed for the present example,

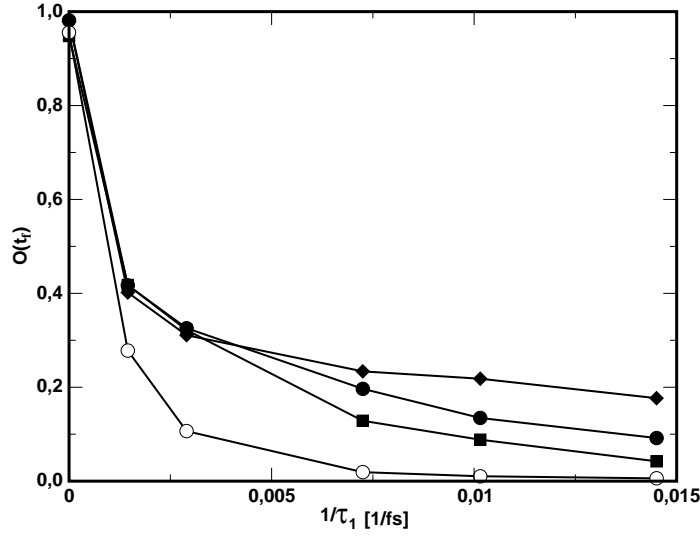


Figure 4.10: ET control efficiency for the model I-1 in dependence on the inverse life-time of the target vibronic state (system parameters according to Tab.4.3). Curves for different values of the penalty factor λ are drawn. Filled squares: $\lambda = 1$, filled circles: $\lambda = 1/5$, and filled diamonds: $\lambda = 1/20$. For comparison the efficiency is shown which is achieved in applying the optimal pulse valid for the absence of dissipation (open circles)

too.

Now we proceed to study the way the presence of a thermal environment may influence the laser pulse control ET. We use the formulation of the OC for the dissipative dynamics explained in section 3.1. To avoid so-called diabatic damping approximation which may lead to the wrong results [KKS01, EKD01] we construct the dissipative part of the QME for the Hamiltonian transformed into the basis of adiabatic states. Subsequently, the dissipative part is transformed back to the basis of diabatic states which is used for the computation. We will consider the state $|\varphi_A\rangle |\chi_{A1}\rangle$ as a target state. Due to the action of the thermal environment all electron-vibrational states are characterized by a finite life-time. In particular, the target state may decay into the acceptor vibrational ground state. To get an impression on the influence of dissipation on the controllability of the ET reaction the coupling strength, i.e. the magnitude of the bath spectral density $J(\omega)$ will be varied.

Before giving a detailed analysis of the control task we try to characterize the general importance of laser pulse control at the presence of dissipation. While trying to control molecular dynamics, the counterproductive influence

of dissipation is usually emphasized. Fig. 4.10 put this into a more quantitative frame. There we have drawn the control yield $O(t_f)$ versus the strength of dissipation represented by an increasing decay rate of the target state (decreasing vibrational life-time τ_{A1} of the first excited vibrational state at the acceptor). To distinguish between different laser pulse intensities the penalty factor λ has been varied, too. All these curves have to be compared with a curve which is obtained applying the OC theory formulated for dissipationless case. What has been only done to get this reference curve is to take the pulse which solves the OC theory in the absence of dissipation and to calculate the control efficiency $O(t_f)$ while increasing dissipation. As can be seen from Fig. 4.10 the application of the OC theory at the presence of dissipation may drastically increase the control efficiency, in particular for an intermediate influence of vibrational relaxation and the largest applied laser pulse intensities. If a generalization to other types of molecular systems might be possible the promising result can be stated that laser pulse control for condensed phase situations would really make sense although the given control task cannot be solved completely. To get more insight into the convergency behavior of the OC algorithm we show in Fig. 4.11 the control yield $O(t_f)$ in its dependence on the number of iteration steps. And indeed, the dissipationless case shows the same rapid convergency as it could be already observed in Fig. 4.9. In contrast, the presence of dissipation results in a somewhat slower convergency which behaves unpredictably and even non-monotonously. And, more iteration steps become necessary. But in any case more than 90 % of the final yield are achieved within about 50 iteration steps (except the curve with a second threshold at about 170 steps). According to our observations this seems to be a universal property of the used iteration procedure, again indicating that the solution of the OC problem may be locked in a local minimum. How to tackle this problem will be discussed later.

Any computation mentioned so far leaves a corresponding optimal laser field. Those related to the calculations of Fig. 4.10 have been displayed in Fig. 4.12. In the absence of dissipation an almost 100% population of the target state is achieved. The laser field extends over the whole interval (t_0, t_f) having enough time to adjust the wave packet motion over the excited PES in order to populate the desired target state at the given time. If dissipation starts to act we observe a concentration of the control field to larger times and a change of some features. The latter behavior is caused by the reduced wave packet motion when increasing the strength of dissipation. The time evolution of the electronic and vibrational state populations related to the laser pulses given in Fig. 4.12 are shown in Fig. 4.13. If dissipation is absent one observes a periodic motion of the population between the donor and acceptor level. After two periods

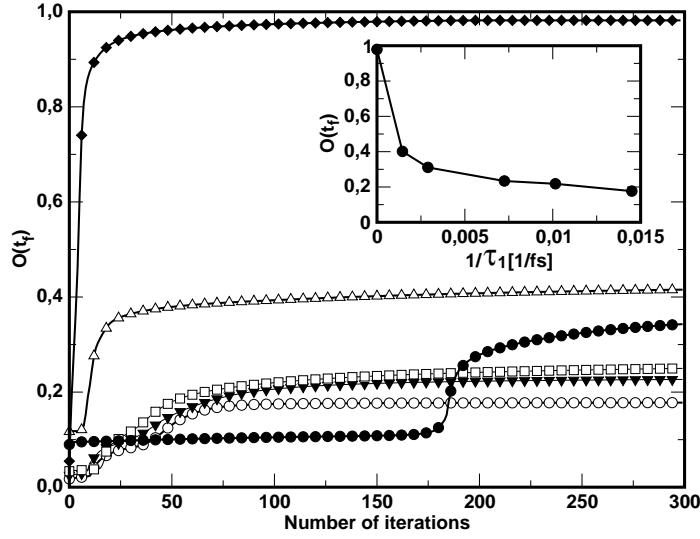


Figure 4.11: ET control efficiency for the model I-1 in dependence on the number of iteration steps taken to solve the OC equations (system parameters according to 4.3). Curves for different inverse life-times of the vibronic target state are shown. Filled diamonds: $1/\tau_1 = 0$, empty triangles: $1/\tau_1 = 1.45 \times 10^{-3}/fs$, filled circles: $1/\tau_1 = 2.9 \times 10^{-3}/fs$, empty squares: $1/\tau_1 = 7.25 \times 10^{-3}/fs$, filled triangles: $1/\tau_1 = 1.01 \times 10^{-2}/fs$ and empty circles: $1/\tau_1 = 1.45 \times 10^{-2}/fs$. Insert: Final control yield as a function of the target state inverse vibrational life-time.

of this motion an almost complete population is achieved of the excited state PES, exhibiting at some points nearly 100% population of the donor excited level, but only about 80% population of the desired acceptor state. From the corresponding part of Fig. 4.13 displaying vibrational populations we see that within the target electronic state, the whole population is already concentrated on the target vibronic level. Finally, we notice the action of the pulse near the end of the control interval which removes the part of the wave packet trapped in the donor level and achieves the complete population of the target state. This is a behavior characteristic for the completely coherent motion of the system. Specially shaped wave packets are iteratively improved while they move coherently on the excited PES.

In part (b) and (c) of Fig. 4.13 the populations are shown for an increasing strength of dissipation. Due to the loss of coherence the algorithm cannot rely on iterative improvement of the wave packet. Instead, the action of the laser pulse concentrate to later times to avoid the depopulation of the target level.

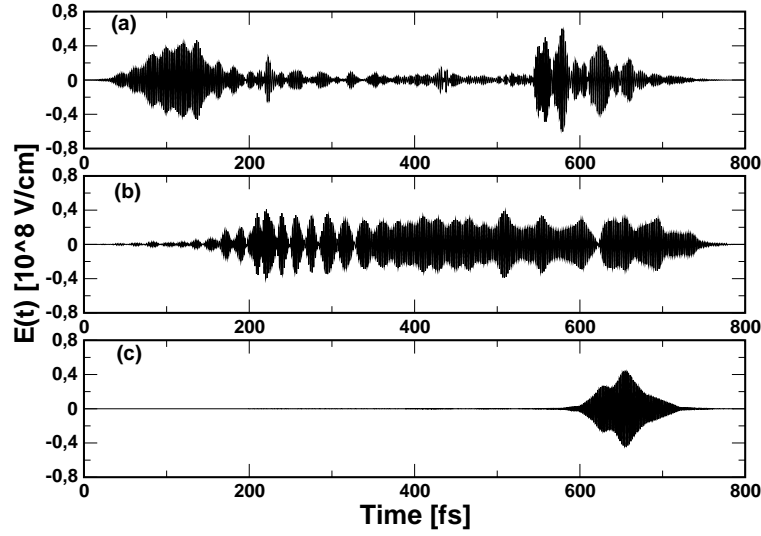


Figure 4.12: Laser pulse control of ET for the model I-2 with increasing dissipation (system parameters according to Tab. 4.3). The optimal pulse is shown for control tasks which differ with respect to the life-time of the target state. Panel a: isolated system, panel b: small dissipation, and panel c: medium dissipation

In the case of medium dissipation (part (b) of Fig. 4.13) the excited donor level is populated first around $t = 200\text{fs}$. And in contrast to the dissipation-less case where population has been directly transferred into the target vibronic level, now population is also transferred into levels positioned above the target level (here the first excited vibrational level). According to vibrational relaxation these higher lying levels are later depopulated into the target state and in this way they contribute to its population.

We may also note that the population of the target level still preserves some oscillatory features from the dissipation-less case. However, these traces of the coherent dynamics are lost if dissipation is further increased and the OC algorithm avoids earlier excitations completely. The whole population is transferred into the target state during the last 200 fs. Looking at the vibronic populations it can be again concluded that a substantial portion of the target state population comes from the decay of higher lying vibrational levels. So our general observation is, that the OC algorithm finds an alternative route to solve the control problem when the strength of dissipation increases. Due to this fact the optimal field computed for the absence of dissipation, although having higher pulse energy, fails to guide the dissipative dynamics (cf. Fig. 4.10). It is of

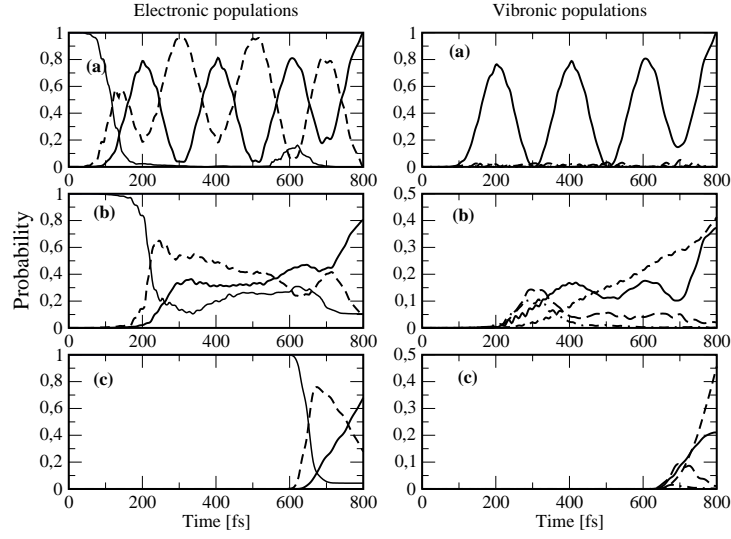


Figure 4.13: Populations of the electronic states (left) and of the vibrational levels in the acceptor state (right) versus time for the ET model I-2 and for the optimal pulses give in Fig. 4.12. Left part: electronic ground state (thin full line), excited donor state (dashed line), acceptor state (full line). Right part: acceptor vibrational ground-state (dashed line), first excited vibrational state (target state, full line), second excited vibrational state (long dashed line), and third excited vibrational state (dashed-dotted line).

some interest to compare the results of the OC calculations with the dynamics being free of any external control and following an ultra-short laser pulse excitation (compare Fig. 4.14 with Fig. 4.13). Due to the lack of dissipation ET proceeds coherently with comparatively low population of the acceptor level, where mainly higher excited vibronic levels are populated (Fig. 4.14 part a right). The population of the target vibronic state is negligible. With increasing dissipation the dynamics in both cases become more similar for the electronic populations. The vibronic populations, however, show still signs of the coherent motion in the control case, in contrast to the case without a control field. The maximum population of the target level achieved around the middle of the studied time window (about 25%) is smaller than that achieved if the laser pulse control has been carried out (more that 35%). For higher coupling-strengths to the environment the results without a control field and in the presence of such a field become almost identical, except for the shift to later times in the case external-field control. A short laser pulse populating the target state in the shortest possible time is close to the optimum for this

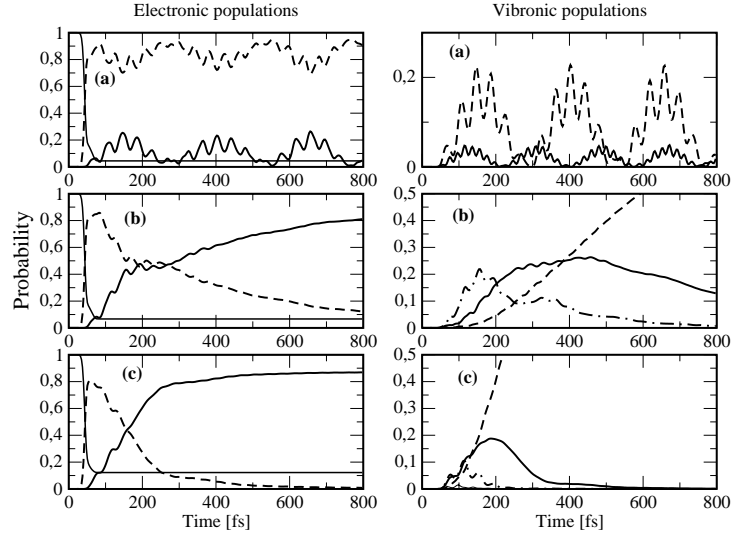


Figure 4.14: Populations of the electronic states (left) and of the vibrational levels in the acceptor state (right) versus time for the ET model I-2 and for an excitation with 50 fs long Gaussian laser pulse. Left part: electronic ground state (thin full line), excited donor state (dashed line), acceptor state (full line). Right part: (a) vibrational states with quantum numbers $N = 2$ (full line) and $N = 3$ (dashed line), (b) and (c): acceptor vibrational ground-state (dashed line), first excited vibrational state (target state, full line), second excited vibrational state (long dashed line), and third excited vibrational state (dashed-dotted line).

particular case.

4.4 Interplay of Vibrational Relaxation and Internal Conversion

In this section we will consider ET control using another Hamiltonian which represents a minimal model for the internal conversion process observed in e.g. betaine 30 [FS96, KWPD94]. The parameters of the model are taken from [FS96] and presented in Tab. 4.4.

In the language of donor–acceptor ET the charge motion described in this model corresponds to ET in the inverted region. The final state of this ET would be the vibrational ground state in the S_0 –state PES. However, to demonstrate the possible ET control we chose as a target state the third excited vi-

m	$U_m^{(0)} - U_g^{(0)}$	$\hbar\omega_{\text{vib}}$	$Q^{(m)}$
g	0.00	0.223 eV	0.0
D	1.305 eV	0.223 eV	-2.483

Table 4.4: Model II. Parameters of the single-mode version inverted region model of the ET with internal conversion (see Fig. 4.8). The transfer integrals have been taken as $V_{ge} = V_{eg} = 0.31$ eV. The transition dipole moment d_{eg} has been set equal to 5.3 D.

brational state in the S_1 -state PES, i.e. $|\varphi_e\rangle|\chi_{e3}\rangle$. This state has been take to have a target somewhat similar to that of the foregoing section. And, it would allow to discuss laser pulse stabilization of an excited state against internal conversion.

Again we start with a discussion of the convergence behavior of the OC algorithm what is displayed in Fig. 4.15. In comparison with ET discussed in previous sections, Fig. 4.11 the convergence seems to be rather fast, and already the initial guess for the laser pulse used to initialize the iterative OC algorithm (a simple Gaussian shaped pulse) reaches a good result. On the other hand, the optimal field obtained when the iteration has been finished differs substantially from the initial guess and exhibits a rather complicated time-dependence. This is due to the non-adiabatic coupling between the ground and the excited state. Apparently, the OC algorithm tries to compensate the fast oscillations caused by this coupling (see the initial part of the electronic populations given in Fig. 4.16). We can also observe, that these oscillations almost disappear at later times. Since these oscillations have a small amplitude, their compensation only results in a small improvement of the control yield compared to the yield achieved with the initial guess for the laser pulse. Noting the insert in Fig. 4.15 we can state that a similar reduction of the control efficiency is obtained as for ET in previous section. And the optimal pulse shows a very similar tendency with an increasing strength of dissipation to concentrates at later times and to populate the target state via a depopulation of levels positioned above the target level.

The laser-guided dynamics obtained from the OC theory has also been compared with the dynamics following after a short excitation with a Gaussian shaped pulse with pulse width $\tau_p = 20fs$, and positioned at the corresponding Frank-Condon window (the figures not shown). The calculation demonstrates that the application of the OC theory leads to a significant enhancement of the

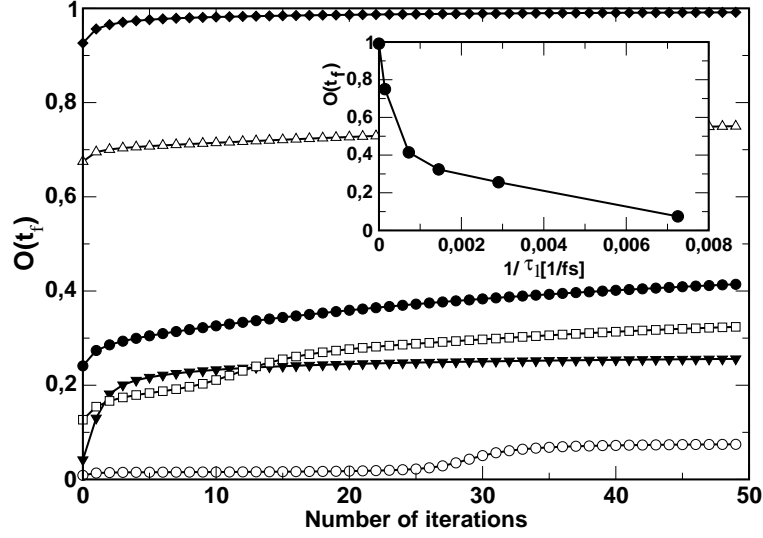


Figure 4.15: ET control efficiency for model II in dependence on the number of iterations necessary to solve the OC equations (system parameters according to Tab. 4.4). Curves for different inverse life-times of the target vibronic state are shown. Filled diamonds: $1/\tau_s = 0$, empty triangles: $1.45 \times 10^{-4}/fs$, filled circles: $7.25 \times 10^{-4}/fs$, empty squares: $1.45 \times 10^{-3}/fs$, filled triangles: $2.9 \times 10^{-3}/fs$, and empty circles: $7.25 \times 10^{-3}/fs$. Insert: control yield versus the inverse life-time of the first excited vibrational level.

yield compared to that one obtained by the 20 fs excitation. And, the calculations also prove that the laser-guided dynamics exhibits a rather organized motion of the population among the electronic levels what is in contrast to the motion one gets after the short excitation.

4.5 Acceleration of the Control Algorithm Convergence

As demonstrated in Fig. 4.15 the iteration algorithm for solving the OC theory may exhibit a fast convergence. Sometimes, however, it first converges to a certain value of $O(t_f)$ where it remains for a comparatively high number of iteration steps. Later, it jumps within several iteration into a new region where a slow convergence follows to a new larger value of $O(t_f)$. This behavior indicates that the OC algorithm has only found a local extremum first. It seems that the algorithm is able to avoid complete pinning in this local extremum but

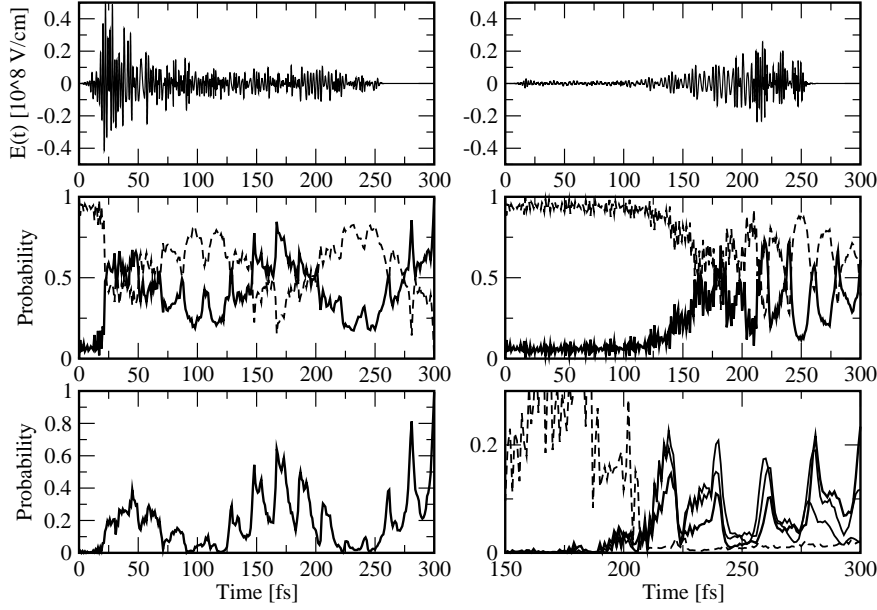


Figure 4.16: ET control in the inverted region, model II. The figure shows the optimal pulse (top), the electronic level populations (center), and the vibronic populations (bottom) for the case of the isolated system (left) and for the case with dissipation ($1/\tau_s = 2.9 \times 10^{-3}/fs$) (right, note the changed scale for the vibrational level populations). On the lowest figures the populations of the vibrational levels are displayed of the target vibrational state (bold solid line), the vibrational ground state (dashed line) and in case of the presence of dissipation also of the two vibrational levels lying over the target state.

the whole procedure takes a significantly long time. We shortly explain how to circumvent such a pinning in a local extremum, and in this manner, how to accelerate the iteration procedure.

The idea here is to randomly add some fluctuations to the control field during the iterative solution of the OC problem. Such a procedure should check whether or not a local optimum is occupied. The easiest way to introduce such fluctuations which perturb the OC algorithm is first to generate a Gaussian pulse of random duration, intensity, frequency and position in time, and second, to add this pulse to the obtained iterative version of the optimal pulse. The random parameters have been chosen from a certain range of them characteristic for a given system, e.g. the frequency of the pulse is chosen between the minimum and maximum transition frequencies possible between vibrational levels of the ground and excited states, respectively.

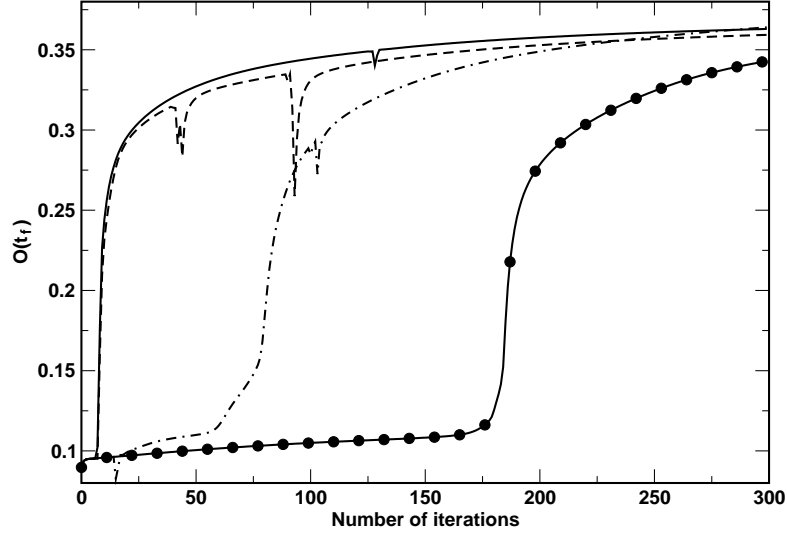


Figure 4.17: Convergence behavior of OC algorithm extended by random fluctuations. Model I-1 with $1/\tau_s = 2.9 \times 10^3/fs$. Fluctuations are applied for 10 successive iterations beginning at the 3rd one (full line, dashed line) as well as the 15th one (dot-dashed line) to induce the transition to the higher optimum, and beginning from the 35th one, the 80th one (dashed line), the 100th one (dot-dashed) as well as the 125th (full line) to check the stability of the extremum. For comparison, the result is plotted following the standard OC approach (full line with filled circles).

The results of our computations for ET from section 4.3 are summarized in Fig. 4.17. The fluctuation of the approximate version of the optimal pulse has been introduced within 10 successive iteration steps starting from the 3rd iteration (full and dashed lines in Fig. 4.17) and the 30th iteration (dot-dashed line in Fig. 4.17), respectively. As it is obvious the procedure moves the solution of the OC problem away from a local extremum, and in all cases the speed of convergence has been significantly enhanced as compared to the ordinary iterative computation. Furthermore, the value for $O(t_f)$ reached after about 150 iterations is even higher than that obtained after 300 iterations following the standard way. If further fluctuations are applied for later iterations a temporary decrease of the OC efficiency appears, but after a few iterations the result continues to converge to the original value. This shows the stability of the extremum, which than can be more likely the global one. But the behavior of the standard OC algorithm in this case indicates that it also converges to a global extremum. This indicates that the results presented in the foregoing

sections remain valid, possibly with a somewhat large value of $O(t_f)$. Such an introduction of random fluctuation into the ordinary OC scheme can be used in general to enhance the convergency and to check the stability of the reached extremum.

4.6 Summary of the Chapter 4

The Chapter 4 has been devoted to the control of the photo-induced ET reactions. First the dissipation-less dynamics has been investigated in section 4.2. As the target states to be populated by the optimal field we have used single vibrational levels in the donor, bridge or acceptor states and wavepackets of the Gaussian form located on a given coordinate Q in the electronic states. It could be shown that in this dissipation-less case the control of the wavepacket position in the DBA system at a give target time can be almost fully controlled. The control is enabled by the iterative action of the laser field, which synchronizes the motion of the different contributions of the excited state wavepacket in such a way that they meet in a given location at a given time.

The extended study including the control of the dissipative ET dynamics is performed in sections 4.3 and 4.4. The detailed investigation of the system dynamics show that the control pathways in presence of the dissipation differ from those found in dissipation-less case. And, as it was anticipated the dissipation acts in rather destructive manner on the controllability of the systems. The control efficiency decreases rapidly with the increase of the strength of the dissipation (see Fig. 4.10). But because the optimal pulses optimized for the dissipation-less case fail much faster to control the dissipative dynamics as the dissipation increases one may conclude that the separate formulation of the OC for dissipative dynamics really make sense. In section 4.5 we have also addressed one technical problem connected with the OC of the dissipative dynamics. During the iterative procedure of the OC algorithm we have applied some additional external stochastic fields in order to check the stability of the OC results. Not only we have found the results rather stable i.e. converging to roughly the same value, but also the speed of the convergence has to be enhanced as a side effect.

Chapter 5

Adapting Optimal Control Theory to Experimental Conditions

We have noted in the earlier discussions that the experimental and theoretical approaches to the optimal search differ substantially. Namely, in the experimental device some input pulse is shaped in the way that it enhances a yield of a given reaction so that the resulting optimal pulse is naturally spectrally limited. On the other hand the theoretical OC defines a target time and can restrict the overall optimal pulse envelop and thus it is naturally restricted in time domain. Also, the description of the experimental situation in the OC theory as it was formulated in Chapter 3 was far too simple to enable the description of the real experiment. The effects like laser pulse spatial profile, the probing of the final state by a weak laser field or the disorder in the molecular ensemble have ultimately be taken into account.

A trivial but crucial difference between the theoretical and experimental approach is that the functional values used to search the optimal pulse in experiment are taken from the response of the real molecular system to the particular laser field, whereas for the theoretical simulation only a model of the molecular system can be used. For small molecules in gas-phase, the model can be taken from quantum chemical calculations (see e.g. [DFG⁺01]). An independent check of the model can be performed by the simulation of well established experiments, e.g. pump-probe spectroscopy etc. Another possible way how to check for the suitability of the theoretical model of the molecular system for the OC simulation would be to compare the measured products of the experimental optimal control with the output of the simulation using the experimental pulse and the theoretical model of the molecule. Entering

the realm of the large systems and the dissipative dynamics there is no hope for calculating the parameters of the molecular model from first principles in recent time. Therefore, simple models have to be used which extract important features of the molecular system in terms of reproducing spectroscopic experiments. This is also the way taken in this work.

The aim of the present chapter is to address some of the problems connected with the application of OC theory results in to recent experiments and to demonstrate its flexibility in describing different experimental situations. In section 5.1 we present a short description of the experimental set-up used for the OC and we analyze its central component, the so-called Liquid-Crystal Spatial Light Modulator (LC-SLM). This is the device which enables a creation of flexible pulse shapes. Analyzing the LC-SLM we define a quantity called *complexity of the control task* in section 5.2 which enables us to classify the control tasks and estimate the experimental feasibility of the control of different system. Section 5.3 is devoted to the problem of controlling with static disorder, which is also closely related to the problem of the inclusion of the finite spatial light profile of the laser pulses. The OC algorithm is generalized for the case of the ensemble of molecules with different orientations of the dipole-moment with respect to the polarized control laser pulse. Finally, the OC is formulated for non-Markovian dynamics in section 5.4 demonstrating that OC theory can cope not only with complicated situation rising from the experimental arrangement, but can also in principle handle the dissipative dynamics beyond the Markov approximation.

5.1 A Standard Experimental Set-Up

We will concentrate now on the basic principles of the experimental OC set-up. Following the suggestion [JR92a] the experimentalists use the measurement of physical quantities their devices provide as a feedback for some kind of optimum search algorithm to provide optimal set of respective parameters. Sometimes one speaks about experiment in this context as about an “analog solution of equations of motion” [JR92a]. Here one refers to the fact, that otherwise equations of motion for the system in question have to be solved to provide input of the searching algorithm.

In the recent practical experimental use a class of optimum search algorithms prevails which takes its main ideas from the evolution of species observed in the nature. In general these algorithms are referred to as Evolutionary Algorithms (EA), where we distinguish at least three main groups, namely Evolutionary Strategies, Evolutionary Programming and Genetic algorithms

[BS], which differ in concrete implementation of the general scheme we introduce in the following. The main idea of EA is the identification of certain parameters of the problem with genes of the living individual and the objective value of the optimization search with its fitness for survival. Thus, having to maximize a function of 10 parameters we have in the simplest case 10 genes and the value of the function represents a fitness of an individual with these genes. For the search to be performed we build up a population of individuals (possibly with randomly chooses genes) and let this population evolve in the survival of the best scheme. In order to obtain a next generation individuals we use the *recombination* of the individuals e.g. random combination of the genes from two of them (mother and father), and *mutation* to enrich the set of genes to explore new parameter areas. The whole procedure is repeated until a certain convergency criterion is met.

The main practical advantage of this algorithm is that it is very effective in avoiding pinning into a local minimum and is applicable also for the problems with large number of parameters. Thinking about a laser experiment we now have to find suitable quantity to be used as a fitness value and some kind of parameterization of the laser pulse to represent genes.

The laser pulse shaping techniques developed in the last decade enable a suitable parameterization of the laser pulse, which can be used in EA. Moreover, these techniques also provide highly flexible laser pulses and thus arrange for a search within correspondingly broad spectrum of parameters. In our consideration we will concentrate on a well-known technique using the LC-SLM. The device is depicted of Figure 5.1.

It consists of two optical grids (G1 and G2), two lenses (L1 and L2) and a set of some 10th of liquid crystal elements (LCE) laying in the center of the device. A short laser pulse of a simple (Gaussian) form enters on the input of the device, it is spectrally decomposed on G1 and focused onto the central plain with LCE. Clearly, through each of the depicted LCE a pulse component with different frequency is traveling. Every LCE can now be addressed by a local voltage enabling to change its refracting index and transparency independently on the other LCEs, and thus enabling to shift the phase and modulate the intensity of the corresponding component of the input laser pulse. After coming through the LCE the components of the laser pulse are focused by L2 on the second grid G2, where a process opposite to the decomposition of the input laser pulse takes place. Due to the modulation of the intensity and the shift of the phase the resulting laser pulse takes a different shape from the input one. If an input pulse with a sufficiently broad spectrum is provided the flexibility of the outcomming laser pulse is limited only by a number of the LC elements in the device. Commercially available shapers dispose with about 128 LCE

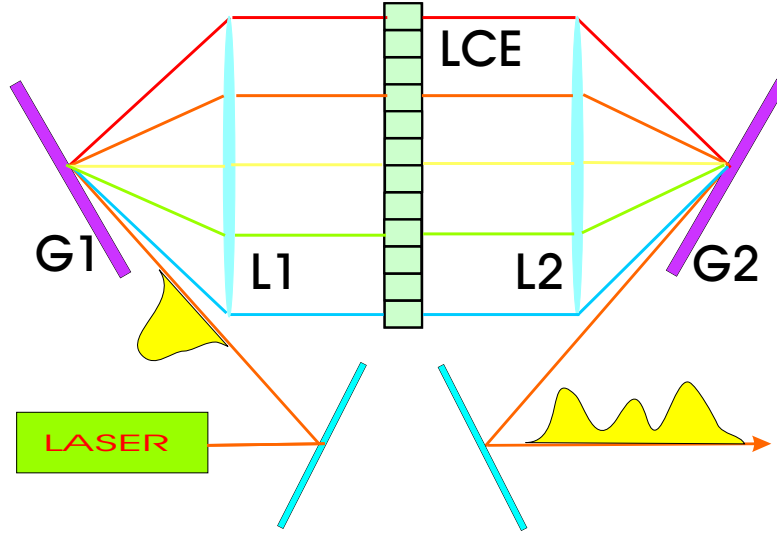


Figure 5.1: A sketch of the LC-SLM. The LC-SLM consists of two optical grids G1 and G2, two lenses L1 and L2, and a central plain with liquid crystal elements LCE.

for intensity modulation and 128 LCE for the phase shift, having thus 256 parameters which can be used in the optimal pulse search.

Bringing together the techniques described in the above discussion one obtains the recent experimental set-up for conducting the OC experiments. Here the output of the experimental measurement (detection of some molecular fragments in the fragmentation experiments [vVBK⁺01] or particular vibrational states [HCP⁺00] etc.) is analyzed by a computer which changes the laser shape choosing new values of the voltages applied to the different LCE in the LC-SLM. This procedure repeats until a convergency is achieved.

There are also other types of modulators used in place of LC-SLM like so-called acousto-optical systems. In these systems the LC elements are replaced by the material in which the acoustic waves change the refracting index. The modulation of the phase and the intensity of the spectral components of the input pulse is in principle possible in a continuous manner (in contrast to the LC-SLM which has some number N of pixels), but in order to use it with EA one also needs some kind of discrete parameterization.

As far as the OC theory is concerned, it is the feasibility of the optimal pulse which decides about the relevance of the theory for the experiment. A prerequisite to achieve the reconstruction of the theoretical pulse with the experimental device would be, of course, the ability to estimate how complicated

is this reconstruction and how efficient such an experimentally reconstructed theoretical pulse would be in solving the task. The discussion of this problems will lead us later to certain definition of the *complexity of the control task*.

5.2 Complexity of the Control Task

In the present section we will demonstrate systematically to which extend the complex field of the optimal pulse can be reproduced in the experiment, and resulting from this to which extend the control task can be solved. This is done by an analysis of molecular systems with a different energy level structure and the consideration of different types of target states. After having applied the OC theory to compute the optimal pulse we discuss the extent the LC-SLM systems reproduces the optimal pulse, and the ability of this approximated optimal pulse to achieve a high yield in the required reaction channel.

Resulting from this study we want to derive a working definition of the *complexity of the control task*. The *complexity* as it will be understood here is a quantity describing the amount of effort which has to be used to achieve a given control task. This is something slightly different from the *controllability* as discussed in Ref. [RZ00], or the notion of the *complexity of the molecular system*, which are properties of the molecular system irrespective of the particular initial and final (target) state. Regarding the complexity of the control task, there may exist e.g. less complex control tasks within an apparently very complex molecular system and vice versa.

Also, while asking for the complexity of the control task one needs to take into account the time scale of the control process. In the OC theory we have always specified the target time t_f at which we wanted to achieve the control task. Demanding different target times, the difficulty connected with the achievement of the control task may vary significantly, in spite of the fact, that the complexity of the system, or its controllability remain the same. Similar situation applies for any other external condition put on the control pulse. From this argument it is evident, that we cannot conclude on the *control task complexity* from analyzing the molecular system only. Rather, the control pulse, its complexity or the amount of effort one has to use to create it should be used to classify the control tasks and to define their complexities. It may seem reasonable to consider a spectrally broader laser pulse for more complicated one. But taking this criterion only a large class of very different laser pulses would fall into the same category. Different laser pulses with the same overall spectral width may have different complicated forms of the spectrum and we may try to define the laser pulse complexity by characterizing the form of its

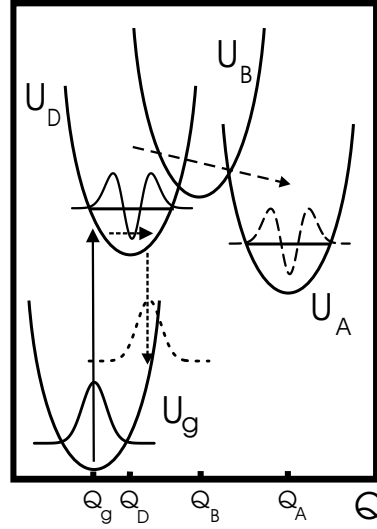


Figure 5.2: Control Tasks to illustrate the Definition of Complexity. The first excited vibrational level on U_D (full line), shifted wavepacket on U_g (dashed line) and first excited level on U_A (long dashed line)

spectra relatively to the spectral width.

Referencing to the previous sections, we notice that the principle of the LC-SLM may be suitable for this task. While reconstructing the laser pulse, we adjust the grid and the lenses so that the whole spectrum falls into the area of LCE. Now, only the number of the LCE in the plane defines the spectral width per element, which further determines the ability of the shaper to reconstruct the fine structure of the pulse. Being able to determine the minimum number of LCE in the shaper which enables a full reconstruction of the pulse, this number characterizes the amount of the effort which has to be used to form the OC pulse from the input one, and thus it is proportional to the *complexity of the control task*. The criterion of the successful reconstruction of the laser pulse is the efficiency the reconstructed laser pulse shows in solving the control task.

In the next section we make some calculations to show that this definition of the complexity is really reasonable in the sense, that it gives results intuitively expected and we also define the complexity more quantitatively.

5.2.1 Control Tasks with Growing Complexity

The molecular systems we will study and the target states to be achieved are shown in Fig. 5.2. The simplest system is given by two electronic states versus a single vibrational coordinate (two-atomic molecule in the gas phase). Since we choose harmonic PES the vibrational spectrum is completely regular. To start with such a – as one may think – oversimplified system is very useful since it allows to put emphasis on what we will understand as the complexity of the control task. This system becomes more complicated if coupled to a thermal environment introducing energy dissipation and dephasing. The regular harmonic oscillator spectrum is transferred to a heterogenous spectrum by coupling the excited-state PES to two additional PES. Such an arrangement is typical for an electron transferring donor bridge acceptor complex. The inhomogeneity of the spectrum can be regulated by the transfer integrals V_{mn} .

The solution of the OC problem for those control tasks introduced in Fig. 5.2 are shown in the upper part of Fig. 5.3 by drawing the respective optimal pulse $\mathbf{E}_{\text{opti}}(t) \equiv \mathbf{n}E_{\text{opti}}(t)$ (\mathbf{n} denotes the polarization unity vector equal for all considered fields). For control task 1 (population of a vibrational level in the excited-state PES) the yield amounts nearly 99%. A somewhat more complicated situation arises in control task 2 where the target state is given by a Gaussian wavepacket in the electronic ground-state (the task corresponds to the well-known pump-dump scheme of Ref. [TR85]). Generally, the OC algorithm provides a sequence of pump and dump pulses over the whole interval (t_i, t_f) . In the present case the vibrational frequency in the excited state PES has been chosen to obtain just a single pump-dump cycle within the 500 fs time window, which leads to a 66% population of the target state. A more complex control task is given by number 3 aimed to guide photoinduced electron transfer through a DBA system. Finally, control task 4 accounts for dissipative effects according to a linear coupling of the active coordinate Q (see Fig. 5.2) to a set of passive (reservoir) coordinates. The Fourier transform $E_{\text{opti}}(\omega)$ of the optimal pulse is drawn in the lower part of Fig. 5.3 together with a Gaussian pulse as an envelope. The overlap of the latter with the respective $E_{\text{opti}}(\omega)$ may be used as quantity characterizing the complexity of the optimal pulse and thus the complexity of the whole control task. In cases 1 to 3 $\alpha = 1$, the task 4 has been studied with $\alpha = 1/5$.

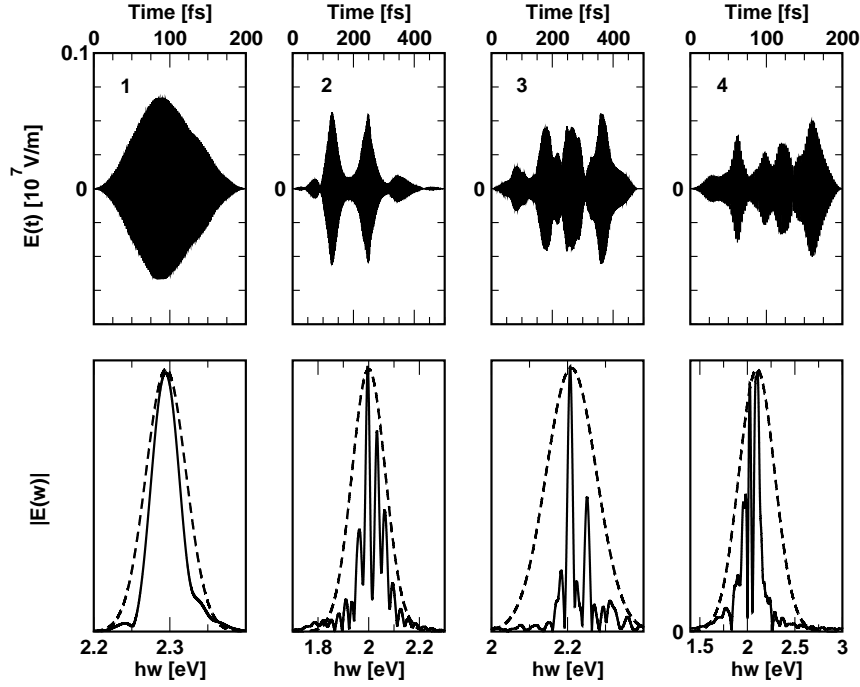


Figure 5.3: The optimal pulse $E_{opti}(t)$ and its Fourier transform $E_{opti}(\omega)$ for the four control tasks as introduced in Fig. 5.2. The additionally shown Gaussian pulse covering $E_{opti}(\omega)$ is used to construct the incoming pulse of the LC-SLM pulse shaping system. The total spectral width covered by the shaper $\Delta\omega^{(sh)}$ is taken as three times the spectral width of the input pulse and reads for the control tasks 1-4: $\Delta\omega_1^{(sh)} = 8.0 \times 10^2 \text{ cm}^{-1}$, $\Delta\omega_2^{(sh)} = 2.6 \times 10^3 \text{ cm}^{-1}$, $\Delta\omega_3^{(sh)} = 2.0 \times 10^3 \text{ cm}^{-1}$ and $\Delta\omega_4^{(sh)} = 5.7 \times 10^3 \text{ cm}^{-1}$. The average spectral width going through a single LC cell can be estimated as $\Delta\omega^{(sh)}/N$.

5.2.2 Pulse-Shaper Analysis and Definition of the Complexity

Now we proceed to define the complexity in a quantitative manner. To this end we look closely on the way in which the control pulse is produced with LC-SLM. Once $E_{opti}(t)$ is known we have to proof to which extend it can be reproduced in the LC-SLM pulse shaping system. As it has been described in detail in Fig. 5.1 a LC-SLM pulse shaper contains two optical grids and in between an array of liquid crystal cells. The first grid realizes a spectral decomposition of the incoming pulse $E_{in}(t)$. The N cells of the array may change the phase and amplitude of every sub-pulse going through the cell.

Afterwards, the second grid unites all N sub-pulses to a common outgoing pulse

$$E_{\text{out}}(t) = \sum_{p=1}^N E_p^{(\text{out})}(t). \quad (5.1)$$

The p 'th sub-pulse of the outgoing field reads

$$E_p^{(\text{out})}(t) = \text{Re} \int_{\omega_p} \frac{d\omega}{\pi} e^{-i\omega t} T_p E_{\text{in}}(\omega). \quad (5.2)$$

Here, $E_{\text{in}}(\omega)$ is the Fourier transform of the complete pulse, and the outgoing sub-pulse is obtained as a superposition of all frequency components around the central frequency ω_p . The latter is the mean frequency corresponding the p 'th cell of the LC-SLM. The frequencies around ω_p are determined by the geometry of the LC part of the modulator. We will consider an idealized pulse shaper neglecting any effect of a lateral extension of the incoming pulse. But it is taken into account that there is not any continuous connection between the frequency interval of sub-pulse p sub-pulse $p+1$ (because of the spatial separation between cell p and $p+1$).

The alternation of every incoming sub-pulse lets deviate $E_{\text{out}}(t)$ drastically from $E_{\text{in}}(t)$. This alternation may be achieved by an independent change of all transmission coefficients $T_p, p = 1, \dots, N$ of the cells. It offers an easy way how to map the optimal pulse $E_{\text{opti}}(t)$ obtained in solving the OC theory for a given problem to an approximate pulse $\tilde{e}_{\text{opti}}(t; N)$ available via a pulse shaper with N cells. To this end we have to identify $E_p^{(\text{out})}(t)$, Eq. (5.2) with the sub-pulse $\tilde{e}_p^{(\text{opti})}(t)$ of $\tilde{e}_{\text{opti}}(t; N)$. To really get the latter quantity we identify $T_p E_{\text{in}}(\omega)$ with the Fourier transform $E_{\text{opti}}(\omega)$ of the optimal pulse. This explains how to choose the transmission of cell p to form the optimal pulse, at least its approximate form $\tilde{e}_{\text{opti}}(t; N)$.

Unfortunately, the ratio $E_{\text{opti}}(\omega)/E_{\text{in}}(\omega)$ may strongly oscillate around the central frequency ω_p of cell p whereas the transmission of the liquid crystal does not. Therefore,

$$E_{\text{opti}}(\omega)/E_{\text{in}}(\omega) \equiv A(\omega) \exp(i\phi(\omega)) \quad (5.3)$$

has to be averaged around ω_p . One can either average the whole expression or choose an independently averaged amplitude \bar{A} and an averaged phase $\bar{\phi}$.

If $\tilde{e}_{\text{opti}}(t; N)$ has been constructed for a given LC-SLM pulse shaper one can proof the way it guides the considered system up to time t_f where one computes $O(t_f; \tilde{e}_{\text{opti}})$. Then, the completeness to fulfill the control task can be

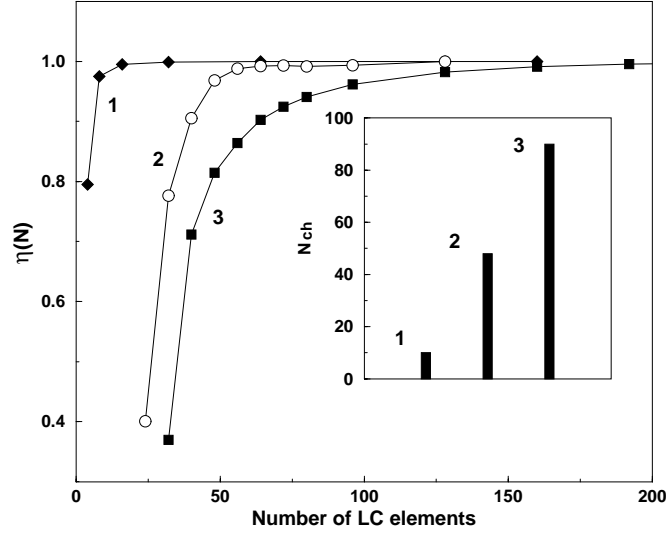


Figure 5.4: The efficiency of the pulse shaper characterized by the ratio η versus the number N of liquid crystal cells in the shaper for the different control tasks of Fig. 5.2. Inset: N_{ch} leading to a 95% yield ordered with respect to the different control tasks.

characterized by

$$\eta(N) = \frac{O(t_f; \tilde{e}_{\text{opti}})}{O(t_f; E_{\text{opti}})} . \quad (5.4)$$

Obviously, the introduced quantity should depend on the cell number N , and in this way on the accuracy we can reproduce the optimal field.

Fig. 5.4 displays $\eta(N)$ versus N for the first three control tasks described in Fig. 5.2. The curves should be confronted with the Fourier-transform $E_{\text{opti}}(\omega)$ of the respective optimal pulse shown in the lower part of Fig. 5.3 together with $E_{\text{in}}(\omega)$. For control task 1 the optimal pulse is mainly determined by the demand of its convergency to zero at times $t = 0$ and $t = t_f$, and it is rather close to the input pulse. $\eta(N)$ clearly shows that the desired optimal form can be achieved with a rather moderate number of liquid crystal cells of the LC-SLM. Control task 2 is characterized by a more complicated target state (displaced vibrational ground-state function at $t = 500$ fs). In $E_{\text{opti}}(\omega)$ we can recognize all the transition frequencies involved in the dynamics. The input pulse which covers the whole spectrum and fits its maximum has the width of $\tau_p = 15$ fs. The laser field consists mainly of two pulses with the delay corresponding to the oscillator period. The time evolution of the level-population (not shown here) demonstrates that they act exactly in accordance

with the pump–dump scheme. According to the 15 fs duration of the incoming pulse $\eta(N)$ approaches 1 for $N < 60$, what is well within the capabilities of commercial pulse shapers. The laser field connecting the initial and the target state for control task 3 is rather complicated and for its reproduction a larger number of liquid crystal cells are necessary. In the present case our task could be accomplished with the 20 fs incoming pulse. According to Fig. 5.4 one notices that $\eta(N)$ converges to 1 for N about 200.

For the control tasks on the Fig. 5.4 we can introduce a characteristic number N_{ch} of liquid crystal cells (in the pulse shaper) necessary to solve the control task. We define N_{ch} by the demand that the ration $\eta(N_{ch})$, Eq. (5.4) amounts the value of 0.95. Accordingly, an ordering of the discussed control tasks with increasing N_{ch} becomes possible (inset of Fig. 5.4). As expected, this ordering coincides very well with the increasing complexity of the optimal pulse (either in its time or frequency dependent form). In this manner we can understand N_{ch} as a number which offerers a combined characterization of the *complexity* of the considered molecular system as well as of the control problem as it was required in our discussion at the beginning of this section. The results obtained from this and other computations (not shown here) suggest that the $\eta(N)$ dependency is rather general and as such the quantitative definition of the complexity introduced here can be regarded as general, too.

5.2.3 Complexity and Dissipation

Similar situation as above can be observed in the case of a relatively simple control task where the system is subject to the influence of increasing dissipation. The results are summarized in Fig. 5.5. The influence of the dissipation results in the control field acting in somewhat later times. This is a tendency already observed in Chapter 4 while studying ET. In Fig. 5.5 (c) the pulse gets spectrally broader and more structured in time as well as in frequency domain. It corresponds to the population of more than one vibrational level. Increasing the strength of dissipation, different mechanisms to populate a desired level are switched on (like indirect population through the relaxation from the above levels), so the critical number N_{crit} grows. Change of the control mechanism in presence of the dissipation has also been demonstrated in section 4.3 in case of ET. With increasing dissipation the absolute efficiency of the control is decreasing as one may see from the insert in Fig. 5.6. Relative efficiency as a function of the number of LC elements N , shows a similar dependency as in forgoing examples from Fig. 5.3.

In section 4.3 it was also shown, that by increasing strength of dissipation over a certain critical point, the control pulse gets shorter and loses compli-

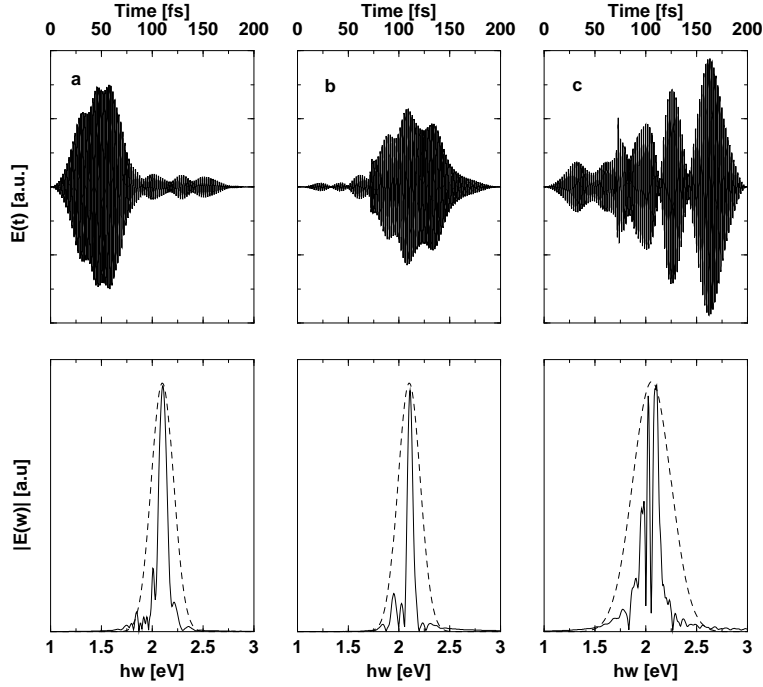


Figure 5.5: The optimal pulse $E_{opti}(t)$ and its Fourier transform $E_{opti}(\omega)$ for the control task 1 including the dissipation. The vibrational life-time of the target level τ_t is used to characterize the strength of dissipation. (a) Without dissipation, (b) $\tau_t = 320 fs$, (3) $\tau_t = 640 fs$.

cated structure, so that the number characterizing complexity according to our definition would become smaller and the definition fails. But to compute reliable value for the complexity we need a OC pulse solving the control task and with strong dissipation the OC theory fails to provide such a control pulse. Thus one may conclude, that the failure of the definition of the complexity is caused by the failure of the OC theory itself. Alternatively, a new definition of the complexity, taking in account the absolute value of the control yield may be used to overcome this problem.

5.2.4 Experimental Relevance of the Optimal Control Theory

From the Figures 5.4 and 5.6 it becomes clear that the values of the characteristic number of cells N_{ch} lies for all given examples within parameters of available experimental devices. Thus, the proof is given, that the experimen-

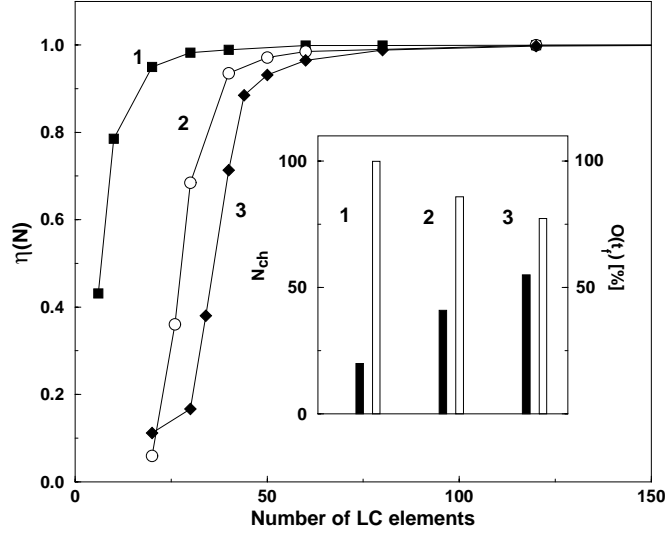


Figure 5.6: The efficiency of the pulse shaper as shown in Fig. 5.4, but for the control task 4, and with different strength of dissipation. The vibrational life-time of the target level τ_t is used to characterize the strength of dissipation. 1. Without dissipation, 2. $\tau_t = 320 fs$, 3. $\tau_t = 640 fs$. Inset: N_{ch} as in Fig. 3 (black bar) and the population of the target state in percentage (white bar).

tal reproduction of the theoretical pulses is possible without any loss of their ability to control the molecular dynamics. For the given examples one also notices the absence of any remarkable discontinuity in the curves showing the extent the control task has been solved by the approximate optimal pulses for different N . However, this regular behavior is disturbed for the calculations with a small number of cells N and whenever there are any control pathways leading to different dynamics in the vicinity of our control path. To check the reliability of the OC results one can use the method introduced in section 4.5.

Concentrating on a single control task at a single type of molecule the decreasing slope of the ration η with increasing N (or of $O(t_f; \mathcal{E}_{opti})$ what can be directly deduced from the experiment) may offer some experimental evidence to which extent the control task has already been solved. It is an enlightening approach to systematically apply pulse shapers where the number of LC cells differs.

The approach discussed in this section enables a theoretical check of the feasibility of the OC pulses and the estimation of their complexities. Also developed here was a simple way how to transfer knowledge of the control pulse from the theory to the experiment and *vice versa*. The parameters of the

LC-SLM to reproduce theoretical pulses can be easily computed.

5.3 Optimal Control with Static Disorder (Orientational Averaging)

The present section will make one step towards performing the OC of the molecular systems under more realistic conditions by considering a special type of the disorder in the system. In the realistic situation, all quantities entering the Hamiltonian, Eq. (4.1) and (4.3) can be subject to fluctuations caused by structural and energetic disorder. Let us characterize such fluctuations by a set of parameters $y_m \equiv \{y_j^{(m)}\}$. It may describe a specific energetic and structural situation in the molecule m or the specific coupling to the environment. Below we will deal with an example of the excitation of a molecular ensemble by a polarized laser field. It depends on the orientation of the dipole-moment of the particular molecule how strong the interaction with the field will be. Therefore, one has to apply a configuration averaging to the quantity $O(t_f; \mathbf{E})$ since it is an ensemble average. With n_{mol} the volume density of the molecules in the probe volume V_0 we can write

$$\langle O(t_f; \mathbf{E}) \rangle_{disorder} = \frac{1}{n_{mol}V_0} \sum_{m \in V_0} O(t_f; \mathbf{E}; y_m). \quad (5.5)$$

The dependence of $O(t_f; \mathbf{E}; y_m)$ on the concrete parameter set y_m can be specified as follows

$$O(t_f; \mathbf{E}; y_m) = tr_S \{ \hat{O} \mathcal{U}(t_f, t_0; \mathbf{E}; y_m) \hat{\rho}(t_0; \mathbf{E}; y_m) \}, \quad (5.6)$$

i.e. disorder effects all parameters involved in the time-propagation and probably the initial state. To be simple enough the possible y_m -dependence of the target operator \hat{O} has been neglected. Accordingly, the optimal field has to be determined via

$$\mathbf{E}(t) = \frac{1}{n_{mol}V_0\lambda} \sum_{m \in V_0} \mathbf{K}(t_f, t; \mathbf{E}; y_m), \quad (5.7)$$

with control kernel

$$\mathbf{K}(t_f, t; \mathbf{E}; y_m) = \frac{i}{\hbar} tr_S \{ \hat{\sigma}(t, \mathbf{E}; y_m) \mathcal{M}(y_m) \hat{\rho}(t; \mathbf{E}; y_m) \} \quad (5.8)$$

referring to a single disorder configuration. If we would like to apply the iteration scheme to determine the optimal field we first note from Eq. (5.7) that the optimal field can be understood as a field which has been averaged

with respect to the various disorder realizations. In contrast the iteration of $\hat{\rho}(t; \mathbf{E}; y_m)$ and $\hat{\sigma}(t, \mathbf{E}; y_m)$ has to be carried out for the various realizations, but these are coupled via the disorder averaged control field.

As an example of the application of the above presented theory we will now discuss a case where the control experiment is carried out using polarized light. This is often the case in fragmentation experiments [vVBK⁺01]. Thus excitation of the molecular systems depends on the orientation of its dipole moment with respect to the polarization plane of the laser pulse. In the fragmentation experiments in gas phase the different orientations of the molecules are caused by their free rotation. The complete theory has to account for the rotation in the equation of motion, however if the rotation period is much longer than the control pulse, one can consider the molecule as non-rotating. We assume this to be the case in the following. For molecules embedded e.g. in a solid the situation gets even easier since the rotation is limited and molecular dipole-moments can be regarded as fixed with respect to the polarization plane of the laser pulse. In our treatment we will assume that the detection of the target state does not differ between different orientations of the molecules, what is again the case in common fragmentation experiments, where the fragments are detected by a mass spectrometer.

In the following study we use the similar initial and target states as before (see section 4.4 and Table 4.4). Generally, the yield of the OC and the control pathway via which the control goal is reached depend on the optimal field strength. Using polarized field the effective field strength felt by individual molecules is different from one to another. Therefore, for different sub-ensembles composed of molecules with a chosen orientation, different control pathways should be applied to optimize the yield of the reaction. But, in the practical case optimal field must have a shape compromising the optima of the sub-ensembles in order to obtain the optimum for the complete ensemble. Thus, we expect a different control pulse if optimizing molecules with identical orientations of the dipole moment from that one optimized for the ensemble with random orientation. Fig. 5.7 illustrates this situation for a single orientation and for an ensemble of orientations. The ensemble has been simulated by taking N mutual orientation angles θ of the dipole-moment and the plane of the polarization of the incoming laser pulse with the equidistant step $\Delta\theta = 2\pi/N$. N is taken so that the results converge. For the presentation in this section we have chosen $N = 20$ which represents a value leading to a well converged result (see Fig. 5.8 and later discussions). We can see that the pulses optimized for the ensemble of orientations and for a single orientation indeed differ. By a careful comparison it can be found that the control pulse obtained with a single orientation allowed has slightly more complicated structure. There are some

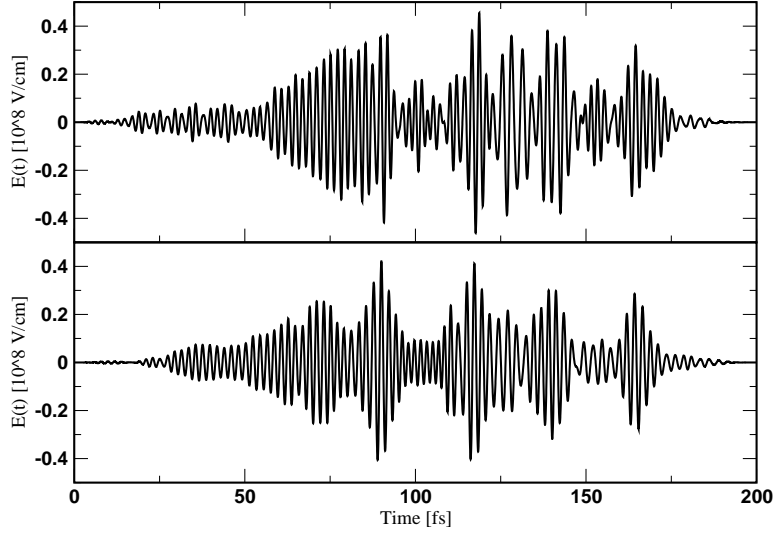


Figure 5.7: Control tasks to illustrate the definition of complexity. The optimal pulse for a single molecule (upper figure) and for an ensemble represented by 20 different orientations (lower figure).

small features with rapid change of the envelope of the pulse which disappear on the pulse optimized for the ensemble so that the latter pulse appears to have a little smoother envelope. This is the result of the averaging over different orientations. It can also be seen that the positions of the sub-pulses are different between both optimal pulses from Fig. 5.7. Although it is not possible to identify a direct reason for the particular structures of the control pulses, Fig. 5.7 demonstrate the differences caused in the shape of the optimal pulse by the effects of orientational averaging.

In our particular case the convergency with respect to the number of orientations has been reached with an ensemble of 20 orientations. It can be clearly seen from the Fig. 5.8, where the control yields $O(t_f; \mathbf{E})$ achieved with control pulses optimized for a given number of orientations has been plotted. We notice that for the case of 1 and 2 orientations chosen according to the above described scheme (i.e. parallel and anti-parallel to the polarization plain of the laser field) we achieve the identical result corresponding to the upper pulse of the Fig. 5.7. For a small number of orientations the control yield oscillates. Clearly, in case of 4 orientations two of them are perpendicular to the polarization plain of the laser field and they do not interact with the field at all. As the number of orientations grows the ensemble covers all the possible orientations and the results converge. Thus, the oscillations are only an artefact of

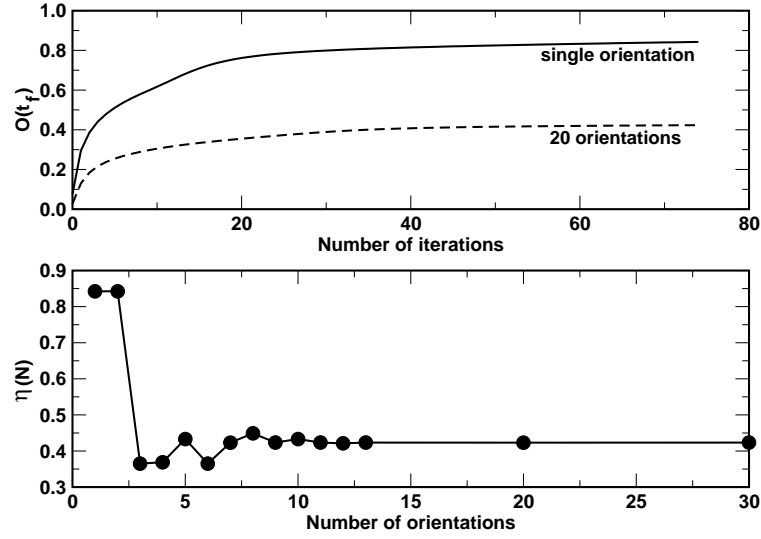


Figure 5.8: Convergency of the OC algorithm with orientational averaging (upper figure). The converged value for an ensemble of 20 orientations is significantly lower than that one for a single orientation, but the speed of the convergency remains the same as in case of a single molecule. Convergency of the results with respect to the number of orientations is also quit high (lower figure). Only about 15 to 20 orientations is necessary to obtain convergency.

the scheme of choosing the ensemble, whereas the converged result represents correctly any big ensemble with a homogeneous layout of the orientations.

Finally, one can ask a question how successful would be the pulse optimized for a single orientation in guiding the ET of an ensemble of the molecules with different orientations, and vice versa, how good would the optimal pulse corresponding the that ensemble guide the ET in case of a single orientation. Since both pulses represent the optimal solutions for their particular molecular systems, while exchanging them we should find the control yield decreasing. Indeed, this is the case in Fig. 5.9. For the particular model system studied here we see only the difference less then 10 percent, but generally even much bigger differences can be expected.

Similar studies including the averaging over the ensembles of molecules subject to the interaction with the laser field depending on the molecule's position has been carried out in Ref. [SRdVR00]. There, the effect of the laser field spatial profile has been taken into account. Thus, the OC theory shows a great flexibility in description of various experimental situations.

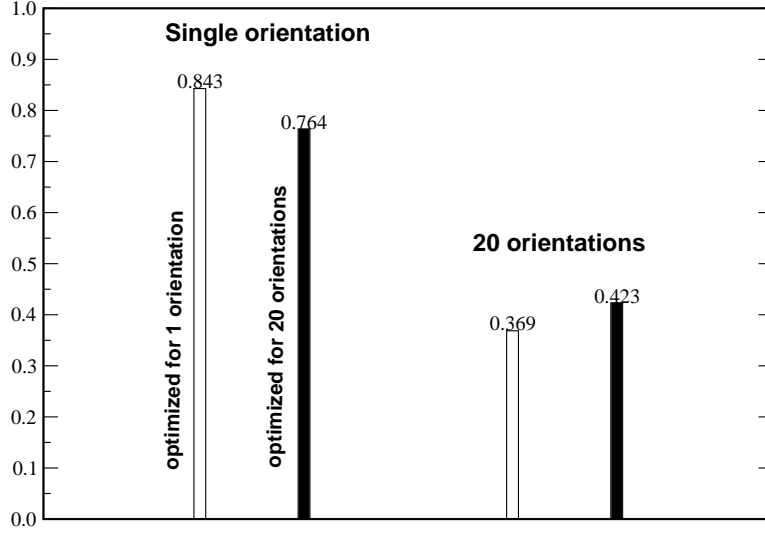


Figure 5.9: Comparison of the yields of the single molecule and the ensemble optimal pulses

5.4 Optimal Control with the Non-Markovian Dissipation

The importance of the memory effects in dissipative dynamics guided by the non-Markovian QME have been studied in the Part II of this thesis. It was found that the memory effects indeed lead to dynamics slightly different from that one obtained from the standard QME (including Markov approximation). As a first step we have considered the dissipation in Markov approximation in Part III. Now, the generalization of OC theory for the case of non-Markovian dissipative dynamics will be presented. To this end we utilize the factorization method explained in Appendix E.

Thus, for the dissipative part of the non-Markovian QME, Eq. (1.10) we write $\hat{D} = \hat{D}_1 + \hat{D}_2$ where \hat{D}_2 corresponds to the time independent part $C_{uv}^{(2)}$ of the correlation function and the contribution \hat{D}_1 stems from the time-dependent part $C_{uv}^{(1)}(t)$ of the correlation function (see Appendix E). In the next step the correlation function $C_{uv}^{(1)}$ which depends on the two time-arguments t and \bar{t} will be replaced by the multiple factorization *ansatz* according to Eq. E.2. Using Eq. E.2 and defining the auxiliary operators $\hat{\sigma}_{s,uv}^{(+)}(t)$ and $\hat{\sigma}_{s,uv}^{(-)}(t)$ which obey the Equations (E.6) and (E.7). The term \hat{D}_2 determined by the time independent part of C_{uv} can be written by introducing the single additional

density operator $\hat{\sigma}$ which can be obtained from Eq. (E.10). All auxiliary operators $\hat{\sigma}_{s,uv}^{(+)}(t)$, $\hat{\sigma}_{s,uv}^{(-)}(t)$ and $\hat{\sigma}$ vanish at the initial time t_0 . The quantities $\hat{\sigma}_{s,uv}^{(\pm)}(t)$ are not hermitian whereas $\hat{\sigma}$ represents a hermitian operator. Furthermore, the equations of motion for $\hat{\sigma}_{s,uv}^{(\pm)}(t)$ does not conserve the respective trace of the operators. However, $\hat{\sigma}$ obeys a trace-conserving equations. The introduction of the auxiliary operators $\hat{\sigma}_{s,uv}^{(\pm)}(t)$ and $\hat{\sigma}$ demonstrates that the time-nonlocality can be removed with any accuracy one needs. Furthermore, the external field exclusively enters the equation of motion via the corresponding Hamiltonians (see Appendix E).

Since we have now time-local equations at hand a generalization of the approach given in section 3.1 to derive a control kernel, Eq. 3.9 is possible. To this end we introduce the column vector of density operators

$$\mathbf{S}(t) = \begin{pmatrix} \hat{\rho}(t) \\ \hat{\sigma}_{s,uv}^{(+)}(t) \\ \hat{\sigma}_{s,uv}^{(-)}(t) \\ \hat{\sigma}(t) \end{pmatrix}. \quad (5.9)$$

The respective equation of motion reads

$$\frac{\partial}{\partial t} \mathbf{S}(t) = -\mathcal{L}_S(t) \mathbf{S}(t) + \begin{pmatrix} -\hat{D}_1(t; \hat{\sigma}_{s,uv}^{(\pm)}) - \mathcal{L}_{mf} \hat{\sigma}(t) \\ \frac{i}{\hbar} \beta_{uv}^{(s)}(t) K_v \hat{\rho}(t) \\ \frac{i}{\hbar} \beta_{vu}^{(s)}(-t) \hat{\rho}(t) K_v \\ -i \mathcal{L}_{mf} \hat{\rho}(t) \end{pmatrix}. \quad (5.10)$$

Introducing the matrix Liouville superoperator

$$\mathbf{L}(t) = \mathcal{L}_S(t) \mathbf{I} + \Delta \mathbf{L}(t), \quad (5.11)$$

where \mathbf{I} denotes the unity matrix and $\Delta \mathbf{L}$ generates the second term on the right hand side of Eq. (5.10), we have the compact notation

$$\frac{\partial}{\partial t} \mathbf{S}(t) = -\mathbf{L}(t) \mathbf{S}(t) \quad (5.12)$$

of the equation of motion. Its solution reads

$$\mathbf{S}(t) = \mathbf{U}(t, t_0) \mathbf{S}(t_0), \quad (5.13)$$

with the matrix time-evolution superoperator

$$\mathbf{U}(t, t_0) = T \exp \left\{ -i \int_{t_0}^t d\tau \mathbf{L}(\tau) \right\}. \quad (5.14)$$

Now it becomes possible to derive the control kernel. To get $\rho(t_f)$ we have to determine $\mathbf{S}(t_f)$ and take the element of the first row. The functional derivative of $O(t_f; \mathbf{E})$ can be carried out in similarity to Appendix H. First we note

$$\frac{\delta \mathbf{S}(t)}{\delta \mathbf{E}(t)} = -i \int_{t_0}^{t_f} d\tau \mathbf{U}(t_f, \tau) \frac{\delta \mathbf{L}(\tau)}{\delta \mathbf{E}(t)} \mathbf{U}(\tau, t_0) \mathbf{L}(\tau). \quad (5.15)$$

The functional derivative gives

$$\frac{\delta \mathbf{L}(t)}{\delta \mathbf{E}(t)} = -\frac{1}{\hbar} \delta(t - \tau) \mathcal{M} \mathbf{I}. \quad (5.16)$$

We insert the result into $O(t_f; \mathbf{E})$ and obtain the control kernel as

$$\mathbf{K}(t_f, t; \mathbf{E}) = \frac{i}{\hbar} \text{tr}_S \left\{ \hat{O} (\mathbf{U}(t_f, t) \mathcal{M} \mathbf{S}(t))_1 \right\}. \quad (5.17)$$

The notation $(\dots)_1$ indicates that we have to take the element of the first row. Note the alternative notation $\mathcal{M} \mathbf{S}(t) = \mathcal{M} \mathbf{I} \mathbf{U}(t, t_0) \mathbf{S}(t_0)$.

The control kernel (5.17) can be calculated by the same iterative procedure as introduced in section 3.1 applied on the Eq. (5.10). Since (5.10) enables to include the memory effects and the external field dependence of the dissipation the formulation of the OC with Eq. (5.17) is the most general formulation available in the literature.

5.5 Summary of the Chapter 5

The present chapter has been devoted to problems directly connected with the application of the results of the OC theory in experiments. In section 5.1 we have first discussed the experimental set-up used in the recent self-learning OC experiments. It was discussed how this set-up with the LC-SLM can be used to perform a search for the OC pulse and corresponding algorithms have been shortly presented.

In section 5.2 we have studied how the pulse-shaping part of the experimental set-up is able to reconstruct the theoretical control pulses. Resulting from the analysis we also came to a working quantitative definition of the complexity of the control task. The reasonability of the definition of the complexity has been tested on a series of control tasks with growing complexity of the electron-vibrational spectra and on the systems subject to vibrational relaxation. The definition of the complexity enabled us to obtain an additional insight into the completeness of the solution of the control task even for recent experiments.

Section 5.3 has been devoted to the problem of OC of the systems with static disorder. The corresponding generalization of the OC scheme has been introduced and the theory has been tested on a model system. As it was expected the OC theory yields different results for disordered systems and those without disorder. The technique developed to account for disorder can be applied for a wide variety of problems including the consideration of the spatial light profile of the laser pulse etc.

Finally, in section 5.4 we have formulated the OC theory for the case of non-Markovian dissipation. With this formulation it would be in principle possible to account for the memory effects and the effects of the field modulation of the dissipation. The presented results show the great adaptability of the OC theory to a variety of problems. The generalizations of the OC theory from sections 5.3 and 5.4 can be combined with further achievements presented in Appendix J and show the way towards its application for the explanation and design of control experiments in the near future.

Part IV

Conclusions and Outlook

In this thesis we have investigated ultrafast laser pulse induced dynamics of dissipative molecular systems. We have applied the density matrix theory for the description of the dynamics of polyatomic molecular systems interacting with thermal bath. The reduced description excluding the so-called passive thermal bath degrees of freedom from the explicit description results in time non-local equation of motion for the reduced density matrix. This leads to so-called memory (non-Markovian) effects. We have concentrated on the identification of memory effects in the system dynamics and on the estimation of how important their inclusion would be for the description of its dissipative dynamics. Based on these studies we have examined in which ways dissipative molecular dynamics can be controlled by laser pulses.

To clearly identify signatures of memory effects the vibrational relaxation dynamics have been compared with and without the memory. A characteristic indication that vibrational relaxation observed in the experiment requires a non-Markovian description is given by the change of the modulation frequency the time evolution of the vibrational populations shows.

Although we have observed memory effects in a special case of the vibrational relaxation dynamics the discussions in this work enables us to draw the following general conclusion. The non-Markovian effects induced by an ultrafast laser field can be identified by an irregular dynamics in times just after the action of the laser field. This irregularity is caused by the sudden change in the dynamics and effective establishing of a new initial state for the system breaking the correlations with the bath. A system with a memory “remembers” this sudden change at least for the duration of the memory time and turns to a Markov dynamics afterwards. A Markovian system develops after the laser field action as if it always was in this newly defined effective initial state.

The discussion of the results of our work suggests that the memory effects can play an important role in the optimal control of dissipative dynamics. While dealing with non-Markovian dynamics we always studied the case of a single short laser pulse which induced the memory effects by effectively setting new initial condition for the propagation of the system density matrix. The control pulses obtained from optimal control theory represent whole trains of such short pulses possibly inducing non-Markovian dynamics during the whole duration of the pulse-train. The optimal control theory formulated including non-Markovian dynamics may clearly obtain significantly different results from the Markovian formulation if the control pulse features become much shorter than the memory time of the system. This gives a future study of the non-Markovian optimal control a new significance.

In our work we have applied the optimal control theory to the problem of

photo-induced electron transfer in a donor–bridge–acceptor systems. The optical field couples the electronic ground state of the molecular system with the certain donor electronic state via a dipole allowed transition. After a photo-excitation and according to the presence of an interstate coupling the electron transfer proceeds from the donor state to the acceptor via intermediate bridge state. If no control is provided and in absence of dissipation the population of the excited state spreads over the whole donor–bridge–acceptor complex. We have studied the feasibility of guiding the wavepacket motion so that we could (i) populate certain vibrational levels of the bridge or acceptor state at a given time or (ii) place a wavepacket of a given shape at a given position at a given time. In order to fulfill the control task the optimal pulse obtained from the optimal control theory excites and de-excites the system with a special timing so that the different parts of the electro-vibration wavepacket meet at a given time on the desired position at the set of potential energy surfaces of the donor–bridge–acceptor complex. The control pulse establishes a vibrational wavepacket moving periodically over the whole donor–bridge–acceptor complex. In this way it has been demonstrated that the problem is completely controllable.

The picture changes if one allows for dissipation e.g. by embedding the system into the condensed matter or dissolving in a solvent. In order to account for the dissipative dynamics we have first formulated the optimal control theory for the dissipative systems in Markov approximation. Such a formulation for a rather general form of dissipation has been provided for the first time in the literature. As expected it was shown that dissipation decreases the control yields of the electron transfer reactions. Comparing the yield obtained for the dissipative system by an optimal pulse designed for the dissipation-less case we can conclude that the optimal control partially compensates for the decrease of the control yield. The mechanism of such a compensation can be demonstrated at the control task where one tries to populate a single vibrational level in the acceptor state. A closer look at the time evolution of the vibrational populations reveals that at the presence of dissipation not only the desired target level but the above laying levels become populated. These levels decay into the target level and enhance its population. Thus one can conclude, that the optimal control algorithm utilizes the natural aspects of dissipative dynamics such as the finite life time of energy levels to achieve the population of the target state.

Further, we have concentrated on problems connected with the application of the results of optimal control theory in experiment. The standard experimental device, the liquid–crystal spatial light modulator has been analyzed and it was shown how to compute its parameters in order to reconstruct the theo-

retical optimal pulse in the experiment and *vice versa*. Comparing the control of systems with energetic spectrum of increasing complexity and prescribing different control tasks in these systems we have come to a certain quantitative definition of the complexity of the control task. This quantity represents the combined characteristics of both the molecular system and the control task and is to some extent even experimentally available. By the control experiments repeated with the light modulators with different numbers of liquid-crystal elements (and thus with different pulse reconstruction capabilities) one may answer the question to which extent a given control task has been fulfilled. This is done by plotting the control yields in dependence on the number of liquid crystal elements used in the experiment and examining the convergency of the resulting curve.

In order to be able to describe more complicated experimental situations the rest of the work has been devoted to certain generalizations of the optimal control theory. Namely, we have studied the problem of a static disorder in the controlled system. We provided a corresponding formulation of the optimal control theory and calculated optimal pulses for the control of electron transfer reaction in the molecular system studied previously, but now with the random orientation of the electric dipole-moment with respect to the linearly polarized laser control field. The results suggest that even here the optimal control theory finds successfully solutions which exhibit high control yield. Thus the flexibility of the optimal control theory has been clearly demonstrated.

It was already argued that due to the presence of ultrafast features in the optimal pulses the consideration of memory effects in the optimal control theory becomes necessary. Therefore, a general formulation of the control equations has been given to provide a basis for the future theoretical studies. Depending on the molecular system in question, (particularly on the type of the bath correlation function which determines the duration of the memory) the non-Markovian optimal control would involve expensive numerical calculation. Consequently, a test of the importance of the non-Markovian dynamics in optimal control has to be conducted on some limited model system before one comes to the implementation of the non-Markovian optimal control theory for general molecular systems.

Recently, experimental attention in the control of molecular systems turns to complex systems including the dissipative systems. Thus the problems dealt with in this work will find more experimental relevance in the near future. To finally achieve a genuine correspondence of the theoretical and experimental results very involved but in principle feasible calculations have to be performed. In such a calculation it would be necessary to consider simultaneously many effects from which we can particularly name:

- the spectral limitation of the control pulse
- the spatial profile of the laser field
- the averaging over disorder
- time non-local target state measurement
- multi-photon transitions.

The time non-local target state measurement refers to experiments where the target state of the system is tested by a weak field probe. Except for the multi-photon transitions, corresponding theoretical formulations already exist in the literature or have been presented in this thesis. The combined use of these methods seems to be straightforward but may become numerically expensive. Also the optimal control calculations with potential energy surfaces obtained for the controlled molecular systems from quantum chemical calculations does not represent any principle obstacle from the theoretical point of view. The optimal control of dissipative dynamics has been shown to be feasible too, although the control yield decreases rapidly with increasing strength of dissipation.

Although the original aim of the optimal control has been motivated by the prospect of efficient governing the dynamics of chemical reactions towards the desired products with possible industrial applications, the concept has become very fruitful in basic research even outside chemistry. Simultaneously with the development of the optimal control the studies has been conducted which suggest to use control methods and the resulting control pulses to actually extract information about the molecular system, e.g. about its potential energy surface. The control of systems in condensed phase bring the prospect of the control of e.g. the dynamics of artificial semiconductor structures like quantum dots. The ability of precise preparation of particular target states may become useful in quantum computing.

With the theoretical apparatus developed and refined in this work we have in hand majority of the means to successfully simulate and explain future control experiments on isolated and open molecular systems and to further extend the optimal control theory.

Part V

Appendices

Appendix A

Nakajima–Zwanzig Equation with External Fields

In section 1.1 we have mentioned the so-called projection operator technique which enables the derivation of an exact equation of motion for the RDO. According to the projection operator technique (see e.g. [MK99]) one gets the reduced statistical operator $\hat{\rho}(t)$ from the complete time-dependent statistical operator $\hat{W}(t)$ by applying the projector (projection superoperator) $\mathcal{P} = \text{tr}_R\{\dots\}\hat{R}$. Here, \hat{R} is a so far arbitrary operator acting on the reservoir DOF, and the trace operation tr_R exclusively concerns the state space of reservoir states. For \mathcal{P} to fulfill the definition of projection operator ($\mathcal{P}^2 = \mathcal{P}$) the trace over \hat{R} has to be equal 1. The aim of this appendix is to review the derivation of the so-called Nakajima–Zwanzig equation (NZE) which represents an exact equation of motion for the RDO. The general form of the NZE has been given in Eq. (1.8) and here the concrete expressions for the initial correlation term \hat{I}_{NZ} and the memory kernel \mathcal{M}_{NZ} will be presented. We use the superoperator notation in this appendix so that we define so-called Liouville superoperators $\mathcal{L}_X \dots = [H_X, \dots]_-$ where H_X are corresponding Hamiltonian operators with $X = S, R, S - R$ etc..

For the derivation of NZE it is advantageous to switch into the interaction picture and to write for the density operator of the compound system $S + R$

$$\hat{W}^{(I)}(t) = \mathcal{U}_{S+R}^\dagger(t, t_0) \hat{W}(t). \quad (\text{A.1})$$

We assume the external field to be incorporated into the system Hamiltonian so that the superoperator $\mathcal{U}_{S+R}^\dagger(t, t_0)$ depends independently on times t_0 and t

and follows as a time-ordered exponential

$$\mathcal{U}_{S+R}(t, t_0) = T \exp \left(-\frac{i}{\hbar} \int_{t_0}^t d\bar{t} \{ \mathcal{L}_{S+R}(\bar{t}) \} \right). \quad (\text{A.2})$$

Applying the projection superoperator \mathcal{P} on $\hat{W}^{(I)}(t)$ we obtain

$$\mathcal{P}\hat{W}^{(I)}(t) = \hat{R} \text{tr}_R \{ \hat{W}^{(I)}(t) \} = \hat{R}\hat{\rho}^{(I)}(t). \quad (\text{A.3})$$

For the later convenience we define so-called orthogonal complement $\mathcal{Q} = 1 - \mathcal{P}$ of the projection superoperator \mathcal{P} . We use the identity $\hat{W}^{(I)}(t) = \mathcal{P}\hat{W}^{(I)}(t) + \mathcal{Q}\hat{W}^{(I)}(t)$ valid for an arbitrary statistical operator \hat{W} on the Liouville-von Neumann equation

$$\begin{aligned} \mathcal{P} \frac{\partial}{\partial t} \hat{W}^{(I)}(t) &= \frac{\partial}{\partial t} \mathcal{P} \hat{W}^{(I)}(t) = -\frac{i}{\hbar} \mathcal{P} \mathcal{L}_{S-R}^{(I)}(t) \hat{W}^{(I)}(t) \\ &= -\frac{i}{\hbar} \mathcal{P} \mathcal{L}_{S-R}^{(I)}(t) \{ \mathcal{P} \hat{W}^{(I)}(t) + \mathcal{Q} \hat{W}^{(I)}(t) \}. \end{aligned} \quad (\text{A.4})$$

Performing the trace over the reservoir DOF on the equation (A.4) we arrive at

$$\frac{\partial}{\partial t} \hat{\rho}^{(I)}(t) = -\frac{i}{\hbar} \text{tr}_R \{ \mathcal{L}_{S-R}^{(I)}(t) (\hat{R} \hat{\rho}^{(I)}(t) + \mathcal{Q} \hat{W}^{(I)}(t)) \}. \quad (\text{A.5})$$

For the expression $\mathcal{Q}\hat{W}^{(I)}(t)$ we can write an equation analogous to Eq. (A.4) for which a formal solution can be found in the form

$$\mathcal{Q}\hat{W}^{(I)}(t) = \mathcal{Q}\hat{W}^{(I)}(t_0) - \frac{i}{\hbar} \int_{t_0}^t d\bar{t} \mathcal{Q} \mathcal{L}_{S-R}^{(I)}(\bar{t}) \hat{R} \hat{\rho}^{(I)}(\bar{t}). \quad (\text{A.6})$$

Finally, we insert (A.6) into (A.5) and change back to the Schrödinger representation. Introducing the abbreviation

$$\langle \dots \rangle_R = \text{tr}_R \{ \dots \hat{R} \} \quad (\text{A.7})$$

we obtain

$$\begin{aligned} \frac{\partial}{\partial t} \hat{\rho}(t) &= \text{tr}_R \{ \mathcal{L}_{S-R} \mathcal{U}_{S+R}(t, t_0) \mathcal{S}(t, t_0) \mathcal{Q} \hat{W}(t_0) \} \\ &- i \left(\mathcal{L}_S(t) + \langle \mathcal{L}_{S-R} \rangle_R \right) \hat{\rho}(t) \\ &- \int_{t_0}^t d\bar{t} \langle \mathcal{L}_{S-R}^{(R)}(t) \mathcal{U}_S(t, t_0) \mathcal{S}(t, \bar{t}) \mathcal{Q} \mathcal{U}_S(\bar{t}, t_0) \mathcal{L}_{S-R}^{(R)}(\bar{t}) \rangle_R \\ &\times \hat{\rho}(\bar{t}). \end{aligned} \quad (\text{A.8})$$

The first term on the right hand-side describes the influence of initial correlations whereas the last term corresponds to the dissipative part of the density operator equation. The quantity \mathcal{S} can be obtained from \mathcal{U}_{S+R} by replacing \mathcal{L}_{S+R} by $\mathcal{Q}\mathcal{U}_S(\bar{t}, t_0)\mathcal{L}_{S-R}$. In this manner \mathcal{S} incorporates the complete perturbation expansion with respect to the system-reservoir interaction.

As it can be seen from the second term on the right-hand side of Eq. (A.8) the reversible part of the density operator equation has been extended by a mean-field type term of the system-reservoir interaction. The quantity $\mathcal{L}_{S-R}^{(R)}(t)$ introduced in the dissipative part of Eq. (A.8) has to be understood as \mathcal{L}_{S-R} translated into an interaction representation defined by \mathcal{L}_R alone.

Finally, we compare the NZE (A.8) with the expression (1.8) so that we can list the concrete forms of the initial correlation term and the memory kernel. It reads

$$\hat{\mathcal{I}}_{NZ}(t, t_0; \hat{W}(t_0)) = \text{tr}_R\{\mathcal{L}_{S-R}\mathcal{U}_{S+R}(t, t_0)\mathcal{S}(t, t_0)\mathcal{Q}\hat{W}(t_0)\}, \quad (\text{A.9})$$

$$\mathcal{M}_{NZ}(t, t_0, \bar{t}) = \langle \mathcal{L}_{S-R}^{(R)}(t)\mathcal{U}_S(t, t_0)\mathcal{S}(t, \bar{t})\mathcal{Q}\mathcal{U}_S(\bar{t}, t_0)\mathcal{L}_{S-R}^{(R)}(\bar{t}) \rangle_R. \quad (\text{A.10})$$

The effective Liouvillian of the system reads now

$$\mathcal{L}_{NZ}(t) = \mathcal{L}_S(t) + \langle \mathcal{L}_{S-R} \rangle_R. \quad (\text{A.11})$$

Appendix B

Quantum Master Equation and the Introduction of the Reservoir Correlation Function

In Appendix A we have presented the concrete form of the NZE. It was argued in section 1.1 that NZE represents only a starting point for an approximative treatment, since its solution requires the same (if not more) effort as solving the Liouville-von Neumann equation for the whole system $S + R$. The goal of this appendix is to derive the equation of motion for RDO in the second order perturbation approximation with respect to the interaction term \mathcal{L}_{S-R} or H_{S-R} . We apply a special factorization of the interaction Hamiltonian (1.9) and also identify so far arbitrary operator \hat{R} with the equilibrium canonical statistical operator of the reservoir \hat{R}_{eq} . Further we assume the initial states of the systems S and R to be uncorrelated so that $\hat{W}(t_0) = \hat{\rho}(t_0)\hat{R}_{eq}$. This assumption turns the initial correlation term (A.9) to zero. During the derivation it will become advantageous to define a quantity called reservoir correlation function which comprises the whole information about reservoir necessary in our second order equation.

We start in the interaction picture with the equation (A.8). Neglecting all contributions in the memory kernel \mathcal{M} involving more than 2 appearances of \mathcal{L}_{S-R} (i.e. dropping \mathcal{S} from A.10) and using the commutator formulation again we obtain

$$\begin{aligned} \frac{\partial}{\partial t}\hat{\rho}^{(I)}(t) &= -\frac{i}{\hbar}\text{tr}_R\left\{\hat{R}_{eq}\left[H_{S-R}^{(I)}(t),\hat{\rho}^{(I)}(t)\right]_{-}\right\} \\ &\quad -\frac{1}{\hbar^2}\int_{t_0}^t d\tau\text{tr}_R\left\{[H_{S-R}^{(I)}(t), (1-\mathcal{P})[H_{S-R}^{(I)}(\tau),\hat{R}_{eq}\hat{\rho}^{(I)}(\tau)]_{-}]_{-}\right\}. \end{aligned} \quad (\text{B.1})$$

The Equation (B.1) is the general second order equation of motion for RDO.

Now, we use the *ansatz* (1.9) assuming the factorized system-reservoir coupling. The first term on the right hand side reads

$$\text{tr}_R \left\{ \hat{R}_{eq} [H_{S-R}^{(I)}(t), \hat{\rho}^{(I)}(t)]_- \right\} = \sum_n [K_n^{(I)}(t) \langle \Phi_n \rangle_R, \hat{\rho}^{(I)}(t)]_- \quad (\text{B.2})$$

with abbreviation $\langle \dots \rangle = \text{tr}_R \{ \dots \}$. Thus the part of the effective Hamiltonian resulting from the system-reservoir interaction has been expressed via a reservoirs average of the reservoir contribution of the interaction Hamiltonian H_{S-R} . Similar possibility appears also in the second term. It takes an especially simple form if we define

$$\Delta \Phi_m(t) = \Phi_m(t) - \langle \Phi_m \rangle_R \quad (\text{B.3})$$

and rewrite all terms in (B.1) similar to

$$\begin{aligned} \langle \Phi_m^{(I)}(t) \Phi_n^{(I)}(\tau) \rangle_R &= \text{tr}_R \{ \Phi_m^{(I)}(t) \Phi_n^{(I)}(\tau) \hat{R}_{eq} \} \\ &= \text{tr}_R \{ \hat{R}_{eq} U_R^\dagger(t, \tau) \Phi_m U_R(t, \tau) \Phi_n \} = \langle \Phi_m^{(I)}(t - \tau) \Phi_n^{(I)}(0) \rangle_R. \end{aligned} \quad (\text{B.4})$$

We define the function

$$C_{mn}(t) = \langle \Phi_m(t) \Phi_n(0) \rangle_R - \langle \Phi_m \rangle \langle \Phi_n \rangle. \quad (\text{B.5})$$

which is called the *reservoir correlation function* and describes a connection between fluctuations of the reservoir operators $\Phi_n(t)$ and $\Phi_m(t)$ at different times. Since Φ_m should be a Hermitian operator one can show that $C_{mn}^*(t) = C_{nm}(-t)$. Using the correlation function, the equation (B.1) can be written as

$$\begin{aligned} \frac{\partial}{\partial t} \hat{\rho}^{(I)}(t) &= -\frac{i}{\hbar} \sum_m \langle \Phi_m \rangle [K_m, \hat{\rho}^{(I)}(t)]_- \\ &\quad - \frac{1}{\hbar^2} \sum_{mn} \int_{t_0}^t d\tau \left(C_{mn}(t - \tau) [K_m^{(I)}(t), K_n^{(I)}(\tau) \rho^{(I)}(\tau)]_- \right. \\ &\quad \left. - C_{mn}^*(t - \tau) [K_m^{(I)}(t), \rho^{(I)}(\tau) K_n^{(I)}(\tau)]_- \right). \end{aligned} \quad (\text{B.6})$$

This equation is known as the *Quantum Master Equation* or *density matrix equation in second Born approximation*.

More concrete expression for the correlation function can be found while working with the Fourier transformation of $C_{mn}(t)$

$$C_{mn}(\omega) = \int_{-\infty}^{\infty} dt e^{i\omega t} C_{mn}(t). \quad (\text{B.7})$$

Introducing the eigenstates $|\alpha\rangle$ of the reservoir Hamiltonian H_R it follows from the definition (B.5)

$$\begin{aligned} C_{mn}(\omega) &= \int_{-\infty}^{\infty} dt e^{i\omega t} \sum_{\alpha\beta} \langle \alpha | \hat{R}_{eq} e^{iHt/\hbar} \Delta\Phi_m e^{-iHt/\hbar} | \beta \rangle \langle \beta | \Delta\Phi_n | \alpha \rangle \\ &= \sum_{\alpha\beta} \int_{-\infty}^{\infty} dt e^{i(\omega - \omega_{\alpha\beta})t} f(E_\alpha) \langle \alpha | \Delta\Phi_m | \beta \rangle \langle \beta | \Delta\Phi_n | \alpha \rangle, \end{aligned} \quad (\text{B.8})$$

where $\omega_{\alpha\beta} = (E_\alpha - E_\beta)$ are the transition frequencies between reservoir energy levels and

$$f(E_\alpha) = \exp(-E_\alpha/k_B T) / \sum_{\beta} \exp(-E_\beta/k_B T) \quad (\text{B.9})$$

represents the thermal distribution function with respect to the reservoir states. Performing the integration which turns exponentials into delta-functions we obtain

$$C_{mn}(\omega) = 2\pi \sum_{\alpha\beta} f(E_\alpha) \langle \alpha | \Delta\Phi_m | \beta \rangle \langle \beta | \Delta\Phi_n | \alpha \rangle \delta(\omega - \omega_{\alpha\beta}). \quad (\text{B.10})$$

This expression gives an explicit way how to compute the Fourier-transformed correlation function when a suitable model of the reservoir is defined. This is done for a reservoir of independent harmonic oscillators linearly coupled to the relevant system in Appendix C.

Appendix C

Microscopic Model for the Correlation Function

In the following the reservoir correlation function will be considered for the case when the reservoir consists of an infinite number of decoupled harmonic oscillators. Let us perform the Taylor expansion of the interaction Hamiltonian H_{S-R} according to the reservoir coordinates and focus on the lowest contribution. Dropping the indices m and n for a while we write

$$H_{S-R} = K(s) \sum_{\xi} c_{\xi} Z_{\xi}. \quad (\text{C.1})$$

Here, c_{ξ} is a system-reservoir coupling constant. The reservoir Hamiltonian $H_R = \sum_{\xi} H_R^{\xi}$ consists of a sum of independent (normal) harmonic modes, with frequencies ω_{ξ}

$$H_R^{\xi} = \hbar\omega_{\xi}(C_{\xi}^{\dagger}C_{\xi} + 1/2), \quad (\text{C.2})$$

where C_{ξ}^{\dagger} and C_{ξ} are the oscillator creation and annihilation operators, respectively. The eigenstates

$$|M_{\xi}\rangle = \frac{1}{\sqrt{M_{\xi}!}}(C_{\xi}^{\dagger})^{M_{\xi}}|0_{\xi}\rangle \quad (\text{C.3})$$

will be labeled with oscillator quantum number M_{ξ} , the eigenenergies read

$$E_M = \sum_{\xi} E_{M_{\xi}} = \sum_{\xi} \hbar\omega_{\xi}(M_{\xi} + 1/2). \quad (\text{C.4})$$

Assuming this we may write using (B.10)

$$C(\omega) = 2\pi \sum_{\xi\xi'} c_{\xi}c_{\xi'} \sum_{NM} f(E_N) \langle N|Z_{\xi}|M\rangle \langle N|Z_{\xi'}|M\rangle \delta(\omega - (E_M - E_N)). \quad (\text{C.5})$$

Inserting

$$\langle N|Z_\xi|M\rangle = \langle N_\xi|Z_\xi|M_\xi\rangle \prod_{\xi' \neq \xi} \delta_{N_{\xi'}, M_{\xi'}} \quad (\text{C.6})$$

into (C.5) enables us to carry out the complete summation over the index M . We have to take in account that we perform the summation over M_ξ and $N_{\xi'}$ if $\xi \neq \xi'$ and over M_ξ only when $\xi = \xi'$. Thus we obtain

$$\begin{aligned} C(\omega) = & 2\pi \sum_{\xi\xi'} c_\xi c_{\xi'} \left\{ \delta_{\xi\xi'} \sum_{M_\xi} |\langle N_\xi|Z_\xi|M_\xi\rangle|^2 \delta(\omega - \omega_{N_\xi M_\xi}) \right. \\ & + (1 - \delta_{\xi\xi'}) \sum_N f(E_N) \sum_{M_\xi \sum_{N_\xi}} \langle N_\xi|Z_\xi|M_\xi\rangle \delta_{N_\xi M_\xi} \\ & \left. \times \langle M_{\xi'}|Z_{\xi'}|N_{\xi'}\rangle \delta_{N_{\xi'} M_{\xi'}} \delta(\omega - \omega_{M_\xi N_\xi} - \omega_{N_{\xi'} M_{\xi'}}) \right\}. \end{aligned} \quad (\text{C.7})$$

Because of the relation $\langle Z_\xi \rangle = 0$, all the terms with $\xi \neq \xi'$ are zero and it reads

$$C(\omega) = 2\pi \sum_{\xi} \sum_{N_\xi M_\xi} c_\xi^2 f(E_{N_\xi}) |\langle N_\xi|Z_\xi|M_\xi\rangle|^2 \delta(\omega - \omega_{M_\xi N_\xi}). \quad (\text{C.8})$$

Finally, we introduce the representation of Z_ξ by the creation and annihilation operators $Z_\xi = \sqrt{\hbar/2\omega_\xi}(C_\xi + C_\xi^\dagger)$ and we get

$$C(\omega) = 2\pi \sum_{\xi} c_\xi^2 \frac{\hbar}{2\omega_\xi} \sum_{M_\xi} f(E_{M_\xi}) ((M_\xi + 1)\delta(\omega - \omega_\xi) + M_\xi \delta(\omega + \omega_\xi)). \quad (\text{C.9})$$

Now we consider the harmonic reservoir to be in equilibrium and introduce the corresponding mean occupation number of the oscillator mode

$$n(\omega) = \sum_M f(\hbar\omega M) M = \frac{\sum_M M e^{-\hbar\omega M/k_B T}}{\sum_N e^{-\hbar\omega N/k_B T}} = \frac{1}{e^{\hbar\omega/k_B T} - 1}. \quad (\text{C.10})$$

We obtain the expression we have been looking for

$$C(\omega) = 2\pi \sum_{\xi} c_\xi^2 \frac{\hbar}{2\omega_\xi} [(n(\omega_\xi) + 1)\delta(\omega - \omega_\xi) + n(\omega_\xi)\delta(\omega + \omega_\xi)]. \quad (\text{C.11})$$

The Eq. (C.11) enables us to write the correlation function in terms of quantities which can be physically interpreted. To that end we define so-called *spectral density*

$$J(\omega) = \sum_{\xi} g_\xi^2 \delta(\omega - \omega_\xi), \quad (\text{C.12})$$

with g_ξ being the dimensionless coupling constant g_ξ given by the relation

$$c_\xi \sqrt{\hbar/2\omega_\xi} = \hbar\omega_\xi g_\xi. \quad (\text{C.13})$$

With this we can finally write

$$C(\omega) = 2\pi\hbar^2\omega^2[1 + n(\omega)][J(\omega) - J(-\omega)]. \quad (\text{C.14})$$

We can see, that in our model describing the reservoir as an infinite set of the harmonic oscillators, the correlation function of is given by a single function $J(\omega)$. Although this function is given as a sum of delta-functions, any macroscopic reservoir would have practically continuous spectral density (see [\[MK99\]](#)).

Appendix D

The Dissipative Part of the Quantum Master Equation and the Reduction to the Excited-State Potential Energy Surface

According to the presence of two different electronic levels in the molecular system from the section 2.1, $\hat{\rho}(t)$ has to be expanded with respect to the electronic states yielding $\hat{\rho}_{ab}(t)$ which is just an operator in the vibrational state-space. For the separation of the density operator into an equilibrium part and a non-equilibrium deviation as introduced in Eq. (2.15) we get

$$\hat{\rho}_{ab}(t) = \delta_{a,b}\delta_{a,g}\hat{r}_{\text{eq}}^{(g)} + \Delta\hat{\rho}_{ab}(t) . \quad (\text{D.1})$$

with

$$\hat{r}_{\text{eq}}^{(g)} = \frac{e^{-H_g/k_{\text{B}}T}}{\text{tr}_{\text{vib}}\{e^{-H_g/k_{\text{B}}T}\}} \quad (\text{D.2})$$

The density operator $\Delta\hat{\rho}_{ab}(t)$ obeys the following equation (cf. Eq. (2.16) and note the neglect of the field-dependence of \mathcal{M})

$$\begin{aligned} & \frac{\partial}{\partial t}\Delta\hat{\rho}_{ab}(t) = \hat{I}_{ab}(t) \\ & - \frac{i}{\hbar}\left(H_a\Delta\hat{\rho}_{ab}(t) - \Delta\hat{\rho}_{ab}(t)H_b\right) - \hat{D}_{ab}(t - t_{\text{field}}; \Delta\hat{\rho}) \\ & + \frac{i}{\hbar}\mathbf{E}(t)\sum_c\left(\mathbf{d}_{ac}\Delta\hat{\rho}_{cb}(t) - \mathbf{d}_{cb}\Delta\hat{\rho}_{ac}(t)\right) \end{aligned} \quad (\text{D.3})$$

Here, the inhomogeneity is given as

$$\hat{I}_{ab}(t) = \frac{i}{\hbar} \mathbf{E}(t) \left(\delta_{ae} \delta_{g,b} \mathbf{d}_{eg} - \delta_{a,g} \delta_{e,b} \mathbf{d}_{ge} \right) \hat{R}_{\text{eq}} \quad (\text{D.4})$$

The dissipative part for the system-bath interaction Hamiltonian $H_{S-R} = \sum_a K_a \Phi_a(Z)$ reads

$$\begin{aligned} \hat{D}_{ab}(t - t_{\text{field}}; \Delta\hat{\rho}) = & \int_0^{t-t_{\text{field}}} d\tau \\ & \left(C_{aa}(\tau) K_a K_a(-\tau) \hat{\sigma}_{ab}(t - \tau, \tau) \right. \\ & + C_{bb}(-\tau) \hat{\sigma}_{ab}(t - \tau, \tau) K_b(-\tau) K_b \\ & - C_{ba}(\tau) K_a(-\tau) \hat{\sigma}_{ab}(t - \tau, \tau) K_b \\ & \left. + C_{ba}(-\tau) K_a \hat{\sigma}_{ab}(t - \tau, \tau) K_b(-\tau) \right). \end{aligned} \quad (\text{D.5})$$

To have a sufficient compact expression we introduced

$$K_a(-\tau) = U_a(\tau) K_a U_a^\dagger(\tau) \quad (\text{D.6})$$

and

$$\hat{\sigma}_{ab}(t - \tau, \tau) = U_a(\tau) \Delta\hat{\rho}_{ab}(t - \tau) U_b(\tau) \quad (\text{D.7})$$

The reservoir correlation functions read (cf. (A.7))

$$C_{ab}(t) = \frac{1}{\hbar^2} \langle U_R^\dagger \Phi_a U_R \Phi_b \rangle_{\text{R}} \quad (\text{D.8})$$

with the time-evolution operators denoted as

$$U_a(t) = e^{-iH_a t/\hbar}. \quad (\text{D.9})$$

In order to simulate the reservoir we provide that a normal mode analysis has been carried out. It results an ensemble of independent harmonic oscillators which will be coupled linearly to the system DOF. Thus, we suppose

$$\Phi_a(Z) = \hbar \sum_{\xi} k_{\xi}(a) Z_{\xi}, \quad (\text{D.10})$$

with k_{ξ} being a coupling constant of a corresponding harmonic oscillator with system DOF. For such a reservoir the correlation function takes the form (see, e.g. [MK99])

$$C_{ab}(t) = \int_{-\infty}^{+\infty} d\omega e^{-i\omega t} (1 + n(\omega)) (J_{ab}(\omega) - J_{ab}(-\omega)), \quad (\text{D.11})$$

with $n(\omega) = 1/(\exp(\hbar\omega/k_B T) - 1)$ being the Bose–Einstein distribution and the quantities

$$J_{ab}(\omega) = \sum_{\xi} k_{\xi}(a)k_{\xi}(b)\delta(\omega - \omega_{\xi}) \quad (\text{D.12})$$

represent the spectral densities of normal modes.

In the case of an arbitrary strength of the applied field all elements of $\Delta\hat{\rho}_{ab}(t)$ have to be considered. Here, we will concentrate on the case of weaker field–strength realizing only marginal population transfer to the excited electronic levels. Then, one can reduce the whole description to the use of the quantity $\Delta\hat{\rho}_{ee}(t)$ describing vibrational dynamics on the excited–state PES initiated by the external–field pulse. It will enter the respective equation of motion in the second order corresponding to a linearization in the field–intensity.

As it is well–known such a result is obtained if one determines $\Delta\hat{\rho}_{eg}$ linearly with respect to \mathbf{E} and inserts the expression into the equation of motion for $\Delta\hat{\rho}_{ee}$. According to Eq. (D.3) one obtains for the electronic off–diagonal density operator

$$\begin{aligned} \frac{\partial}{\partial t}\Delta\hat{\rho}_{eg}(t) &= -\frac{i}{\hbar}\left(H_e\Delta\hat{\rho}_{eg}(t) - \Delta\hat{\rho}_{eg}(t)H_g\right) \\ &- \hat{D}_{eg}(t - t - \text{field}; \Delta\hat{\rho}_{eg}) + \frac{i}{\hbar}\mathbf{E}(t)\mathbf{d}_{eg}\hat{r}_{\text{eq}}^{(g)}. \end{aligned} \quad (\text{D.13})$$

Solving this equation and inserting the result into the equation of motion for $\Delta\hat{\rho}_{ee}$ gives the desired closed description of the vibrational dynamics in the excited electronic state. To have an analytical expression we replace \hat{D}_{eg} by a time–local expression $\hat{\Gamma}_e\Delta\hat{\rho}_{eg} + \Delta\hat{\rho}_{eg}\hat{\Gamma}_g$ and the respective deviation $\Delta\hat{D}_{eg}$ from this expression. On the one hand side this procedure enables us to derive an analytical formula for the field–dependent source term in the equation of motion for $\Delta\hat{\rho}_{eg}$. And, on the other hand side, we can improve the result step by step. The operators $\hat{\Gamma}_a$ realize dephasing and are given as

$$\hat{\Gamma}_a = \int_0^{\infty} d\tau C_{aa}(\tau)K_aK_a(-\tau). \quad (\text{D.14})$$

Instead of a contribution proportional to $\Delta\hat{\rho}_{eg}$, now the equation of motion for $\Delta\hat{\rho}_{ee}$ contains a source term and reads

$$\begin{aligned} \frac{\partial}{\partial t}\Delta\hat{\rho}_{ee}(t) &= \frac{i}{\hbar}\left(H_e, \Delta\hat{\rho}_{ee}(t)\right)_- \\ &- \hat{D}_{ee}(t - t_{\text{field}}; \Delta\hat{\rho}_{ee}) + \hat{F}_{ee}(t, t_{\text{field}}; \mathbf{E}), \end{aligned} \quad (\text{D.15})$$

For the source term one gets

$$\begin{aligned}
& \hat{F}_{ee}(t, t_{\text{field}}; \mathbf{E}) \\
&= \frac{1}{\hbar^2} \int_{t_{\text{field}}}^t d\bar{t} (\mathbf{d}_{eg} \mathbf{E}(t)) (\mathbf{d}_{ge} \mathbf{E}(\bar{t})) \tilde{U}_e(t - \bar{t}) \hat{\rho}_{\text{eq}}^{(g)} \tilde{U}_g^+(t - \bar{t}) \\
&+ \text{h.c.},
\end{aligned} \tag{D.16}$$

The evolution operators $\tilde{U}_e(t)$ and $\tilde{U}_g(t)$ are defined according to

$$\tilde{U}_a(t) = \exp -\frac{i}{\hbar} \left(H_a - i\hbar \hat{\Gamma}_a \right), \tag{D.17}$$

i.e. they are formed by non-hermitian Hamiltonian including dephasing operators $\hat{\Gamma}_a$.

Appendix E

Solution of Non-Markovian Equations: Factorization of the Correlation Function

Although the general form of the correlation function $C(t)$ does not allow for the direct transformation of the non-Markovian equation of motion into a time-local form, there are some special forms of $C(t)$ which allow it. In principle, all functions $f(t)$ which can be decomposed as

$$f(t - \tau) = g(t)h(\tau) \quad (\text{E.1})$$

when substituted for the correlation function in (1.10) result in its direct transformation into the time local form.

To characterize the retardation effects and to construct time-local equations of motion it will be of great advantage to change the notation of the dissipative part. Therefore, we write the dissipative part of Eq. (1.10) as $\hat{D} = \hat{D}_1 + \hat{D}_2$ and identify \hat{D}_2 with the contribution given by the time-independent part $C_{uv}^{(2)} = - \langle \Phi_u \rangle_R \langle \Phi_v \rangle_R / \hbar^2$ of C_{uv} , Eq. (1.13). The first contribution \hat{D}_1 follows from the time-dependent first term in Eq. (1.13). We start to give an alternative notation for \hat{D}_1 . It is obvious from Eq. (1.10) that we can write $\hat{D}_1 = \sum_u [K_u, \hat{\Sigma}_u]_-$ (where $\hat{\Sigma}_u$ is easily deduced from Eq. (1.10) and K_u is a system part of the system-bath interaction Hamiltonian H_{S-R} defined in Eq. (1.9)). This expression removes the time non-locality from the QME. Unfortunately, one cannot derive a separate equation of motion for $\hat{\Sigma}_u$. This only becomes possible if the various correlation function $C_{uv}^{(1)}$, which depend on the two time-arguments t and \bar{t} can be replaced by the following multiple

factorization *ansatz*

$$C_{uv}^{(1)}(t - \bar{t}) = \frac{1}{\hbar^2} \sum_s \alpha_{uv}^{(s)}(t) \beta_{uv}^{(s)}(\bar{t}) . \quad (\text{E.2})$$

Such an expression may be constructed by a double expansion with respect to an orthogonal set of functions. Providing the multiple factorization of $C_{uv}^{(1)}$ we can introduce the following new auxiliary density operators (note the use of the interaction representation)

$$\hat{\sigma}_{s,uv}^{(I+)}(t) = \frac{i}{\hbar} \int_{t_0}^t d\bar{t} \beta_{uv}^{(s)}(\bar{t}) U_S^+(\bar{t}, t_0) K_v \hat{\rho}(\bar{t}) U_S(\bar{t}, t_0) , \quad (\text{E.3})$$

and

$$\hat{\sigma}_{s,uv}^{(I-)}(t) = \frac{i}{\hbar} \int_{t_0}^t d\bar{t} \beta_{vu}^{(s)}(-\bar{t}) U_S^+(\bar{t}, t_0) \hat{\rho}(\bar{t}) K_v U_S(\bar{t}, t_0) , \quad (\text{E.4})$$

which remove the time-nonlocality in \hat{D}_1 to give

$$\begin{aligned} \hat{D}_1(t) &= \frac{i}{\hbar} \sum_{u,v} \sum_s \\ &[K_u, \alpha_{uv}^{(s)}(t) \hat{\sigma}_{s,uv}^{(+)}(t) - \alpha_{vu}^{(s)}(-t) \hat{\sigma}_{s,uv}^{(-)}(t)]_- . \end{aligned} \quad (\text{E.5})$$

The equations of motion for the auxiliary operators read

$$\frac{\partial}{\partial t} \hat{\sigma}_{s,uv}^{(+)}(t) = -\frac{i}{\hbar} [H_S(t), \hat{\sigma}_{s,uv}^{(+)}(t)]_- + \frac{i}{\hbar} \beta_{uv}^{(s)}(t) K_v \hat{\rho}(t) , \quad (\text{E.6})$$

and

$$\frac{\partial}{\partial t} \hat{\sigma}_{s,uv}^{(-)}(t) = -\frac{i}{\hbar} [H_S(t), \hat{\sigma}_{s,uv}^{(-)}(t)]_- + \frac{i}{\hbar} \beta_{vu}^{(s)}(-t) \hat{\rho}(t) K_v , \quad (\text{E.7})$$

We note that the term stemming from initial correlations can be handled in a similar manner [MT99]. However, for the description of the external field influence initial correlations are of less importance as discussed in section 2.3.

Next we deal with term \hat{D}_2 determined by the time-independent part of C_{uv} . It can be rewritten by introducing a single additional density operator $\hat{\sigma}$

$$\hat{D}_2(t, t_0) = -\frac{i}{\hbar} [H_{\text{mf}}, \hat{\sigma}(t)]_- . \quad (\text{E.8})$$

Using the interaction representation the new operator reads

$$\hat{\sigma}^{(I)}(t) = \frac{i}{\hbar} \int_{t_0}^t d\bar{t} U_S^+(\bar{t}, t_0) [H_{\text{mf}}, \hat{\rho}(\bar{t})]_- U_S(\bar{t}, t_0) . \quad (\text{E.9})$$

This expression can be related to the following equation of motion (in the Schrödinger representation)

$$\frac{\partial}{\partial t} \hat{\sigma}(t) = -\frac{i}{\hbar} [H_S(t), \hat{\sigma}(t)]_- - \frac{i}{\hbar} [H_{mf}, \hat{\rho}(t)]_- . \quad (\text{E.10})$$

The introduction of the auxiliary operators $\hat{\sigma}_{s,uv}^{(\pm)}$ and $\hat{\sigma}$ demonstrates that the time-nonlocality can be removed with any accuracy one needs. In which manner the two types of auxiliary operators contribute depends on the properties of the reservoir correlation functions. If the time-independent part dominates the dissipation one may have the chance to find an analytical solution of the non-Markovian QME (cf. Section 2.4).

Before dealing with techniques based on a certain expansion of the density operator and the QME we refer to methods which try to solve the non-Markovian QME directly, i.e. in the time-domain. In [Ima94] the introduction of the fictitious bath modes to simulate a spectral density of the bath has been suggested. Behind this idea is the common observation that a given non-Markovian process can be related to a Markovian process of a system with a larger set of DOF. The easiest way would be to enlarge the system in question by a single fictitious harmonic-oscillator mode. If the latter interacts with a zero-correlation time bath, the spectral density obtained after tracing over the fictitious mode turns out to be of a Lorentzian shape. Although originally suggested for the Monte Carlo wavefunction method [Ima94], where the scaling of the problem (related to the involved level number) is much more favorable than that of the density matrix approach, it is obvious that the system cannot be enlarged by more than a few fictitious modes. Therefore, the flexibility to choose a particular shape of the effective spectral density is rather small.

The scaling problem can be avoided if we view the fictitious bath modes only as a numerical trick for the decomposition of the spectral density. To this end the following parameterization of the correlation function has been suggested in [MT99] (for a single electronic state, see also [KP97])

$$J(\omega) = \frac{1}{2} \sum_{s=1}^{\nu} J_s \frac{\pi \omega}{[(\omega + \omega_s)^2 + \gamma_s^2][(\omega - \omega_s)^2 + \gamma_s^2]} , \quad (\text{E.11})$$

where the parameters J_s , ω_s and γ_s are arbitrary and real. It is the great advantage of such a generalized multi-Lorentzian form that an analytical determination of the time-dependent correlation function according to Eq. (D.11) becomes possible. One obtains (note the absence of electronic quantum numbers)

$$\text{Re } C(t) = \sum_{s=1}^{\nu} \frac{J_s}{\omega_s \gamma_s} \left(\coth \left(\frac{\beta}{2} (\omega_s + i\gamma_s) \right) e^{i\omega_s t - \gamma_s t} \right)$$

$$\begin{aligned}
& + \sum_{s=1}^{\nu} \frac{J_s}{\omega_s \gamma_s} \left(\coth \left(\frac{\beta}{2} (\omega_s - i\gamma_s) \right) e^{-i\omega_s t - \gamma_s t} \right) \\
& + \frac{2i}{\beta} \sum_{s=1}^{n'} J(i\nu_s) e^{-\nu_s t} ,
\end{aligned} \tag{E.12}$$

and

$$\text{Im } C(t) = -i \sum_{s=1}^{\nu} \frac{J_s}{\omega_s \gamma_s} \left(e^{i\omega_s t - \gamma_s t} - e^{-i\omega_s t - \gamma_s t} \right) , \tag{E.13}$$

where $\nu_s = 2\pi s k_B T$ are the Matsubara frequencies. If formulated for the difference time-argument $t - \bar{t}$ the real and imaginary part of the correlation function are just of the type introduced in Eq. (E.2). Therefore, the original QME can be completed by the equations of motion for the auxiliary density operators, Eqs. (E.3) and (E.4).

The resulting equations would represent the time local equivalent to the original time non-local Eq. (1.10) if the parameterization (E.11) is exact. Although this is not the case it has been noted in [MT99] that it gives a good approximation for an Ohmic spectral density even if one incorporates only a few terms in the expansion Eq. (E.11). But the main advantage of this method is that one can easily account for an external field influence. So, the approach is suitable for strong field problems as well as for problems of laser pulse control of molecular dynamics, e.g. in the framework of the optimal control scheme (see Part III of this work).

Appendix F

Solution of Non-Markovian Equations: Laguerre Polynomial Expansion

To obtain the solution of the non-Markovian density matrix equation (2.32) we expand all parts with respect to the Laguerre polynomials

$$L_n(t) = \frac{1}{n!} e^t \frac{d^n}{dt^n} (t^n e^{-t}) \quad n = 1, 2, \dots \quad (\text{F.1})$$

Therefore, we note their orthogonality with respect to the scalar product

$$(f, g) = \int_0^\infty dx e^{-x} f(x) g(x) . \quad (\text{F.2})$$

In carrying out the expansion the time-argument t has to be replaced by the dimensionless variable x

$$x = t/t_{\text{char}} , \quad (\text{F.3})$$

where the time-constant t_{char} roughly fixes the characteristic time-interval in which the function to be expanded by Laguerre polynomials can be properly described. Since we will consider the correlation functions decaying on a time-scale of some $10fs$ we set $t_{\text{char}} = 10fs$.

Carrying out the expansions for the density matrix we get

$$\sigma_{MN}(t_{\text{char}} x) = \sum_{n=0}^{\infty} \sigma_{MN}^{(n)} L_n(x) . \quad (\text{F.4})$$

If we set $t = 0$ this expression reduces to (note $L_n(x = 0) = 1$)

$$\sigma_{MN}(t = 0) = \sum_{n=0}^{\infty} \sigma_{MN}^{(n)} . \quad (\text{F.5})$$

Using the scalar product (F.2) the expansion coefficients of the density matrix introduced in Eq. (F.4) are obtained as

$$\sigma_{MN}^{(n)} = \int_0^\infty dx e^{-x} L_n(x) \sigma_{MN}(t_{char} x) . \quad (F.6)$$

The algebraic equations determining the expansion coefficients are obtained from the expansion of the original equation of motion (2.32). To do this we use the relations [MBS98, AS72]

$$\int_0^x d\bar{x} L_n(x - \bar{x}) L_m(\bar{x}) = L_{n+m}(x) - L_{n+m+1}(x) \quad (F.7)$$

and

$$\frac{\partial}{\partial x} L_n(x) = - \sum_{m=0}^{n-1} L_m(x) . \quad (F.8)$$

It results the recurrence relation for the density matrix expansion coefficients $\sigma_{MN}^{(n)}$

$$\begin{aligned} & \sum_{KL} \left((it_{char} \omega_{MN} + 1) \delta_{MK} \delta_{NL} + t_{char}^2 \mathcal{M}_{MN, KL}^{(0)} \right) \sigma_{KL}^{(n)} \\ &= \sigma_{MN}(t=0) \\ &- \sum_{m=0}^{(n-1)} \left(\sigma_{MN}^{(m)} + t_{char}^2 \sum_{KL} \mathcal{M}_{MN, KL}^{(n-m)} - \mathcal{M}_{MN, KL}^{(n-m-1)} \right) \sigma_{MN}^{(m)} \\ &+ t_{char} F_{MN}^{(n)} . \end{aligned} \quad (F.9)$$

If the coefficients $\mathcal{M}_{MN, KL}^{(n)}$ as well as $F_{MN}^{(n)}$ are known the density matrix can be deduced.

Computing the memory kernel expansion coefficients $\mathcal{M}_{MN, KL}^{(n)}$ in similarity to Eq. (F.6) a detailed inspection of relation (2.33) demonstrates that we have to handle contributions of the type

$$\tilde{C}^{(n)} = \int_0^\infty dx L_n(x) e^{i\Delta\tilde{\omega}x} e^{-x} C_{ee}(\pm t_{char} x) . \quad (F.10)$$

Here, $\Delta\tilde{\omega} = t_{char} \Delta\omega$ where $\Delta\omega$ denotes one of the various transition frequencies.

To calculate the above given type of integrals we proceed as follows. First we note that $C_{ee}(t)$ follows from an inverse Fourier transformation according to Eq.

(D.11). In the general case this Fourier transformation has to be carried out numerically, and, consequently, the values of the function $C_{ee}(t)$ are given for a set of points t_0, t_1, \dots, t_N on the time axes (corresponding to x_0, x_1, \dots, x_N). Such a set can be interpolated by so-called cubic splines [PTVF92], which result in a function, analytical by-parts and continuous up to the second derivative. Then, between any two points x_j, x_{j+1} of the set, the function $C_{ee}(xt_{char})$ is represented by a cubic polynomial and the integral (F.10) turns to a sum of the integrals

$$\tilde{C}_{\text{spl}}^{(n,j)} = \int_{x_j}^{x_{j+1}} dx L_n(x) e^{i\Delta\tilde{\omega}x} e^{-x} C_{\text{spl}}^{(j)}(\pm xt_{char}) , \quad (\text{F.11})$$

with $C_{\text{spl}}^{(j)}(t)$ being a spline interpolation of $C_{ee}(\pm t)$ in the interval $[t_j, t_{j+1}]$. For all of these integrals special recurrence formulas can be derived. Accordingly, the complete expansion coefficient, Eq. (F.10) can be computed in any degree of accuracy, for any order of the polynomial expansion, and any value of $\Delta\omega$. Details on the derivation of the recursion formulas are given in appendix G.

In the same manner we can calculate the expansion coefficients $F_{MN}^{(n)}$ of the filled term in Eq. (2.32). Therefore, $F_{MN}(t_{char}x)$ is determined for the discrete set of time-arguments t_0, t_1, \dots, t_N and the respective spline approximation is used to calculate $F_{MN}^{(j)}(t_{char}x)$ according to Eq. (F.11).

It has been already highlighted in [MBS98] and can be made obvious by an inspection of Eq. (F.9) that the accuracy of the memory kernel expansion determines the accuracy we can compute the density matrix elements. Having at hand a sufficient good approximation of the memory kernel for the time interval $[t_1, t_2]$ one may expect that the density matrix expansion results in the same accuracy.

Appendix G

Evaluation of the Correlation Function Expansion Coefficients

In Appendix F we claimed that, based on the spline approximation of the correlation function, the integrals (F.11) can be evaluated analytically. Here we give some details of this procedure. The function $C_{\text{spl}}^{(j)}(t)$ introduced in (F.11) is an interpolation of the correlation function by cubic splines, i.e.

$$\begin{aligned} C_{\text{spl}}^{(j)}(xt_{\text{char}}) &= \alpha(x)C_{ee}(x_j t_{\text{char}}) + \beta(x)C_{ee}(x_{j+1} t_{\text{char}}) \\ &+ \gamma(x)C'''(x_j t_{\text{char}}) + \delta(x)C'''(x_{j+1} t_{\text{char}}) . \end{aligned} \quad (\text{G.1})$$

The four different expansion coefficients can all be expressed by the first one which reads

$$\alpha(x) = \frac{x_{j+1} - x}{\Delta x} \equiv \frac{1}{\Delta x}(L_1(x) - L_1(x_{j+1})) . \quad (\text{G.2})$$

Here, we introduced $\Delta x = x_{j+1} - x_j$. The remaining three coefficients are

$$\beta(x) = 1 - \alpha(x) , \quad (\text{G.3})$$

$$\gamma(x) = \frac{(\Delta x)^2}{6}(\alpha^3(x) - \alpha(x)) , \quad (\text{G.4})$$

and

$$\delta(x) = -\frac{(\Delta x)^2}{6}(\alpha^3(x) - 3\alpha^2(x) + 2\alpha(x)) . \quad (\text{G.5})$$

The second derivative C'' of $C_{ee}(xt_{\text{char}})$ at $x = x_j, x_{j+1}$ are computed using a standard interpolating algorithm [PTVF92]. The above given relations indicate that it is necessary to compute integrals of type Eq. (F.11) but with $C_{\text{spl}}^{(j)}(xt_{\text{char}})$

replaced by $\alpha(x)$ up to its third power. In carrying out these integrations it is useful to generate recurrence formulas. Therefore we define

$$a_n^{(m)} = \int_{x_j}^{x_{j+1}} dx (L_1(x))^m L_n(x) e^{i\Delta\tilde{\omega}x} e^{-x}. \quad (\text{G.6})$$

In particular we have $a_0^{(1)} = a_1^{(0)}$, and

$$a_0^{(0)} = -\frac{1}{1 - i\Delta\tilde{\omega}} \left[e^{-(1-i\Delta\tilde{\omega})x} \right]_{x_j}^{x_{j+1}}, \quad (\text{G.7})$$

where the abbreviation $[g(x)]_b^a = g(a) - g(b)$ has been introduced. These expression enables us to express the required integrals as

$$\int_{x_j}^{x_{j+1}} dx \alpha(x) L_n(x) e^{i\Delta\tilde{\omega}x} e^{-x} = \frac{1}{\Delta x} (a_n^{(1)} - a_n^{(0)}), \quad (\text{G.8})$$

$$\begin{aligned} & \int_{x_j}^{x_{j+1}} dx \alpha^2(x) L_n(x) e^{i\Delta\tilde{\omega}x} e^{-x} \\ &= \frac{1}{\Delta x^2} \left(a_n^{(2)} - 2L_1(x_{j+1})a_n^{(1)} + (L_1(x_{j+1}))^2 a_n^{(0)} \right), \end{aligned} \quad (\text{G.9})$$

and

$$\begin{aligned} & \int_{x_j}^{x_{j+1}} dx \alpha^3(x) L_n(x) e^{i\Delta\tilde{\omega}x} e^{-x} = \frac{1}{\Delta x^3} \left(a_n^{(3)} - \right. \\ & \left. 3L_1(x_{j+1})a_n^{(2)} + 3(L_1(x_{j+1}))^2 a_n^{(1)} - (L_1(x_{j+1}))^3 a_n^{(0)} \right). \end{aligned} \quad (\text{G.10})$$

Accordingly, the announced recursion formulas which are essential for an efficient computation of a_n^m read

$$\begin{aligned} a_n^{(0)} &= \frac{1}{1 - i\Delta\tilde{\omega}} \left\{ \left[e^{i\Delta\tilde{\omega}x} e^{-x} (L_{n-1}(x) - L_n(x)) \right]_{x_j}^{x_{j+1}} \right. \\ &\quad \left. - i\Delta\tilde{\omega} a_{n-1}^{(0)} \right\}, \end{aligned} \quad (\text{G.11})$$

and similarly for the other integrals

$$\begin{aligned} a_n^{(1)} &= \frac{1}{1 - i\Delta\tilde{\omega}} \left\{ [L_1(x) e^{i\Delta\tilde{\omega}x} e^{-x} (L_{n-1}(x) - L_n(x))]_{x_j}^{x_{j+1}} \right. \\ &\quad \left. + a_{n-1}^{(0)} - a_n^{(0)} - i\Delta\tilde{\omega} a_{n-1}^{(1)} \right\}, \end{aligned} \quad (\text{G.12})$$

$$a_0^{(2)} = -\frac{1}{1-i\Delta\tilde{\omega}} \left\{ [(L_1(x))^2 e^{i\Delta\tilde{\omega}x} e^{-x}]_{x_j}^{x_{j+1}} + 2a_1^{(0)} \right\}, \quad (\text{G.13})$$

$$\begin{aligned} a_n^{(2)} &= \frac{1}{1-i\Delta\tilde{\omega}} \left\{ [(L_1(x))^2 e^{i\Delta\tilde{\omega}x} e^{-x} (L_{n-1}(x) - L_n(x))]_{x_j}^{x_{j+1}} \right. \\ &\quad \left. + 2a_{n-1}^{(1)} - 2a_n^{(1)} - i\Delta\tilde{\omega}a_{n-1}^{(2)} \right\}, \end{aligned} \quad (\text{G.14})$$

$$a_0^{(3)} = -\frac{1}{1-i\Delta\tilde{\omega}} \left\{ [(L_1(x))^3 e^{i\Delta\tilde{\omega}x} e^{-x}]_{x_j}^{x_{j+1}} + 3a_0^{(2)} \right\}, \quad (\text{G.15})$$

and

$$\begin{aligned} a_n^{(3)} &= \frac{1}{1-i\Delta\tilde{\omega}} \\ &\times \left\{ [\{ (L_1(x))^3 e^{-i\Delta\tilde{\omega}x} e^{-x} (L_{n-1}(x) - L_n(x)) \}]_{x_j}^{x_{j+1}} \right. \\ &\quad \left. - 3a_{n-1}^{(2)} - 3a_n^{(2)} - i\Delta\tilde{\omega}a_{n-1}^{(3)} \right\}. \end{aligned} \quad (\text{G.16})$$

At the first glance the given formulas look to complex to be useful for integrating a function of a single variable. But according to our efforts to reach a sufficient precision they seem to give the only way to get precise results even for Laguerre polynomials of the order 10^5 or higher. Moreover these formulas if accompanied by a routine to compute Laguerre polynomials via standard recurrence formulas [PTVF92] can be put in a very compact computer code. Finally we note that the given spline interpolation scheme to integrate a product of a smooth and a highly oscillating function such as polynomials of a high order and/or $\exp\{i\tilde{\omega}x\}$ may be used in many other cases.

Appendix H

Derivation of the Control Kernel

The control kernel Eq. (3.8) follows as the functional derivative of the expectation value introduced in Eq. (3.5). The latter expression shows that one has to determine the respective derivate of the reduced density operator. To perform the derivative we first note the more explicite structure of the time–evolution superoperator introduced in Eq. (3.4). It reads (T guarantees proper time–ordering)

$$\mathcal{U}(t, t_0; \mathbf{E}) = T \exp \left\{ -i \int_{t_0}^t d\tau (\mathcal{L}_{\text{mol}} + \mathcal{L}_{\text{F}}(\tau) - i\mathcal{D}) \right\}. \quad (\text{H.1})$$

Accordingly the functional derivate of $\hat{\rho}(t_f)$ follows as

$$\frac{\delta \hat{\rho}(t_f)}{\delta \mathbf{E}(t)} = -i \int_{t_0}^{t_f} d\tau \mathcal{U}(t_f, \tau; \mathbf{E}) \frac{\delta \mathcal{L}_{\text{F}}(\tau)}{\delta \mathbf{E}(t)} \mathcal{U}(\tau, t_0; \mathbf{E}). \quad (\text{H.2})$$

Noting

$$\frac{\delta \mathcal{L}_{\text{F}}(\tau)}{\delta \mathbf{E}(t)} = -\frac{1}{\hbar} \delta(\tau - t) \mathcal{M} \quad (\text{H.3})$$

expression (H.2) is easily converted into the final result, Eq. (3.8) for the control kernel.

Appendix I

The Reverse Time Evolution Superoperator

To have a more specific version of the time evolution superoperator at hand we specify the dissipative superoperator \mathcal{D} introduced in Eq. (3.3). According to the standard QME (see for example [MK99, LM00]) we set

$$-\mathcal{D}\hat{\rho} = -\sum_u \left(K_u \Lambda_u \hat{\rho} + \hat{\rho} \Lambda_u^+ K_u - \Lambda_u \hat{\rho} K_u - K_u \hat{\rho} \Lambda_u^+ \right). \quad (\text{I.1})$$

These dissipative terms correspond to a second-order perturbational treatment of the type of system reservoir coupling introduced in Eq. (1.9). Although not necessary in general we will additionally assume that the single operators K_u are hermitian. The operators Λ_u are obtained from the time dependent operators $K_u(t)$ (defined in the Heisenberg picture with respect to H_{mol} and thus incorporating any order in the transfer integrals V_{mn}) and the reservoir correlation functions $C_{uv}(t)$ as [MK99, LM00]

$$\Lambda_u = \sum_v \int_0^\infty d\tau C_{uv}(\tau) K_v(-\tau) \quad (\text{I.2})$$

To justify the representation Eq. (3.9) for the control kernel and to give a definition of the reverse time evolution superoperator we first note the general form of any superoperator. i.e. of the time evolution superoperator, too. It is given by [LM00]

$$\begin{aligned} \mathcal{U}(t, t_0) \hat{\rho}(t_0) &= \hat{A}(t, t_0) \hat{\rho}(t_0) + \hat{\rho}(t_0) \hat{B}(t, t_0) \\ &+ \sum_j \hat{C}_j(t, t_0) \hat{\rho}(t_0) \hat{D}_j(t, t_0). \end{aligned} \quad (\text{I.3})$$

Here, the $\hat{A}(t, t_0)$, $\hat{B}(t, t_0)$, $\hat{C}_j(t, t_0)$, and $\hat{D}_j(t, t_0)$ are ordinary operators acting from the left or from the right on the initial value $\hat{\rho}(t_0)$ of the reduced density operator. The set of operators can be somewhat restricted if we note that $\hat{\rho}(t)$ is a hermitian operator

$$\hat{\rho}(t) = \mathcal{U}(t, t_0)\hat{\rho}(t_0) = \hat{\rho}^+(t) = \left(\mathcal{U}(t, t_0)\hat{\rho}(t_0)\right)^+. \quad (\text{I.4})$$

If all contributions to \mathcal{U} are considered to be linearly independent one obtains $\hat{B} = \hat{A}^+$ and $\hat{D}_j = \hat{C}_j^+$. This gives

$$\begin{aligned} \mathcal{U}(t, t_0)\hat{\rho}(t_0) &= \hat{A}(t, t_0)\hat{\rho}(t_0) + \hat{\rho}(t_0)\hat{A}^+(t, t_0) \\ &+ \sum_j \hat{C}_j(t, t_0)\hat{\rho}(t_0)\hat{C}_j^+(t, t_0). \end{aligned} \quad (\text{I.5})$$

We use this relation to change from Eq. (3.8) to Eq. (3.9). In a first step we rewrite Eq. (3.8) in replacing \mathcal{U} which carries out the time evolution from t to t_f according to Eq. (I.5)

$$\begin{aligned} K(t_f, t; \mathbf{E}) &= \frac{i}{\hbar} \text{tr}_S \{ \hat{O} \left(\hat{A}(t_f, t) [\mathcal{M}\hat{\rho}(t)] + [\mathcal{M}\hat{\rho}(t)] \hat{A}^+(t_f, t) \right. \\ &\quad \left. + \sum_j \hat{C}_j(t_f, t) [\mathcal{M}\hat{\rho}(t)] \hat{C}_j^+(t_f, t) \right) \}. \end{aligned} \quad (\text{I.6})$$

A rearrangement of the different terms in the trace leads to

$$\begin{aligned} K(t_f, t; \mathbf{E}) &= \frac{i}{\hbar} \text{tr}_S \{ \left(\hat{A}^+(t_f, t) \hat{O} + \hat{O} \hat{A}(t_f, t) \right. \\ &\quad \left. + \sum_j \hat{C}_j^+(t_f, t) \hat{O} \hat{C}_j(t_f, t) \right) \mathcal{M}\hat{\rho}(t) \}. \end{aligned} \quad (\text{I.7})$$

The derived expression confirms the existence of $\tilde{\mathcal{U}}$, Eq. (3.10) and demonstrates how to obtain this quantity if \mathcal{U} is given in the form of Eq. (I.5).

To derive an equation of motion for $\hat{\sigma}$, Eq. (3.10) with respect to a dependence on the intermediate time t we first take notice of Eq. (H.1) and get

$$\frac{\partial}{\partial t} \mathcal{U}(t_f, t) = \mathcal{U}(t_f, t) (i\mathcal{L}_{\text{mol}} + i\mathcal{L}_{\text{F}}(t) + \mathcal{D}). \quad (\text{I.8})$$

Generalizing the control kernel written in the form of Eq. (3.9) to a quantity which depends via $\hat{\rho}$ on a second independent time-argument \bar{t} the time derivative with respect to t yields

$$\begin{aligned} \frac{\partial}{\partial t} K(t_f, t, \bar{t}; \mathbf{E}) &= \\ \frac{i}{\hbar} \text{tr}_S \{ \hat{\sigma}(t) (i\mathcal{L}_{\text{mol}} + i\mathcal{L}_{\text{F}}(t) + \mathcal{D}) \mathcal{M}\hat{\rho}(\bar{t}) \}, \end{aligned} \quad (\text{I.9})$$

A rearrangement of the terms in the bracket leads to the required equation of motion for $\hat{\sigma}$

$$\frac{\partial}{\partial t}\hat{\sigma}(t) = -i\mathcal{L}_{\text{mol}}\hat{\sigma}(t) - i\mathcal{L}_{\text{F}}(t)\hat{\sigma}(t) + \tilde{\mathcal{D}}\hat{\sigma}(t) , \quad (\text{I.10})$$

with the dissipative part

$$\begin{aligned} \tilde{\mathcal{D}}\hat{\sigma}(t) = \\ \sum_u \left(\Lambda_u^+ K_u \hat{\sigma}(t) + \hat{\sigma}(t) K_u \Lambda_u - \Lambda_u^+ \hat{\sigma}(t) K_u - K_u \hat{\sigma}(t) \Lambda_u \right) \end{aligned} \quad (\text{I.11})$$

which is essentially different from \mathcal{D} , Eq. (I.1). Eq. (I.10) tells us how to perform the reverse time propagation in Eq. (3.10).

Appendix J

Further Generalizations of the Optimal Control Theory

J.1 Spectral Limitation of the Laser Pulse

Although it was not directly the aim of the present work to develop new methods to reduce the spectral width of the OC pulse and we work throughout this thesis with unrestricted field, the importance this aspect for the application of OC results in experiment is such, that we find it necessary to discuss this problem here. At the moment, there exist only few attempts to introduce the spectral limitations on the the optimal field within OC theory [HMdVR01, HMdVR02]. The results will be shortly reviewed here.

The first method discussed here uses a special projection method to eliminate the unwanted components of the optimal field spectrum and to restrict it onto a given spectral interval. A spectrally broad laser pulse would coherently excite many eigenstates of the molecular system, while the reduced one should excite only few of them. Thus, we define a projector onto a specified subset of the N eigenstates $|\nu_n\rangle$ of the field free Hamiltonian H_{mol} . The states in the projector will be weighted with a shape function $W(n)$,

$$P = \sum_{n=1}^{N^*} W(n) |\nu_n\rangle \langle \nu_n|. \quad (\text{J.1})$$

In [HMdVR01] the shape function was chosen to represent a Gaussian distribution,

$$W(n) = \exp \left\{ - \left(\frac{\nu - \nu_0}{\Delta\nu} \right)^2 \right\}. \quad (\text{J.2})$$

Here ν_0 is the maximum and $\Delta\nu$ is the width of the desired eigenstate distribution. Once the parameters of the distribution are chosen one applies the projector in Eq. (3.19) for the optimal laser field to restrict its spectra. This results in the splitting of the Eq. (3.19) into the desired spectrally restricted part and the un-wanted one which should be eliminated. We obtain for the control kernel

$$\begin{aligned} \mathbf{K}(t, t_0, t_f; \mathbf{E}) = & -Im\left\{ \left(\sum_{k,l=1}^N W(l)^2 a_l^{\dagger(i)} a_k^{(f)} \delta_{kl} \right) \right. \\ & \times \left. \left(\sum_{k,l=1}^N W(l)W(k) \langle \nu_l | a_l^{\dagger(f)} \mu a_k^{(i)} | \nu_k \rangle \right) \right\} + \dots \end{aligned} \quad (\text{J.3})$$

Here we used complex numbers $a_l^{(i)} = \langle \nu_l | \psi_i(t) \rangle$. Numerically the formula is applied in each step of the OC propagation. The propagation is performed with the unrestricted wavefunctions, only the optimal field is created with the restriction. The method has been successfully applied in [HMdVR01] to calculate the optimal pulses to control the dynamics of K_2 molecule. A significant simplification of the laser pulses in terms for their experimental feasibility has been reported.

Another method to put a spectral pressure on the optimal pulse has been developed in [HMdVR02]. The method is based on the observation, that the standard OC algorithm naturally selects the transitions with the highest transition dipolemoment from those contributing to the control yield. Therefore, an artificial two level system with very high transition dipolemoment and the transition frequency required from the restricted optimal pulse is added and optimized simultaneously with the original molecular system. This results in the new type of the objective functional

$$J(t_0, t_f; \mathbf{E}) = O_{mol}(t_f, \mathbf{E}) + O_{art.}(t_f, \mathbf{E}) + \frac{1}{2} \int_0^{t_f} \lambda(t) |\mathbf{E}(t)|^2 dt. \quad (\text{J.4})$$

Thus additionally to the propagation of the coupled equations (3.11) and (3.12) we are obliged to propagate similar set of equations for the artificial two level system. The optimal electric field is computed as a sum of the fields produced from the OC algorithm for both systems. Because the additional computational effort for propagating the two level system is rather minor the method could be successfully used. It is demonstrated in [HMdVR02] that the method is indeed able to distill the right frequencies from the optimal pulse.

The methods presented above demonstrate the ability of the OC theory upon some generalizations to achieve spectral limited control pulses. The gen-

eralizations presented here are simple enough so that they can be combined with other refinements of the OC theory presented in following sections.

J.2 Generalized Target States

The formulation of OC theory introduced so far tries to maximize a certain observable at a certain time. However, it would be of a great interest to relax this strict demand somewhat. For example, if a wavepacket has been excited in a particular electronic level, the demand should be sufficient to have this wavepacket localized in a certain part of the respective PES in a certain time interval. Indeed, since the coordinates Q are continuous functions the OC theory becomes ill defined if we try to maximize $Q(t_f) = \text{tr}_S\{\hat{\rho}(t_f)Q\}$. It would be more appropriate to introduce into the control function $\mathcal{F}(Q(t_f) - \bar{Q})$, where \bar{Q} is a value of the coordinate to be achieved and $\mathcal{F}(x)$ is a ordinary function of the argument x vanishing at $x = 0$, e.g. $\mathcal{F}(x) = x^2$. Now we try to minimize the deviation of $Q(t_f)$ from the given value \bar{Q} .

The formulation of the OC theory using the control functional $J(t_f; \mathbf{E})$, Eq. (3.6) enables one to formulate the control task for a target state which deviates from those discussed in this thesis so far. Up to now the target state of the control task has been defined via a pure state, i.e. $|\phi_{\text{target}}\rangle$ or by a hermitian operator, i.e. a mixed state

$$\hat{O} = \sum_{\alpha} o_{\alpha} |\psi_{\alpha}\rangle \langle \psi_{\alpha}|, \quad (\text{J.5})$$

where o_{α} and $|\psi_{\alpha}\rangle$ are the *eigenvalues* and *eigenstates* of the operator \hat{O} , respectively. The latter case would result in

$$O(t_f; bfE) = \sum_{\alpha} o_{\alpha} O_{\alpha}(t_f; \mathbf{E}). \quad (\text{J.6})$$

Here, every O_{α} corresponds to the case where \hat{O} in Eq. (J.5) has to be defined with the projector $|\psi_{\alpha}\rangle \langle \psi_{\alpha}|$.

The control task defined via Eq. (J.6) can be somewhat relaxed in setting $\mathcal{F}(O_{\alpha}(t_f; \mathbf{E}) - \hat{O}_{\alpha})$ instead of $O_{\alpha}(t_f; \mathbf{E})$ (the function \mathbf{F} are not necessarily identical for all α). This scheme can be used to achieve an incoherent population of certain molecular levels. Therefore, we identify the \hat{O}_{α} with given level populations \hat{P}_{α} and set, e.g.

$$O(t_f; \mathbf{E}) = \frac{1}{2} \sum_{\alpha} (O_{\alpha}(t_f; \mathbf{E}) - \bar{P}_{\alpha})^2, \quad (\text{J.7})$$

where the index α only runs over a few numbers.

Noting this generalization of the Eq. (3.5) and thus of the control functional, Eq. (3.6) it becomes immediately clear that we have to work with the set of K_α of control kernels. According to Eq. (3.8) they would contain the prefactors $O_\alpha(t_f; \mathbf{E}) - \bar{P}_\alpha$. Here, we define

$$\begin{aligned} \mathbf{K}_\alpha(t_f, t; \mathbf{E}) &= \frac{\delta O_\alpha(t_f)}{\delta \mathbf{E}(t)} \\ &= \frac{i}{\hbar} \text{tr}_S \{ |\psi_\alpha\rangle \langle \psi_\alpha| \mathcal{U}(t_f, t; \mathbf{E}) \mathcal{M} \mathcal{U}(t, t_0; \mathbf{E}) \hat{\rho}(t_0) \} \\ &= \frac{i}{\hbar} \text{tr}_S \{ \hat{\sigma}(t; \mathbf{E}) \mathcal{M} \hat{\rho}(t; \mathbf{E}) \}. \end{aligned} \quad (\text{J.8})$$

Instead of a single density operator for back propagation we have the set

$$\hat{\sigma}_\alpha(t; \mathbf{E}) = \tilde{\mathcal{U}}(t_f, t; \mathbf{E}) |\psi_\alpha\rangle \langle \psi_\alpha|. \quad (\text{J.9})$$

Once the various control kernels, Eq. (J.8) have been introduced the functional equation defining the optimal pulse has to be generalized to

$$\mathbf{E}(t) = \frac{1}{\lambda(t)} \sum_\alpha (O_\alpha(t_f; \mathbf{E}) - \hat{P}_\alpha) \mathbf{K}_\alpha(t_f, t; \mathbf{E}) \quad (\text{J.10})$$

including now the prefactors $O_\alpha(t_f; \mathbf{E}) - \hat{P}_\alpha$.

To solve the control task in a manner given by the two equations (3.11) and (3.12) we have to notice that the control field is composed by different contributions.

J.3 Probe–Pulse Absorption as the Target of the Optimal Control

The absorption spectrum of a probe pulse which has been applied in addition to the laser pulse guiding the molecular system in the required manner represents an observable to which one has a direct access in an optical experiment. It is usually derived from expression describing the amount of field energy exchanged with the medium

$$S(t) = - \int d^3 \mathbf{r} \frac{\partial \mathbf{E}_{probe}(\mathbf{r}, t)}{\partial t} \mathbf{P}_{probe}(\mathbf{r}, t). \quad (\text{J.11})$$

Here, \mathbf{E}_{probe} is the probe pulse field-strength which can be written as (in contrast to the control field)

$$\mathbf{E}_{probe}(\mathbf{r}, t) = \mathbf{n}_{probe} E_{probe}(t) \exp\{i(\mathbf{k}_{probe}\mathbf{r} - \omega_{probe}t) + c.c. \} \quad (\text{J.12})$$

It includes field polarization vector \mathbf{n}_{probe} , amplitude $E_{probe}(t)$, wavevector \mathbf{k}_{probe} and frequency ω_{probe} . The respective polarization (dipole density) induced by the probe pulse has to be deduced from the complete polarization field \mathbf{P} . If any inhomogeneous broadening is absent it reads (n_{mol} is volume density of molecules)

$$\mathbf{P}(t) = n_{mol} tr_S\{\hat{\rho}(t; \mathbf{E}) \hat{\mu}\}. \quad (\text{J.13})$$

The total field \mathbf{E} is given as a sum of the probe field \mathbf{E}_{probe} and the control field \mathbf{E}_c . Since the probe field is usually assumed to be weak compared to the control field one can carry out a linearization of $\mathbf{P}(t)$ with respect to \mathbf{E}_{probe} . Changing to the total energy exchange between the probe pulse and the medium one obtains (note the neglect of the time-derivative of the probe field amplitude)

$$\begin{aligned} S_{total} &= \int_{t_0}^{\infty} dt S(t) = 2\omega_{probe} V_0 \\ &\times Im \int_{t_0}^{\infty} dt \int_{t_0}^t d\bar{t} e^{\{i\omega_{probe}(t-\bar{t})\}} E_{probe}^*(t) E_{probe}(\bar{t}) \mathbf{K}(t, \bar{t}; \mathbf{E}_c). \end{aligned} \quad (\text{J.14})$$

Since a linearization with respect to the weak-field part of the complete laser pulse has been carried out a derivative appears allowing the introduction of the control kernel according to Eq. (3.8).

Bibliography

- [ABB⁺98] A. Assion, T. Baumert, M. Bergt, T. Brixner, B. Kiefer, V. Seyfried, M. Strehle, and G. Gerber. *Science*, 282:919, 1998.
- [Abr61] A. Abragam. *The Principles of Nuclear Magnetism*. Clarendon, Oxford, 1961.
- [AS72] M. Abramovitz and I. A. Stegun. *Handbook of Mathematical Functions*. Dover, New York, 1972.
- [BBK⁺99] M. Bergt, T. Brixner, B. Kiefer, M. Strehle, and G. Gerber. *J. Phys. Chem. A*, 103:10381, 1999.
- [BBS⁺97] T. Baumert, T. Brixner, V Seyfried, M. Strehle, and G. Gerber. *Appl. Phys. B*, 65:779, 1997.
- [BBz⁺00] R. Bartels, S. Backus, E. zeek, L. Misogutti, G. Vdovin, I. P. Christov, M. M. Murnane, and H. C. Kapteyn. *Nature*, 406:164, 2000.
- [BDNG00] T. Brixner, N. H. Damrauer, P. Niklaus, and G. Gerber. *Nature*, 414:57, 2000.
- [BG95] T. Baumert and G. Gerber. *Isr. J. Chem.*, 34:103, 1995.
- [BHM97] M. L. Brewer, J. S. Hulme, and D. E. Manolopoulos. *J. Chem. Phys.*, 106:4832, 1997.
- [BJWM00] M. H. Beck, A. Jäckle, G. A. Worth, and H.-D. Meyer. *Phys. Rep.*, 324:1, 2000.
- [BKG01] T. Brixner, B. Kiefer, and G. Gerber. *Chem. Phys.*, 267:241, 201.
- [BKP99] H.-P. Breuer, B. Kappler, and F. Petruccione. *Phys. Rev. A*, 59:1633, 1999.

- [BKT93] A. Bartana, R. Kosloff, and D. J. Tannor. *J. Chem. Phys.*, 99:196, 1993.
- [Blu89] Karl Blum. *Density Matrix Theory and Applications*. Plenum Press, New York, 2nd edition, 1989.
- [BMP94] J. R. Brinati, S. S. Mizrahi, and G. A. Prata. *Phys. Rev. A*, 50:3004, 1994.
- [BS] Th. Bäck and H.-P. Schwefel. *Evolutionary Computation*, 1.
- [BS86] P. Brumer and M. Shapiro. *Chem. Phys. Lett.*, 126:54, 1986.
- [BTS98] K. Bergmann, H. Theuer, and B. W. Shore. *Rev. Mod. Phys.*, 70:1003, 1998.
- [BYS⁺99] C. J. Bardeen, V. V. Yakovlev, J. A. Squier, K. R. Wilson and S. D. Carpenter, and P. M. Weber. *J. Biomed. Opt.*, 4:362, 1999.
- [BYW⁺97] C. J. Bardeen, V. V. Yakovlev, K. R. Wilson, S. D. Carpenter, P. M. Weber, and W. S. Warren. *Chem. Phys. Lett.*, 280:151, 1997.
- [CS79] S. Chaturvedi and J. Shibata. *Z. Phys. B*, 35:297, 1979.
- [Dak94] Y. Dakhnovskii. *J. Chem. Phys.*, 100:6492, 1994.
- [DC95] Y. Dakhnovskii and R. D. Coalson. *J. Chem. Phys.*, 103:2908, 1995.
- [DCM92] J. Dalibard, Y. Castin, and K. Molmer. *Phys. Rev. Lett.*, 68:580, 1992.
- [DEKC95] Y. Dakhnovskii, D. G. Evans, H. J. Kim, and R. D. Coalson. *J. Chem. Phys.*, 103:5461, 1995.
- [DFG⁺01] Ch. Daniel, J. Full, L. González, C. Kaposta, M. Krenz, C. Lupulescu, J. Manz, S. Minemoto, M. Opel, P. Rosendo-Francisco, Š. Vajda, and L. Wöste. *Chem. Phys.*, 267:247, 2001.
- [Ein56] Albert Einstein. *Investigations on the Theory of the Brownian Movement*. Dover, New York, 1956.

- [EKD01] D. Egorova, A. Kühl, and W. Domcke. *Chem. Phys.*, 268:105, 2001.
- [EMB⁺98] A. Efimov, M. D. Moores, N. M. Beach, J. L. Krause, and D. H. Reitze. *Opt. Lett.*, 23:1915, 1998.
- [Fey48] R. P. Feynman. *Rev. Mod. Phys.*, 20:367, 1948.
- [FH65] R. P. Feynman and A. R. Hibbs. *Quantum Mechanics and Path Integrals*. McGraw-Hill, New York, 1965.
- [FS96] C. Fuchs and M. Schreiber. *J. Chem. Phys.*, 105:1023, 1996.
- [FV63] R. P. Feynman and F. L. Vernon. *J. Ann. Phys.*, 24:118, 1963.
- [GBF98] E. Gaizauskas, A. Berzanskis, and K.-H. Feller. *Chem. Phys.*, 235:123, 1998.
- [Ger01] Gerber. *Physikalische Blätter*, 2001.
- [Gev02] E. Geva. *J. Chem. Phys.*, 116:1629, 2002.
- [GH98] M. Grifoni and P. Hänggi. *Phys. Rep.*, 304:229, 1998.
- [GN99a] P. Gaspard and M. Nagaoka. *J. Phys. Chem.*, 111:5676, 1999.
- [GN99b] P. Gaspard and M. Nagaoka. *J. Phys. Chem.*, 111:5668, 1999.
- [GP92] N. Gisin and I. C. Percival. *J. Phys. A*, 25:5678, 1992.
- [GPM96] I.A. Goychuk, E. G. Petrov, and V. May. *Chem. Phys. Lett.*, 253:428, 1996.
- [GPM97] I.A. Goychuk, E. G. Petrov, and V. May. *J. Chem. Phys.*, 106:4522, 1997.
- [GR92] G. Gangopadhyay and D. S. Ray. *Phys. Rev. A*, 46:1507, 1992.
- [GRSB90] U. Gaubatz, P. Rudecki, S. Schiemann, and K. Bergmann. *J. Chem. Phys.*, 92:5363, 1990.
- [HCP⁺00] M. Heid, T. Chen, R. Pausch, H. Schwoerer, and W. Kiefer. *J. Chinese Chem. Soc.*, 47:637, 2000.
- [Her94] M. F. Hermann. *Ann. Rev. Phys. Chem.*, 45:83, 1994.

- [HMdVR01] Th. Hornung, M. Motzkus, and R. de Vivie-Riedle. *J. Chem. Phys.*, 115:3105, 2001.
- [HMdVR02] Th. Hornung, M. Motzkus, and R. de Vivie-Riedle. *Phys. Rev. A*, 65:R021493, 2002.
- [HWC⁺] J. L. Herek, W. Wohlleben, R. J. Cogdell, D. Zeidler, and M. Motzkus. *Nature*, 417.
- [Ima94] A. Imamoglu. *Phys. Rev. A*, 50:3650, 1994.
- [JB99] J. Jortner and M. Bixon. *Adv. Chem. Phys.*, 106:107, 1999.
- [JR92a] R. S. Judson and H. Rabitz. *Phys. Rev. Lett.*, 68:1500, 1992.
- [JR92b] R. S. Judson and H. Rabitz. *Phys. Rev. Lett.*, 68:1500, 1992.
- [KKS01] U. Kleinekathöfer, I. Kondov, and M. Schreiber. *Chem. Phys.*, 268:121, 2001.
- [KP97] M. V. Korolkov and G. K. Paramonov. *Phys. Rev. A*, 55:589, 1997.
- [KTF94] V. M. Kenkre, A. Tokmakoff, and M. D. Fayer. *J. Chem. Phys.*, 101:10618, 1994.
- [KWPD94] S. Krempl, M. Winterstetter, H. Plöhn, and W. Domcke. *J. Chem. Phys.*, 100:926, 1994.
- [Lan08] P. Langevin. *Co. R. Acad. Sci. Paris*, 146:530, 1908.
- [LCD⁺87] A. J. Leggett, S. Chakravarty, A. Dorsey, M. P. A. Fisher, A. Garg, and W. Zwerger. *Rev. Mod. Phys.*, 59:1, 1987.
- [Lin74] G. Lindblad. *Commun. Math. Phys.*, 48:119, 1974.
- [LM00] O. Linden and V. May. *Eur. Phys. J. D*, 12:473, 2000.
- [LV91] J. P. Lavoine and A. A. Villayes. *Phys. Rev. Lett.*, 67:2780, 1991.
- [Mak98] N. Makri. *J. Phys. Chem. A*, 102:4414, 1998.
- [Man97] T. Mančal. *Czech. J. Phys.*, 48:463, 1997.

- [MAS99] K. Mukai, S. Abe, and H. Sumi. *J. Phys. Chem.*, 103:6096, 1999.
- [MBS98] T. Mančal, J. Bok, and L. Skála. *J. Phys. A: Math. Gen*, 31:9429, 1998.
- [Men95] M. Menšík. *J. Phys.: Condens. Matter*, 7:7349, 1995.
- [MK99] Volkhard May and Oliver Kühn. *Charge and Energy Transfer Dynamics in Molecular Systems*. Wiley-VCH, Berlin, 1999.
- [MKM02] T. Mančal, U. Kleinekathöfer, and V. May. *J. Chem. Phys.*, 2002.
- [MM00] T. Mančal and V. May. *Eur. Phys. J. B*, 18:633, 2000.
- [MM01] T. Mančal and V. May. *J. Chem. Phys.*, 114:1510, 2001.
- [MM02] T. Mančal and V. May. *Chem. Phys. Lett.*, 2002.
- [MS98] D. Meshulach and Y. Silberberg. *Nature*, 396:239, 1998.
- [MT99] Ch. Meier and D. J. Tannor. *J. Chem. Phys.*, 111:3365, 1999.
- [MW95] J. Manz and L. Wöste. *Femtosecond Chemistry*. VCH, Weinheim, 1995.
- [Nak58] S. Nakajima. *Prog. Theor. Phys.*, 20:948, 1958.
- [OF89] Y. Ohtsuki and Y. Fujimura. *J. Chem. Phys.*, 91:3903, 1989.
- [Pau28] W. Pauli. *Festschrift zum 60. Geburtstage A. Sommerfelds*. Hirzel, Leipzig, 1928.
- [PDR88] A. P. Pierce, M. A. Dahleh, and H. Rabitz. *Phys. Rev. A*, 37:4950, 1988.
- [PK98] M. B. Plenio and P. L. Knight. *Rev. Mod. Phys.*, 70:101, 1998.
- [PLZ92] E. D. Potter, Q. Lin, and A. H. Zewail. *Chem. Phys. Lett.*, 200:605, 1992.
- [PTVF92] William H. Press, Saul A. Teukolsky, William T. Vetterling, and Brian P. Flannery. *Numerical Recipes in FORTRAN*. Cambridge University Press, Cambridge, 2nd edition, 1992.

- [RdVRMK00] H. Rabitz, R. de Vivie-Riedle, M. Motzkus, and K. Kompa. *Science*, 288:824, 2000.
- [Red65] A. G. Redfield. *Adv. Mag. Res.*, 1:1, 1965.
- [Ris89] H. Risken. *The Fokker-Planck Equation*. Springer-Verlag Berlin Heidelberg, 1989.
- [RM00] Th. Renger and V. May. *Phys. Rev. Lett.*, 84:5228, 2000.
- [RM02] Th. Renger and R. Marcus. *J. Chem. Phys.*, 116:9994, 2002.
- [RWM00] S. Ramakrishna, R. Willig, and V. May. *Phys. Rev. B*, 110:R16330, 2000.
- [RZ00] S. A. Rice and M. Zhao. *Optical Control of Molecular Dynamics*. Wiley, New York, 2000.
- [SB82] L. Skála and O. Bílek. *Phys. Stat. Sol. B*, 114:K51, 1982.
- [SB92] M. Shapiro and P. Brumer. *J. Chem. Phys.*, 102:5863, 1992.
- [Sch81] L. S. Schulman. *Techniques and Applications of Path Integration*. John Wiley and Sons, New York, 1981.
- [SdVR99] K. Sundermann and R. de Vivie-Riedle. *J. Chem. Phys.*, 110:1896, 1999.
- [SG96] M. A. Sepulveda and F. Grossmann. *Adv. Chem. Phys.*, 96:191, 1996.
- [SJF93] N. F. Scherer, D. M. Jonas, and G. R. Fleming. *J. Chem. Phys.*, 99:153, 1993.
- [SM97] H. Schirrmeister and V. May. *Chem. Phys.*, 220:1, 1997.
- [SM98] H. Schirrmeister and V. May. *Chem. Phys. Lett.*, 297:383, 1998.
- [SRdVR00] K. Sundermann, H. Rabitz, and R. de Vivie-Riedle. *Phys. Rev. A*, 62:13409, 2000.
- [SSO92] A. Suarez, R. Silbey, and I. Oppenheim. *J. Chem. Phys.*, 97:5101, 1992.
- [ST77] N. H. F. Shibata and Y. Takahashi. *J. Stat. Phys.*, 17:171, 1977.

- [Sun98] V. Sundström. (ed.) femtochemistry 97. *J. Chem. Phys. A*, 102:23, 1998.
- [SWR88] S. Shi, A. Woody, and H. Rabitz. *J. Chem. Phys.*, 88:6870, 1988.
- [TKR86] D. J. Tannor, R. Kosloff, and S. A. Rice. *J. Chem. Phys.*, 85:5805, 1986.
- [TR85] D. J. Tannor and S. A. Rice. *J. Chem. Phys.*, 83:5013, 1985.
- [vK92] N. van Kampen. *Stochastic Processes in Physics and Chemistry, 2nd edition*. North-Holland, Amsterdam, 1992.
- [vVBK⁺01] Š. Vajda, A. Bartelt, E.-C. Kaposta, Th. Leisner, C. Lupulescu, Sh. Minemoto, P. Rosendo-Francisco, and L. Wöste. *Chem. Phys.*, 267:231, 2001.
- [VVL91] A. A. Villayes, J. C. Vallet, and S. H. Lin. *Phys. Rev. A*, 43:5030, 1991.
- [WAB99] T. C. Weinacht, J. Ahn, and P. H. Bucksbaum. *Nature*, 397:233, 1999.
- [Wei93] U. Weiss. *Quantum Dissipative Systems*. World Scientific, Singapore, 1993.
- [Wil99] K. Wilson. Festschrift. *J. Chem. Phys. A*, 103:10021, 1999.
- [WK98] A. M. Weiner and A. M. Kan'an. *IEEE J. Select. Topics Quant. Electron.*, 4:317, 1998.
- [WL93] T.-M. Wu and R. F. Loring. *J. Chem. Phys.*, 99:8936, 1993.
- [WWB99] T. C. Weinacht, J. L. White, and P.H. Buckbaum. *J. Phys. Chem.*, 103:10166, 1999.
- [YD01] T. J. York and Y. Dakhnovskii. *J. Phys. Chem. B*, 105:8278, 2001.
- [YGW⁺93] Y. J. Yan, R. E. Gillian, R. M. Whitnell, K. R. Wilson, and S. Mukamel. *J. Phys. Chem.*, 97:2320, 1993.
- [YMS97] D. Yelin, D. Meshulach, and Y. Silberberg. *Opt. Lett.*, 22:1793, 1997.

- [YOR99] W. Zhu Y. Ohtsuki and H. Rabitz. *J. Chem. Phys.*, 110:9825, 1999.
- [ZBR98] W. Zhu, J. Botina, and H. Rabitz. *J. Chem. Phys.*, 108:1953, 1998.
- [Zew94] A. H. Zewail. *Femtochemistry: Ultrafast dynamics of the Chemical Bond*. World Scientific, Singapore, 1994.
- [Zew96] A. H. Zewail. *Femtochemistry: Ultrafast Chemical and Physical Processes in Molecular Systems*. World Scientific, Singapore, 1996.
- [Zew97] A. H. Zewail. *Adv. Chem. Phys.*, 101:3, 1997.
- [ZR98] W. Zhu and H. Rabitz. *J. Chem. Phys.*, 109:385, 1998.
- [ZW94] R. Zimmermann and J. Wauer. *J. Luminescence*, 58:271, 1994.
- [Zwa60] R. Zwanzig. *J. Chem. Phys.*, 33:1338, 1960.

Danksagung

Ich möchte mich an dieser Stelle ganz herzlich bei allen Mitgliedern der Arbeitsgruppe Halbleitertheorie um Herrn Prof. Roland Zimmermann bedanken für die sehr freundliche Arbeitsatmosphäre in der mir die Arbeit am Thema meiner Promotion viel Spaß gemacht hat. Dabei ist an erster Stelle mein Betreuer Dr. habil. Volkhard May zu nennen, der mich vor 4 Jahren in seine Gruppe aufgenommen hat und in beide Themen meiner Doktorarbeit eingeführt hat. Er fand sich zu jeder Zeit bereit über Physik zu diskutieren, mich bei der Lösung aller Problemen zu begleiten und trug die Sorge dafür, daß die äußeren Rahmenbedingungen meiner Arbeit stets gewährleistet waren.

Besonderer Dank gebührt Ben Brüggemann und Dr. Axel Esser, die sich in unserer Arbeitsgruppe ausser anderem auch um die Computer gekümmert haben auf denen der numerische Teil dieser Arbeit ausgeführt wurde. Mein spezieller Dank ist dem Prof. Dr. Vincenzo Savona gewiß, mit dem ich die Deutschkurse besucht habe und der für viel Spaß und Unterstützung sorgte.

Herrn Dr. Ulrich Kleinekathöffer von der TU Chemnitz möchte ich herzlich danken für einen stimulierenden Aufenthalt in der Gruppe von Herrn Prof. M. Schreiber im Herbst 2000.

Die Arbeit wurde im Rahmen des Sonderforschungsbereiches 450 *Analyse und Steuerung ultraschneller photoinduzierter Reaktionen* gemacht, sodaß meinen Dank auch den vielen Leuten aus verschiedenen Teilprojekten gilt, die sich an interessanten Seminaren im SFB beteiligt haben.

Ich bedanke mich bei meiner Familie und meiner Freundin für ihre große Unterstützung und viel Gedult bei meiner 4 Jahre lange Abwesenheit.

Lebenslauf

Persönliches:

Name: Tomáš Mančal
23. April 1974 geboren in Vlašim, Tschechische Republik
Nationalität: tschechisch
Familienstand: ledig

Ausbildung:

1988 - 1992 Gymnasium in Vlašim, Tschechische Republik
1992 - 1997 Studium der Physik an der Karls-Universität Prag
1997 Diplomarbeit zum Thema: *Lösung der Verallgemeinerten
Ratengleichung für ein Modellsystem in Wechselwirkung
mit einem thermodynamischen Bad*
1997 - 1998 Vorbereitung auf das Promotionsstudium,
Karls-Universität Prag
1998 - 2002 Promotion an der Humboldt-Universität zu Berlin
Thema: *Laser Pulse Control of Dissipative Dynamics
in Molecular Systems*
unter Betreuung von Dr. habil. V. May

Aufstellung der wissenschaftlichen Veröffentlichungen

Zeitschriftenartikel im Rahmen der Dissertation

1. **T. Mančal and V. May**, *Optimal Control Theory of Ultrafast Molecular Dynamics: Are the Results of Interest for the Experiment?*, Chem. Phys. Lett., in press
2. **T. Mančal, U. Kleinekathöffer and V. May**, *Femtosecond laser pulse control of electron transfer processes*, J. Chem. Phys., 117 (2002) 636
3. **T. Mančal and V. May**, *Retardation effects in the dynamics of open quantum systems*, Chem. Phys. 268 (2001) 201
4. **T. Mančal and V. May**, *Laser pulse control of ultrafast electron transfer reactions*, Europ. Phys. J. D, 14 (2001) 173
5. **T. Mančal and V. May**, *Non-Markovian Dissipation of Molecular Vibrational Energy via Multi-Quantum Processes*, Chem. Phys. Lett., 334 (2001) 179
6. **T. Mančal and V. May**, *Interplay of Non-Markovian Relaxation and Ultrafast Optical State Preparation in Molecular Systems: The Laguerre Polynomial Method*, J. Chem. Phys., 114 (2001) 1510
7. **T. Mančal and V. May**, *Non-Markovian Relaxation in an Open Quantum System: Polynomial Approach to the Solution of the Quantum Master Equation*, Eur. Phys. J. B, 18 (2000) 633

Tagungsbeiträge im Rahmen der Dissertation

1. **T. Mančal and V. May**, *Laser Pulse Control of Molecular Dynamics: Considerations of some experimental constraints*, **Frühjahrstagung der Deutschen Physikalischen Gesellschaft**, 11. - 15. März 2002, Regensburg, Germany : oral contribution
2. **T. Mančal and V. May**, *Optimal Control of Molecular Dynamics*, **Vth Femtochemistry Conference**, 2. - 6. September 2001, Toledo, Spain : poster contribution; also published in *Femtochemistry and Femtobiology: Ultrafast Dynamics in Molecular Science* (World Scientific, 2002)
3. **T. Mančal and V. May**, *Optimal Control of Molecular Dynamics*, **The Seventh European Conference on Atomic and Molecular Physics and The 2001 AMOP & CPP Spring Meeting of DPG**, 2. - 6. April 2001, Berlin : poster contribution
4. **T. Mančal and V. May**, *Non-Markovian Dissipative Wavepacket Dynamics in Open Quantum Systems*, **Workshop in Theoretical Chemistry**, 15. - 18. Februar 2000, Mariapfarr, Österreich : oral contribution
5. **T. Mančal and V. May**, *Nichtmarkovsche Dynamik in offenen Molekularsystemen: Relaxation und Elektronentransfer*, **Frühjahrstagung der Deutschen Physikalischen Gesellschaft**, 13. - 16. März 2000, Potsdam : poster contribution
6. **T. Mančal, D. H. Schirrmeister and V. May**, *Memory effects in the Light-Driven Dissipative dynamics of molecular systems*, **Frühjahrstagung der Deutschen Physikalischen Gesellschaft**, 22. - 26. März 1999, Münster : oral contribution

Weitere Veröffentlichungen

1. **V. Čápek and T. Mančal**, *Phonon mode cooperating with particle serving as Maxwell gate and rectifier*, J. Phys. A: Math. Gen., 35 (2002) 2111
2. **V. Čápek and T. Mančal**, *Isothermal Maxwell Daemon as a Molecular Rectifier*, Europhys. Lett., 48 (1999) 365

3. **T. Maňcal, J. Bok and L. Skála**, *Short time de-excitation dynamics of a two level electron system. Non-perturbative solution of the master equation*, J. Phys. A: Math. Gen. 31 (1998) 9429
4. **T. Maňcal** *Non-perturbative Solution of Generalized Master Equation*, Czech. J. Phys., 48 (1998) 463

Selbständigkeitserklärung

Hiermit erkläre ich, die vorliegende Arbeit selbständig ohne fremde Hilfe verfaßt zu haben und nur die angegebene Literatur und Hilfsmittel verwendet zu haben.

Tomáš Mančal
Berlin, den 11. September 2002